AN INVESTIGATION INTO THE DEPENDANCE OF ELECTRICAL PROPERTIES ON MICROSTRUCTURE IN POLYCRYSTALLINE BARIUM TITANATE

by

P.C.Williams

being a thesis submitted to the University of Aston in Birmingham in support of an application for admission to the Degree of Master of Science.

20th. January 1969. University of Aston in Birmingham.

P.C. Williams.

P.C.Williams.

MEMORANDEM

Except where mentioned, all the experimental work described in this thesis was carried out solely by the author between December 1966 and December 1968, under the supervision of Mr.B.M. Farazmand of the University of Aston in Birmingham.

None of the work contained herein has been presented before in a degree thesis to this or any other University.

In the author's opinion the main contributions presented in this thesis are:-

(i) A detailed investigation of the factors which influence the electrical phenomena exhibited by polycrystalline barium titanate

(ii) A contribution to the material available concerning grain growth in porous compacts

(iii) The development of ceramic capacitor voltage dividers for use on high voltage electrical power systems which have superior operating characteristics to those already in general use.

ACKNOWLEDGEMENTS

The author wishes to acknowledge the help and advice given to him during the course of the project by Professor E.J.Davies and Professor J.E.Flood of the University of Aston in Birmingham, to thank Mr.B.M.Farazmand for his assistance and enthusiasm in his role as Internal Supervisor and other members of the Academic and Non-Academic staff of the University who generously gave their time or facilities in the furtherance of the project.

The author wishes to thank in particular Mr.N.Grimes of the Physics Department, University of Aston, for his assistance and guidance with problems associated with the Crystallographic Analysis of Ceramic Specimens.

SYNOPSIS

It has been recognised for some considerable time that the intrinsic properties of particular materials determined from single crystals are not always reflected in the properties of polycrstalline materials of the same composition.

In particular, it is known that samples of polycrystalline ceramics are invariably more complex than their single-crystal form. The differences which occur may be seen to depend upon the processing and thermal history of the material, in the size and distribution of grains, the number, size and distribution of voids, and the nature of the boundaries between the grains.

Ceramic barium titanate is a typical example of this type of material. Various investigators have stated that the dielectric properties of the material are influenced by the microstructure, but relatively few direct correlations have been reported.

A survey of the literature available revealed that, in every case, the investigators had based their work on test pieces formed by pressing powders of varying purity in a punch and die using organic additives as binders.

Whilst this method of compaction can be used to good advantage when producing commercial grade bodies, it would appear to be quite unsatisfactory for the fabrication of laboratory test pieces, the inhomogeneous nature of the material, caused by differential compaction, producing warping and (in extreme cases) cracking of the fired ceramic. The strains present within this type of body would obviously contribute towards the electrical properties of the material and could, perhaps, produce effects which might mask the true nature of the test pieces, and so produce the discrepancies observed in the reported literature.

In order to determine the true nature of the material, ceramic test pieces were produced by pressing powders of known composition in a water-filled die, a method known to produce homogeneous powder compacts. These were then fired under closely controlled conditions together with samples of the same powders pressed in the conventional manner (with a punch and die),

care being taken to remove all possible sources of impurity during this process.

Metal electrodes were then applied to discs of the ceramics and electrical measurements were made over a wide temperature range (-70° to 150°C). Specimens from each batch of test pieces were examined in detail, using advanced physical methods, in order to determine their exact structure.

A detailed correlation of physical and electrical properties then followed, together with a direct comparison with specimens pressed by the conventional method.

INDEX

CHAPTER 11 - Conclusions

CHAPTER 12 - Future Work

CHAPTER 1

1.1. OBJECTIVE

The objective of this project was to correlate the electrical properties exhibited by polycrystalline barium titanate with the physical structure of the material.

1.2. DEFINITION

High-permittivity ceramic materials are defined as those materials, usually mixed oxides, which have porous crystalline structures and which exhibit anomolously-high relative electrical permittivity.

1.3. CONVENTIONS EMPLOYED IN THIS THESIS

1.3.1. Unless otherwise stated,all temperatures refer to the Celsius Scale.

1.3.2. The M.K.S. system of units is adopted throughout,unless otherwise stated.

1.3.3. All abbreviations are in accordance with B.S.1991 (1963).

1.3.4. Crystallographic studies are referred to using the Magun-Hermann notation.

1.3.5. The computor programme is written in Algol.

1.3.6. Barium titanate ($BaTiO_3$), and other simple chemical compounds, are refered to by use of the appropriate chemical formulae.

1.4. List of Principle Symbols

Symbol	Term	Unit
a	Cell dimension in 'a' direction	°A
A	Electrode area	m^2
b	Cell dimension in 'b' direction	°A
c	Cell dimension in 'c' direction	°A
c	Curie Constant	
C	Capacitance	F
d	Spacing of contributing planes	°A
D	Electric Displacement	C/m^2
E	Electrical Stress	V/m
f	Shape factor	
G	Gibbs Function	
i	Instantaneous Current	A
I	Steady or R.M.S. value of Current	A
I_o	Peak intensity of refracted x-ray beam	Counts/sec.
Ip	Peak intensity of incident x-ray beam	Counts/sec.
K	Scale Factor	
m	With a mirror plane parallel to the preceeding axis	
/m	With a mirror plane normal to the axis referred to before the oblique stroke	
n	n fold axis	
$\bar{n}$	n fold rotation	
p	Number of contributing planes	
P	Polarization	Coulombs/m^2
Ps	Spontaneous Polarization	Coulombs/m^2
S	Entropy	Btu/lb - degF.
t	Sample thickness	M
Tc	Transition temperature	°C.
To	Calculated temperature	°C.
U	Internal Energy	Btu./lb.
V	Voltage	V

Symbol	Term	Unit
α	Activation field	
β_1	X-ray characteristic half-height width	Radians
β_2	X-ray generator half-height width	Radians
ϵ_o	Permittivity of free space 8.85×10^{-12} M.K.S. Units	
ϵ_r	Relative permittivity	
λ	Wavelength	°A
ρ	Resistivity	-m.
2θ	Bragg Angle	Radians

CHAPTER 2

2. SURVEY OF LITERATURE APPERTAINING TO BARIUM TITANATE

Although the compound barium titanate had been known for a considerable time, its ferroelectric nature was not discovered until 1945 (1). Structural and electrical investigations followed and the properties of the single crystal material became well documented.

2.1. The Single Crystal Material

2.1.1. Static Properties

In its single crystal form (unclamped) the material is found to undergo several phase transitions at specific temperatures. Kay and Vousden (1949) (2) measured the unit cell dimensions over a wide range of temperature, indentifying the phase changes.

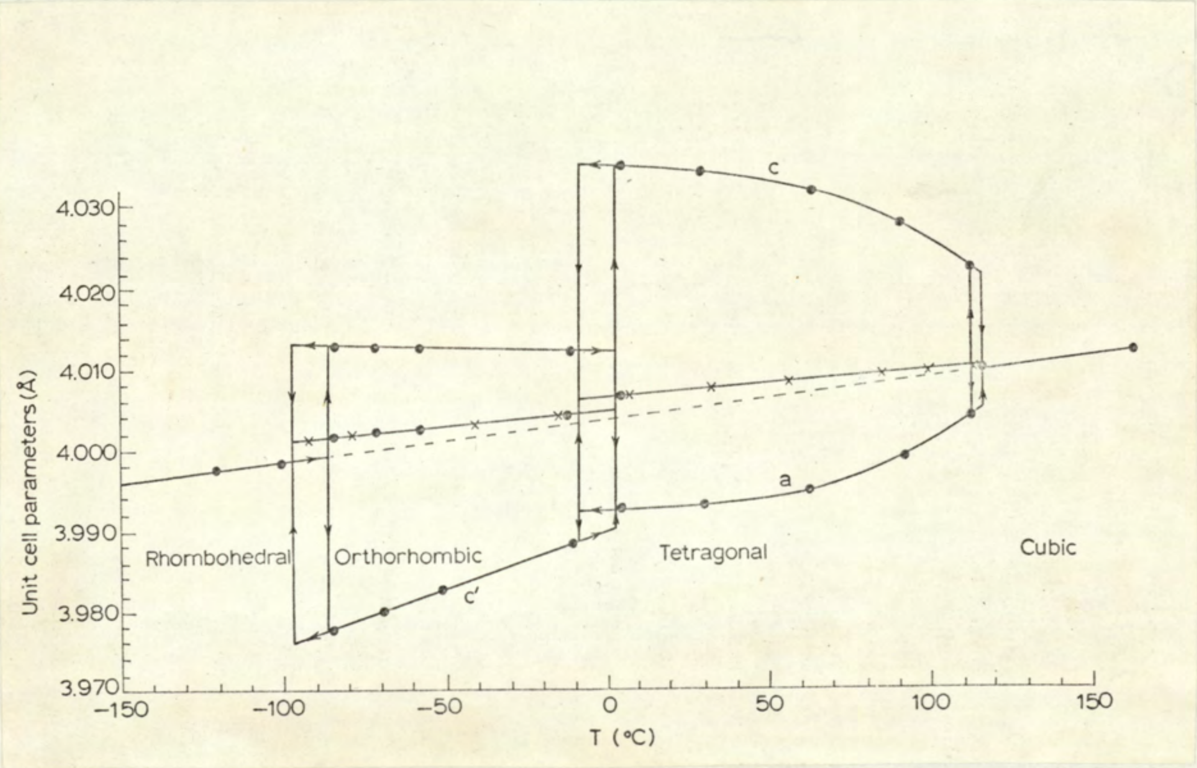

Figure 2.1. Dimensions of the unit cell of $BaTiO_3$ against temperature Kay and Vousden (1949) (2)

$BaTiO_3$ is found to have phase transition points at -70°; 0 and 120°C. The transitions occuring are rhombic to orthorhrombic, orthorhombic to tetragonal and tetragonal to cubic respectively.

Merz (1949) (1950) (3) (4) found that the temperature dependence of the dielectric constant of single crystal $BaTiO_3$ is related to the structural changes found by Kay and Vousden (above).

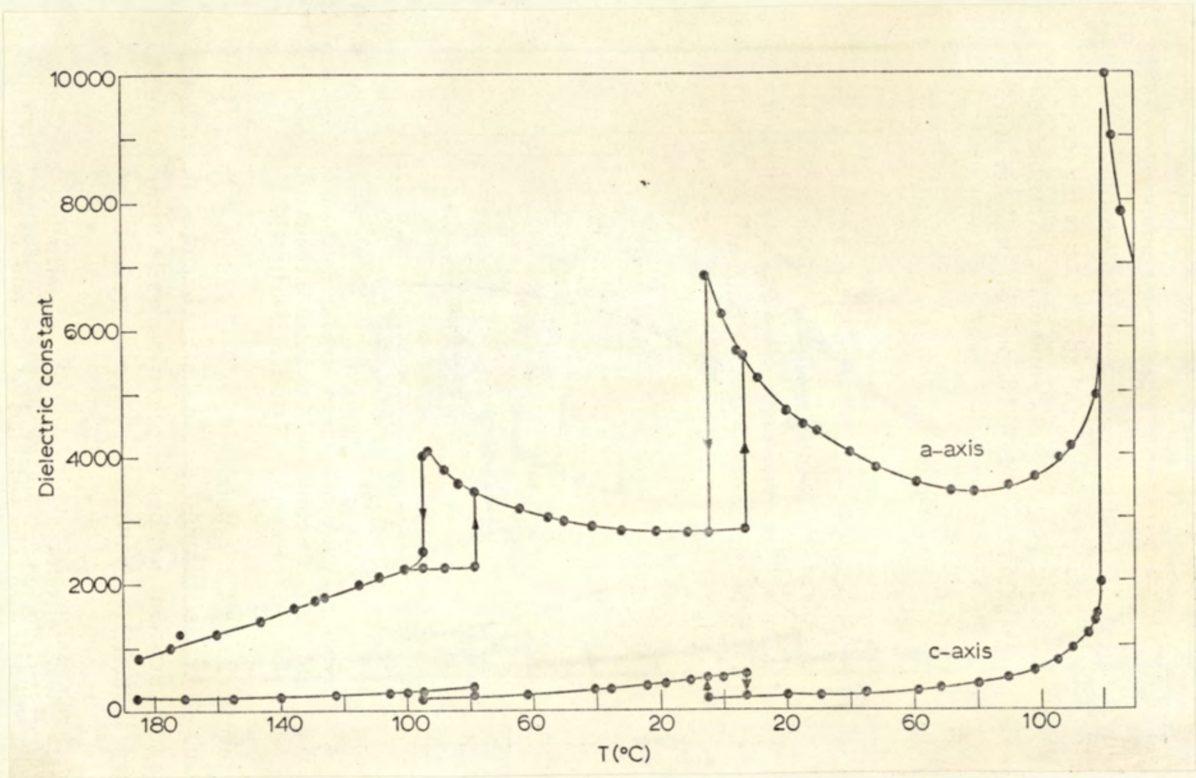

Figure 2.2. Dielectric constant of single crystal $BaTiO_3$ as a function of temperature for both 'a' and 'c' axees. Merz 1949 (3).

The characteristic exhibits three anomolous peaks at the phase transition points. The gradient of the curve just below the 120°C transition point suggests that, for a perfect crystal, there might be a discontinuity at this point, which leads to the conclusion that the transition is of the first order.

Above the Curie point (at which $\varepsilon_r \widehat{=} 10^4$), the dielectric constant falls off rapidly following the Curie-Weiss law

i.e. $$\frac{T-To}{c} = \varepsilon$$

The Curie constant c has a value between 1.5×10^5 and 6.5×10^5 degrees, depending upon the texture of the crystal under test (5).

2.1.1.1. Effect of Applied Pressure

The transition points of the material may be shifted by the application of three and two dimensional pressure.

Merz (1950) (4), investigating the effects of three-dimensional pressure on the transition points, reports that the Curie point is depressed linearly by pressures of up to 10,500 atm., the transition point falling at a rate of -5.8×10^{-3}°C/atm. For the tetragonal-orthorhombic transition, the point lowers by 3×10^{-9}°C/atm. up to a pressure of 500 atm when it reverses.

The application of two dimensional pressure produces an opposite effect. Forsbergh (1954)(6) compressed a single crystal along its tetragonal axis and found an increase in the Curie temperature, the pressure-transition point characteristic having the parabolic relationship $\delta T = 3.1 \times 10^{-17} . p^2$ up to pressures of 10^4 atm. The reason for this fact is clear; the pressure must force the sample in the tetragonal state at temperatures at which the material should be cubic.

2.1.1.2. Effect of Applied Field

Electric fields have the effect of elevating the Curie point of $BaTiO_3$ single crystals. Samples at a temperature slightly above their Curie point are found to be forced back into the ferroelectric state by the application of high electric fields. Kanzig and Maikoff (1951) (7) reporting the shift to be in the order of

$$1.2 \times 10^{-2}\text{°C. per KV/m.}$$

Merz (1953) (8) later obtained similar measurements when studying the double hysteresis loops which occur during the forced transition period.

Twinning

When a single crystal undergoes transition from the cubic to the tetragonal state, the crystal will transform into a single tetragonal state only if it is perfect, crystals subject to any stress either from neighbouring crystals or from internal imperfections will twin in such a way as to reduce the stress to a minimum (12).

Two types of twin are known, those in which the tetrad axes are at approximately 90° and those at which the axes are 180° to each other. The boundary walls of both types of twin can be moved by the application of electric fields and this is known as switching.

2.1.2. Dynamic Properties

The switching time (ts) for polarization reversal in single-crystal barium titanate has been found to follow an exponential relationship over the mid-field range (9,10)

i.e. $ts = to \exp \left[\frac{\alpha}{E}\right]$ where α and to are constants. 2.1.

Measurements by Stadler (1958) (11) indicate that the switching time follows a power law for high fields

i.e. $ts = KE^{-n}$ where K and n are constants. 2.2.

Field optical measurements indicate that polarization reversal can occur at any value of field, no matter how small (8), thus confirming the implication from equation (2.1) that no definite coercive field exists for barium titanate.

Optical investigations into the mechanism of polarization reversal in single crystal $BaTiO_3$ by Merz (1954) and Millar (1958)(9) (13) established that domain formation and growth takes place in four distinct stages:-

(i) new domains are nucleated at the crystal surface
(ii) the domains grow forward through the thickness of the crystal
(iii) they expand sideways
(iv) they coalesce until the whole crystal is switched

2.2. Polycrystalline Material

2.2.1. Early Work

The early investigations of $BaTiO_3$ were carried out using specimens of the polycrystalline ceramic material, single crystals of satisfactory quality for experimental purposes being difficult to manufacture at that time.

Experimental results obtained from differing sources, however, reveal large discrepancies in the measured values for the phase transition points. For example, under similar conditions, Megaw (1946) (14) gives the Curie point for $BaTiO_3$ as 120°C, Rushman and Strivens (1946) (15) as 127°C, and Vul (1946) suggests the transition to take place over the range 122° to 129°C. It was concluded, therefore, that accurate qualitative and quantitative measurements are only possible using good single crystals. It was only later, when ceramic materials began to be used for industrial applications, that there was any attempt made to correlate electric properties with the crystalline structure of the ceramic material.

2.2.2. Dielectric Studies

One of the first papers on this subject was the results of an investigation by Egerton and Koonce (1955) (17) into the effects of the firing cycle on electrical properties of ceramic $BaTiO_3$. The structural changes occuring in pure and commercial grade samples during firing were observed using an electron microscope. Samples were fired in both conventional and induction-heated furnaces. It was found that, as the firing time and temperature increased, the crystal in the samples generally grew larger and the grain-boundary condition improved up to an optimum point, beyond which a slow deterioration occured. The dielectric properties accompanied these changes, rising to an optimum point and then declining slowly.

Unfortunately, the work took no account of the physical properties, or the chemical purity of the starting material and did not describe the processes used to form the test pieces. The conclusion, that the final properties of ceramic barium titanate may be controlled to some extent by the firing cycle to which it is subjected, can therefore only be treated as a generalisation.

Eubank et al (1952) (18), in a more extensive survey, obtained a number of more conclusive results from their investigations. Samples of $BaTiO_3$ powders were produced by a variety of methods, and these were subsequently fired over a range of closely controlled conditions.

A dependence of the Curie point on structure was noted, the transition point being found to vary with the calcination temperature of consituent materials (barium carbonate ($BaCO_3$) and titanium dioxide (TiO_2)). A dependence of the maximum dielectric constant on the stoichiometric proportions of these constituents was also noticed, the dielectric constant moving upwards with an increasing excess of barium oxide and decreasing with an increasing excess of titanium dioxide.

In this work, starch and glycerine were used as binders and the samples were fired on zirconia plates or between platinum sheets. No investigations were made into the effects of these techniques on the final fired samples, although a slight reaction in between the samples and the platinum sheets was noticed.

2.2.3. Structural Studies

2.2.3.1. Course Grained Material

Early structural studies of $BaTiO_3$ ceramics involved work on materials formed by calcination of $BaCO_3$ and TiO_2, the ceramic formed usually possessing a rather coarse grain structure.

During the course of an extensive programme on the reproducibility of $BaTiO_3$ ceramics of varying compositions, Kulscar(1956) (19) found that the microstructure of the materials considered could be studied successfully, using the conventional metallurgical techniques of polishing and etching.

Samples for examination were prepared as for metallurgical examination, using diamond-abrasive kerosene lubricant for the final polishing step.

The samples were etched in an aqueous solution of 5% HCL with a little HF. The etchant successfully revealed the crystal structure of Ba TiO_3 ceramics (including domain structures in some cases), but the author does not discuss the possible mechanisms of its action. Cook (1956) (20), working on the same project, analysed the domain patterns obtained and concluded that the etchant used by Kulcsar revealed 90° domains, sets of which are bounded by (110) planes.

DeVries and Burke (1957) (21) enlarged upon previous work and examined specimens, having known compositions in both the normal state and under electrical stress (d.c.). During this work, antiparallel (180°), domains were identified and measurements indicated that the 90° and 180° domains found in the ceramic form were smaller than those which exist in single crystals of $BaTiO_3$.

The samples used were found to contain complex banded structures, which were considered to be due to stress configurations caused by mutual impingement of the randomly orientated grains forming the crystal matrix.

The structural changes due to fields occurring during the phase transition at the Curie point and the normal re-arrangement of domains under electrical stress were observed by this technique. In the latter case, slight growth of 90° domains occurred on application of the field but the 180° domains were eliminated.

Examination of specimens by optical methods is not entirely satisfactory, however the surface detail being somewhat obscure even at the highest magnification. Accordingly, Tennery and Anderson (1958) (22) investigated the possibility of using an electron microscope to study domain structures and produced satisfactory results using carbon-backed platinum - 13% rhodium pershadowed replicas. The domain structure of the materials investigated were revealed; 90° and 180° domains and their boundaries being clearly shown.

The dependance of the Curie point upon the calcination temperature of $BaCO_3$ and TiO_2 during the preparation of $BaTiO_3$ and the relationship which exists between the stoichiometric proportion of the constituents and the dielectric properties of the fired material, indicate that the reaction of the constituents is, in many ways, responsible for the variations which exist between the properties exhibited by the ceramic and the single crystal forms.

Templeton and Pask (1959) (23) investigated the reactions which occur during calcination and found that a diffusion controlled reaction occurs, the compounds appearing in varying quantities depending upon their relative rates of diffusion. It was observed that, during firing, excesses of $BaCO_3$ inhibited crystal growth, whilst excesses of TiO_2 enhanced it.

The situation which arises when the stoichiometric proportion of the constituent material varies may be more easily appreciated by referring to the phase diagram for the system BaO - TiO_2 produced by Rase and Roy (1955) (24).

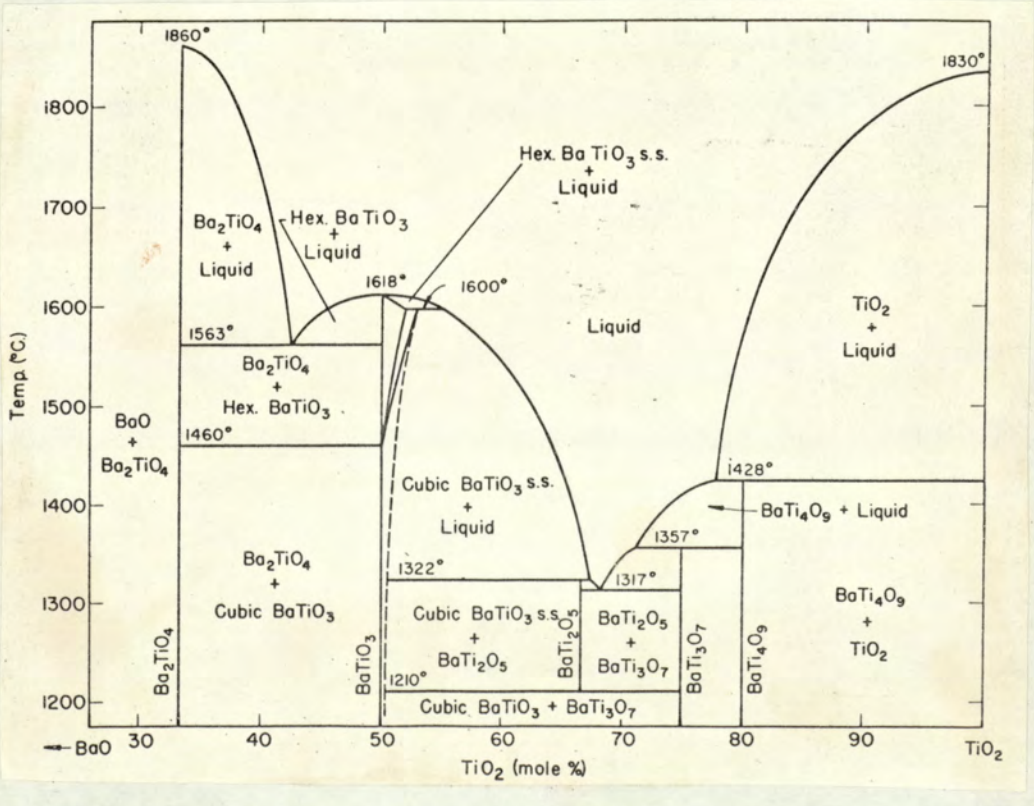

Fig. 3.2 Phase equilibrium diagram for the system BaO - TiO_2. Rase and Roy (1955)(23).

From the diagram it is apparent that any small variation from 50 mole % of either constituent compound will generally result in a mixture or solution of two materials during the firing process. Whether or not these compounds will exist after firing, may well depend upon the heating-cooling cycle of the furnace used or on the stability of the material. what is certain is that the crystal matrix formed on cooling to room temperature will not be of the form BaO - TiO$_2$, but will be more complex.

The optimum conditions for firing BaTiO$_3$ test samples may also be deduced from the phase diagram, maximum densities being achieved by firing mixtures having slight excess TiO$_2$ between 1,322° and 1,460°C.

2.2.3.2. Fine Grained Material

During work using very pure specimens of BaTiO$_3$, various investigators (17) (25) reported anomalously high values of permittivity, (4000 - 6000), when the materials used were sintered to bodies having an average grain size of approximately 1 micron.

Usually, the methods of obtaining BaTiO$_3$ powders of very small grain size, calcination and wet ball milling can considerably affect the purity and hence the electrical properties of the final ceramic. Other methods of producing such powders are therefore essentially for full investigation of the anomalous behaviour of fine-grained high-permittivity ceramics.

A method of production of fine-powders was reported by Gallagher et al (1963) (26). Pure BaTiO$_3$ powders or pure powders of partially-substituted BaTiO$_3$ (Sr and Zr) were prepared of near-perfect stoichiometry by the controlled calcination of the corresponding mixed oxalates, which were produced by precipitation from solution.

The selection of calcination conditions was found to have a marked effect upon the microstructure and conductance of the final fired samples of both pure and substituted ceramics. The time, temperature and atmospheric conditions of calcination determined the particle size and reactivity of the powders produced.

Kiss et al.(1966) (28) synthesized titanate powders of fine particle size by the isothermal pyrolysis of barium titanium oxalate and the controlled hydrolysis of titanium esters by barium compounds.

The $BaTiO_3$ powders were produced in samples having narrow particle size distributions over the range 500 - 3,000°A and 80 - 1,000°A, respectively.

The work was extended by Harkulich et al.(1966) (29), who attempted control of grain size in $BaTiO_3$ fine powders by the addition of Ta_2O_5 and by the close control of firing conditions, using a fast cycle kiln. Results obtained using Ta_2O_5 indicated successful inhibition of grain growth, but control using the fast-cycle furnace was not so acceptable (as secondary crystallisation was found to occur in the compacts during firing).

Barium titanium citrate is decomposed by heat to form fine grained barium titanate (30). The authors, Payne and Anderson, used powders formed by this method to study grain growth inhibition by Ta_2O_5.

The results which were obtained differed somewhat from those obtained by Harkulich et al, but it can be considered that the discrepancy is due to a difference in firing conditions (Harkulich et al. did not report the conditions under which their samples were fired).

The work of the two authors above is considered by both to be grain-growth inhibition studies but, from their experimental observations of changes in the intrinsic properties of the ceramics produced, it must be considered that the reaction is one of solid solution as distinct from one of inhibition. The work of Baxter et al (1959) (31) into the effects of additives on the ferroelectric nature of $BaTiO_3$ supports this theory.

2.2.4. Correlations of Structural and Dielectric Properties in Polycrystalline $BaTiO_3$

Several investigators show correlations between structure and dielectric properties in polycrystalline $BaTiO_3$. Egerton and Koonce (1955) (17), using commercial-grade powder, found that ceramic samples when fired over a range of temperatures show dielectric properties which follow the structural changes in the material. With increasing time or temperature crystals in the samples examined became larger, with improved grain boundary conditions which resulted in better structure. An optimum point was eventually reached, beyond which the crystal structure began to deteriorate. The dielectric properties followed the changes, reaching an optimum value and then declining slightly. With chemically-pure starting materials (using a fast cycle kiln) specimens of small particle size were produced. High dielectric constants were observed with the samples produced by this method. The maximum fired density occurred at 1,275°C. Samples fired to higher temperatures had less than maximum density, with generally increased particle size and decreased dielectric constant. Increased piezoelectric constants were observed with these changes.

Henry and Illyn (1965) (32) attempted to eliminate many of the variables present in an investigation of the type attempted by Egerton and Koonce (17). Using an ultrapure $BaTiO_3$ powder prepared from barium titanium oxalate, ceramic discs were made for test purposes. The discs were fired on zirconia plates dusted with ultrapure $BaTiO_3$ or on waster tiles. A variety of structures were produced, ranging from those having an average particle size of 5µ up to those having a particle size of 20 µ.

It was concluded that control of grain size in ultrapure material is possible by heat treatment alone.

Dielectric measurements made on each disc indicated high values of dielectric constant for the fine-grained samples (approximately 3,000). However, as the grain size increased the dielectric constant fell to its more normal value, (approximately 1,600 for the coarser materials). Samples with intermediate grain size showed intermediate values of dielectric constant. In general, it was noticed that the piezoelectric constant varied inversely with dielectric constant, being small with the fine grained samples and large with large grained samples.

The work does not profess to eliminate every variable which can be present in this type of work, but it does go some way in eliminating many of the major sources of error made by other workers.

2.3. Doped Polycrystalline Materials

Barium titanate will form solid solution with a large number of compounds. The majority of systems studied involve the replacement of Ba^{2+} ions by other divalent ions (such as Ca^{2+} and Pb^{2+}) and Ti^{4+} ions by other tetravalent ions (like Zr^{4+} and Sn^{4+}) but several systems having lattice defects have been also studied. Partial or complete solid solution of the substitutional type generally have the typical perovskite structure form ABO_3.

The literature presently available on this subject is large and it is proposed to deal only with major topics of interest in this survey.

The first recorded investigation of a substituted $BaTiO_3$ system, by Rushman and Strivens (1946) (15), established a relationship between electrical and structural properties in the system $SrTiO_3$ - $BaTiO_3$ - $PbTiO_3$ (see Fig. 2.4.).

Structural data for the work was determined by Megaw (1946) (33).

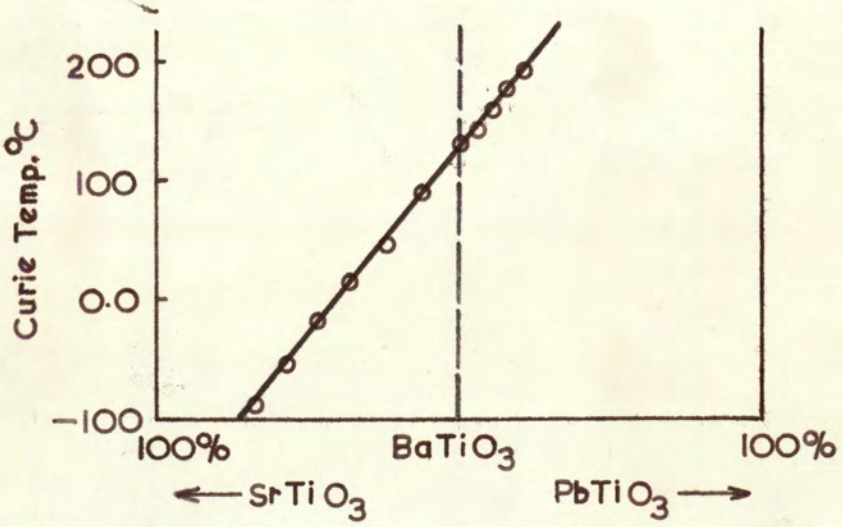

Figure 2.4. Variation of Curie Point in the system $SrTiO_3$ - $BaTiO_3$ - $PbTiO_3$ Rushman and Strivens (1946).

Addition of $SrTiO_3$ was found to depress the Curie point linearly, whilst the addition of lead titanate elevated it.

The main features of the dielectric polarization phenomena occuring in both cases were explained in terms of the variation in spacing of the constituent atoms within the crystal lattice of the materials.

Verbitskaya et al (1958) (34) measured the lattice constants in the system $BaTiO_3$ - $BaZrO_3$ and produced a phase diagram for the system.

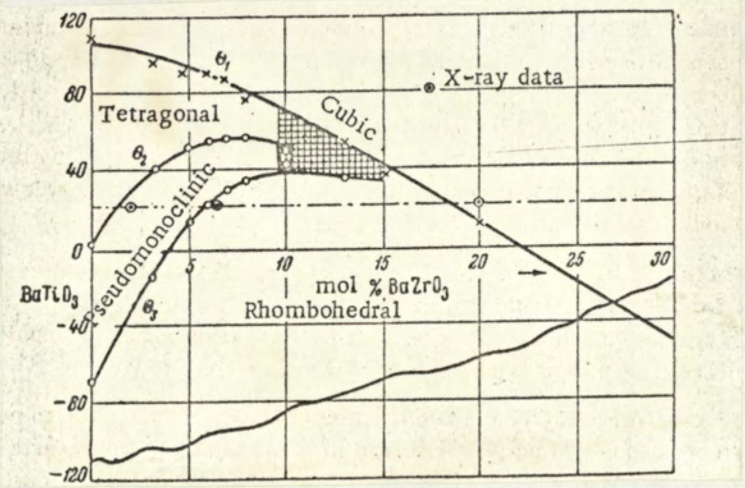

Figure 2.5. Phase diagram for the system $BaTiO_3$ - $BaZrO_3$ Verbitskaya et al (1958) (34).

The changes in symmetry and lattice constants of the solid solutions up to 30% $BaZrO_3$ were found to be dependant upon the composition.

From dielectric measurements, the Curie point of the material is found to fall with increasing concentrations of $BaZrO_3$. The two lower transition points rose, however, and the three points merged at a concentration of 30% $BaZrO_3$. This single peak existed until a concentration of 50% $BaZrO_3$ was reached, when the peak disappeared and the material became nonferroelectric.

The phase diagram found was seen to resemble (i) the corresponding diagram for the system $BaTiO_3$ - $BaSnO_3$ established earlier (35) and (ii) the system $BaTiO_3$ - $BaHfO_3$ established later (36).

Whilst the above type of solid solution has been extensively investigated, only brief attention has been given to those systems having lattice defects. Several authors have, however, published work on this subject. Subbarao and Shirane (1959)(37) made a dielectric and structural study of the systems $Ba(TiNb)O_3$ and $Ba(TiTa)O_3$; Van Loan and Chakrabarty investigated the systems $BaTiO_3$ - UO_2 and $BaTiO_3$ - $BaUO_3$ (38) and Harkulich et al (29) inhibited grain growth in $BaTiO_3$ by using varying amounts of Ta_2O_5.

On the basis of the results from these papers,it is generally seen that substitutions of this type have profound influence upon the properties of the solid solutions. Subbarao and Shirane (37) found that the Curie point of their materials was lowered by only small amounts of doping agent, the doping substance being incorporated in the $BaTiO_3$ lattice.

Van Loan and Chakrabarty (38), during their investigation,found a dependance of the system upon the firing atmosphere. In general, the amount of solid solution formed was small,but considerable change in dielectric properties occurred as a result.

The work of Harkulich et al (29), primarily an attempt at grain growth control in $BaTiO_3$,must be considered in part to be extension of the work of Subbarao and Shirane (37) discussed above.

Whilst the addition of Ta_2O_5 did undoubtedly control the final fired grain size of fine grained $BaTiO_3$ specimens,the assumption made that any change in grain size can be correlated directly with corresponding changes in dielectric properties must be erroneous,as the doping agent Ta_2O_5 was found by Subbarao and Shirane to enter the crystal lattice of $BaTiO_3$. The assumption that Ta_2O_5 remains at the crystal boundaries and operates over a distance to affect the dielectric properties is therefore also invalid.

2.4. AGING IN BARIUM TITANATE

2.4.1. Aging Phenomena in Single Crystal $BaTiO_3$

Several ferroelectric materials,and in particular $BaTiO_3$,show an effect known as decay upon repeated reversals of spontaneous polarization. The change is shown in $BaTiO_3$ as a decrease in the spontaneous polarization of the crystal,accompanied by a rise in the coercive field.

In $BaTiO_3$,decay does not occur if the sample is switched with a sinewave or squarewave,but does occur if the sample is switched with pulses of wide spacing. The pulse amplitude and pulse pattern are important in determining the rate of decay.

Two types of decay are apparent. The first occurs when the crystal is subjected to electrical pulses and is characterised by rapid decrease in polarization. The crystal will recover from this type of decay if subjected to a low frequency sinewave or a d.c. potential of appropriate polarity. The second, an irreversible change, is observed during switching at high frequencies as a distortion of the dielectric hysteresis loop and an increase in coercive field, with no significant change in polarization.

No decay is observed if liquid electrodes (usually a solution of LiF) are used in place of the more usual evaporated metal electrodes (39).

2.4.2. Aging Phenomena in Polycrystalline $BaTiO_3$

Gradual diminution of the permittivity of ceramic $BaTiO_3$ occurs on cooling the material through its Curie point. The effect proceeds rapidly at first and then continues at a gradually diminishing rate for a considerable period of time.

Marks (1948) (40) suggested a linear decrease in permittivity with log t, where t is the time over several decades. Plessner (1956)(41) confirmed this theory, finding both permittivity and power factor decreasing with log t over a period of years.

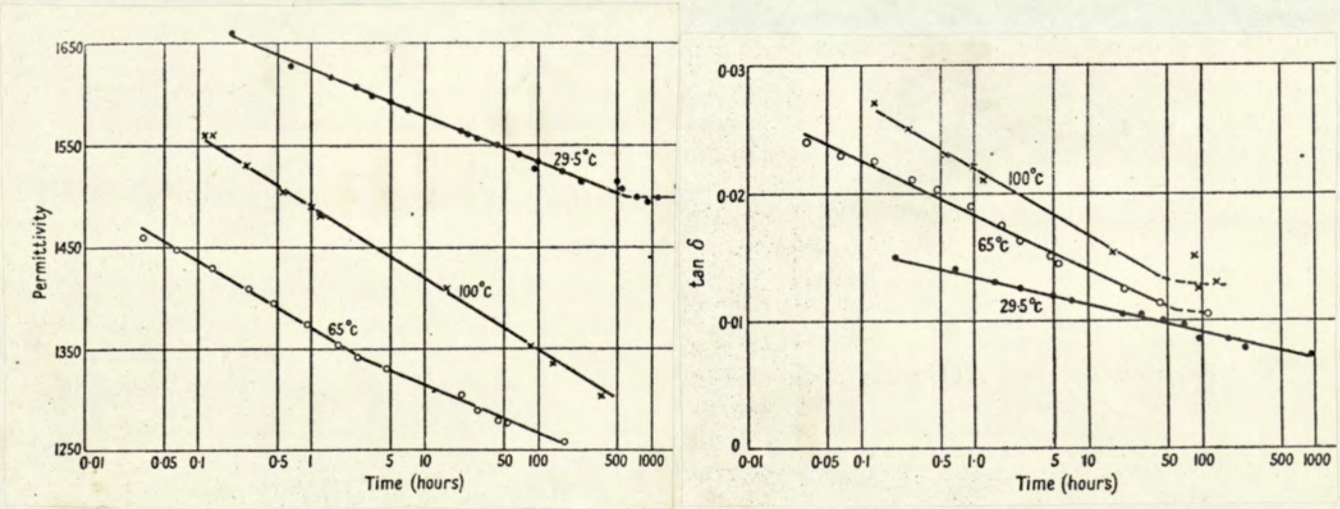

Figure 2.6. Aging of permittivity and tan δ of one sample of $BaTiO_3$ at three different temperatures Plessner (1956)(41).

CHAPTER 3

3. THEORETICAL CONSIDERATIONS RELATING TO FERROELECTRIC MATERIALS

3.1. CRYSTAL CLASS

A crystal has a structure which continues to infinity in all directions, the unit of repeat imagined to be precisely the same throughout (the unit cell). Three primitive non coplaner translations a, b and c from an arbitary lattice point to neighbouring lattice points define the unit cell.

It is found that certain unit cells have common shapes and certain common symmetries which allow recognition of seven crystal systems. The crystal systems are divided amongst thirty two classes, known as point groups, eleven of which are centrosymmetrical classes and twenty-one non-centrosymmetrical classes.

Symmetry considerations can show that some of the thirty two crystal classes cannot possess certain physical properties, (e.g. no centrosymmetrical crystal can possess a finite polarization), but they never show that a particular crystal must exhibit a certain property; the effect could, in principle, be infinitely small in the particular system considered.

Figure 3.1. The 32 Point Groups

		Centrosymmetric		Non-Centrosymmetric				
				Polar		Not Polar		
	Triclinic	1		1				
Biaxial	Monoclinic	2/m		2	m			
	Orthorhombic	mmm		mm2			222	
	Tetragonal	4/m	4/mmm	4	4mm	4	42m	422
Uniaxial	Trigonal	3	3m	3	3m		32	
	Hexagonal	6/m	6/mmm	6	6mm	6	6m2	622
Optically isotropic	Cubic	m3	m3m			432	43m	23

3.2. FERROELECTRICITY

The phenomenon of ferroelectricity was discovered by Valasek (1921) (42) during an investigation of Rochelle salt (sodium potassium tartrate tetrahydrate). Megaw (14) defines ferroelectrics fundamentally as those cystals possessing reversible polarization, as shown by a dielectric hysteresis loop.

Figure 3.2. Ferroelectric Hysteresis Loop (Schematic).

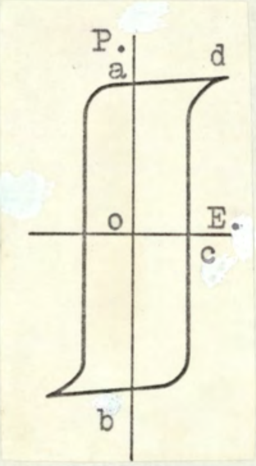

Ferroelectric cystals are characterised by several particular physical properties in addition to dielectric hysteresis.

1. They show disappearance of hysteresis at a certain temperature, the Curie point.
2. They have a domain structure, which may be visible in polarized light.
3. They have a high dielectric constant, rising to a peak at the Curie point.
4. The falling-off of their dielectric constant above the Curie point follows a Cuie-Weiss law.
5. They possess a pseudosymmetric structure.
6. Their symmetry places them in a polar class.
7. They have a transition at the Curie point to a form of higher symmetry.
8. The Curie point is raised (or a lower Curie point lowered) by the application of a biassing field.
9. There is a sudden appearance of surface charges at the transition.

3.3. DYNAMIC PROPERTIES OF FERROELECTRIC MATERIALS

From the previous definition, the fundamental physical property of all ferroelectrics is the property of polarization reversal. The reversal process, commonly called switching, can be studied by electrical or optical methods. The former technique is to observe the displacement current flowing in the crystal by measurement of the real current flowing in an external circuit connecting the two electrodes, whilst the latter is to directly observe moving domains in those crystals where such observations are possible.

3.3.1. Electrical Methods

3.3.1.1. Switching Circuit

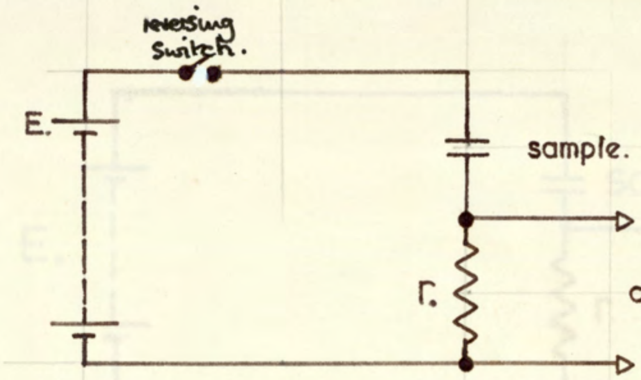

Figure 3.3. Schematic circuit for the electrical study of polarization reversal in ferroelectrics.

Square pulses of alternate polarity are applied to the crystals. As the spontaneous polarization reverses, a displacement current flows in the crystal. The real current flowing in the resistor can be displayed on an oscilloscope.

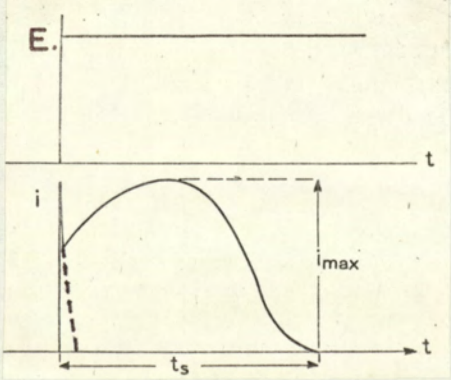

Figure 3.4. Applied field and switching current v. time for a typical ferroelectric material (barium titanate). The pecked curve is that curve which is obtained when the applied field is parallel to the

polarization and no switching occurs.

Switching time t_s, is defined as that time necessary for the switching current i to drop to a certain fraction, usually 90% of its maximum value, i(max.).

$$i = \frac{dP}{dt}.$$

Integrating from t = o to t = ∞.

$$2P_s = \int i dt = i_{(max)}.t.f.$$

$$\text{where} \qquad f = \frac{i}{i(max)} . d(t/t_s). \qquad 3.1$$

is a shape factor obtained from an exponentially-decaying switch pulse. If this factor f remains constant, measurement of the maximum current, $i_{(max)}$ is equivalent to measurement of the switching time t_s.

3.3.1.2. Dielectric Hysteresis

The dielectric-hysteresis phenomenon may be observed experimentally by use of a Sawyer-Tower bridge (Sawyer and Tower(1930).(43)).

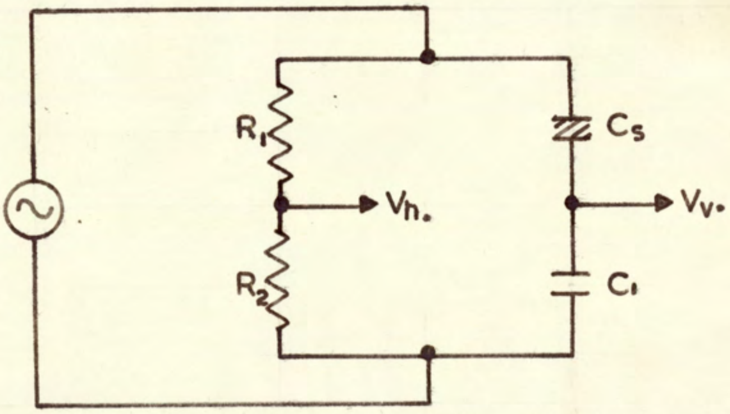

Figure 3.5. Circuit for the Investigation of Dielectric Hysteresis Loops.

From this circuit, the electric displacement D produced by an applied electric field E is shown on an oscilloscope.

The relationship

$$D = \varepsilon_0 E + P \qquad 3.2$$

holds for any point on the loop where ε_0 is the permittivity of free space.

Differentiating:-

$$\varepsilon = \varepsilon_0 + \eta \qquad 3.3$$

Where ε is the permittivity $\left(\frac{dD}{dE}\right)$ and η is the susceptibility $\left(\frac{dP}{dE}\right)$

3.3.1.2.1. Spontaneous Polarization P_s.

The existence of a hysteresis loop implies that the substance possessess a spontaneous polarization, that is, a polarization which exists when the applied field is zero.

N.B. P_s = Number of dipoles per unit volume x moment of one dipole

In Figure 3.2 the spontaneous polarization is given by the length oa.

Spontaneous polarization must vary with temperature in ferroelectric material, eventually becoming zero at the Curie temperature.

3.3.1.2.2. Coercive Force Ec.

The coercive force Ec is given in Figure 3.2. by the length oc. In ferroelectric material it is an ill-defined quantity, being dependant upon temperature frequency and waveform. In addition, it has been shown by Merz (1954)(9) that in most ferroelectric materials switching of the dipoles will occur in time, by any field, no matter how small.

3.3.2. Optical Techniques for the Study of Ferroelectric Domains

3.3.2.1. Observation with Polarized Light

Ferroelectric domains are homogeneous regions within ferroelectric crystals each containing large numbers of dipoles all aligned in the same direction. In each domain the polarization is orientated in a different direction, the area between adjacent domains being known as a domain wall. Since the polarization points in different directions on opposite sides of the domain wall, the bifringence is usually different in adjacent domains and can therefore be made visible by observing the crystal with a polarizing microscope.

3.3.2.2. Etching

A number of ferroelectric materials may be etched chemically, the etch rate for different orientations of polarization being markedly different. For example, Hooton and Merz (1955)(44) found that the surface next to the positive end of domains in barium titanate etches more rapidly than the surface next to the negative end. The etch rate in the 'A' direction is intermediate between the two.

This technique is usually used for the study of the static behaviour of domains, but use of combined liquid electrode material and etchant enables partial study of their dynamic characteristics to be made also.

In this technique, a train of pulses of one polarity is applied to the crystal. Each pulse partially switches the domains and, if the partially switched states are stable, the separate parts of the switching transient fit together to form a patchwork version of the total switching transient shown in Figure 3.4.

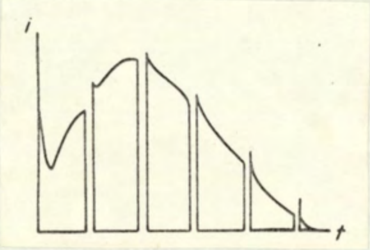

Figure 3.6. Patchwork Switching Currents

If pauses of sufficient length to cause noticable etching of the crystal are allowed between each pulse, a series of contours form in the crystal surface showing the boundaries of differently etched regions and the position of sucessive positions of the domain walls during the off periods.

The technique has the limitation that possible rearrangement or backswitching of the domains cannot be observed, and it may not be justifiable to assume that the motion of domain walls studied by this method is the same as that which is obtained by applying a single very long pulse.

3.3.3. Nucleation and Growth of Ferroelectric Domains

Polarization reversal in ferroelectric materials is governed by the mechanisms of domain nucleation and growth. The following steps are apparent in the process

(i) nucleation of new domains
(ii) forward growth of domains through the thickness of the crystal
(iii) sideways expansion of domains
(iv) co-alescence of domains

The nucleation of domains appears to be dependant upon the magnitude of the applied field, but crystal surface texture and electrode material play some part in the mechanism. The exact mechanisms of domain growth may be particular to each material. The mechanisms existing in barium titanate are discussed in Chapter 4.

3.4. STATIC PROPERTIES OF FERROELECTRIC MATERIALS

3.4.1. Anomalous Characteristics

Most ferroelectric materials exhibit a phase transition temperature or Curie point, at which the material changes from a ferroelectric to a non-ferroelectric state. At these particular temperatures the materials possess very high 'anomalous' values of permittivity, the maximum point rising to a sharp peak.

Above the transition temperature the temperature dependance of the permittivity characteristic usually follows the Curie-Weiss law:-

$$\varepsilon_r = \left(\frac{C}{T-To}\right). \quad \text{where } T > Tc.$$

Tc Transition temperature, e.g. barium titanate:-

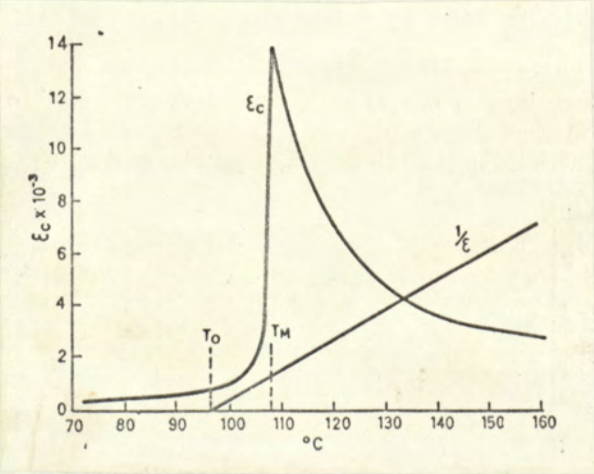

Fig.3.7
Anomalous behaviour of barium titanate about its Curie Point, (120°c) Merz (1953)(8).

3.4.2. Structural Properties and Spontaneous Strain in Ferroelectrics

Since the outset of spontaneous polarization at the Curie point is caused by either the formation of dipoles or the ordering process of existing dipoles, it is easily shown that the crystallographic structure must change at the Curie point, the temperature dependance of the structural changes being closely related to the temperature dependance of the polarization.

3.4.2.1. Pressure Dependance of the Dielectric Properties

Generally, the effect of pressure on ferroelectric materials must be to produce a change in the Curie temperature and dielectric constant of the material. The close relationship between dipole moment and crystal lattice deformation as a direct consequence of large piezoelectric coupling, common in ferroelectrics, shows that ferroelectricity can be suppressed if spontaneous deformation at the Curie point is prevented by mechanical forces.

3.4.2.2. Dielectric Properties as a Function of Applied Field

Application of high electric fields to many ferroelectrics appears to influence the temperature at which structural transitions take place in the material. In general, it may be stated that the field needed to inhibit transition from one state to another is strongly temperature dependant and highly critical. However, at temperatures reasonably above the Curie point (10°C.) induced transitions may be impossible to produce even with very high fields.

A consequence of this shift in transition temperature is that the dielectric hysteresis loop observed when the material is in the forced state is distorted, becoming a double loop.

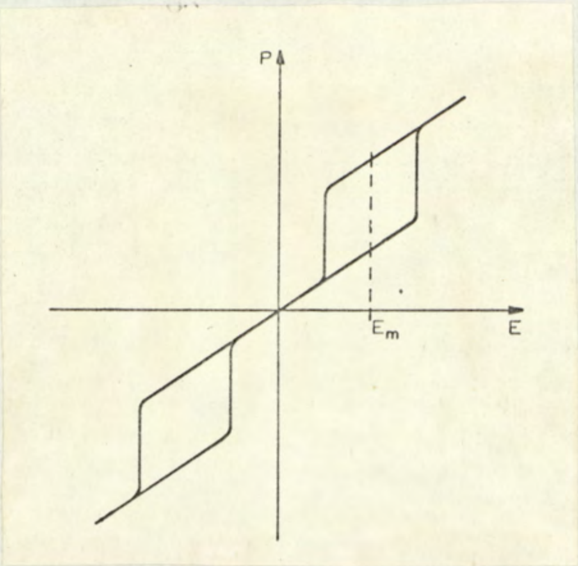

Figure 3.8. Typical double hysteresis loop observed in $BaTiO_3$ a few degrees above the Curie Point

The shape and temperature dependance of the double loop may be studied using Thermodynamic theory. The temperature range within which forced transition may take place may then be predicted for particular materials.

3.5. CRYSTAL STRUCTURE

The theoretical considerations discussed up to this point deal with the properties exhibited by a single crystal of ferroelectric materials. The situation existing in the polycrystalline material, where it exists, is more complex, the single crystal properties being modified by the structure of the cystal matrix.

3.5.1. Sintering of Solid Materials

Grain sizes in ceramic materials is a function of firing temperature and time. The observed densification rates during sintering of powder compacts are nonlinear (45) quantitative studies by Kingery and Berg (1955) (46) suggested that the initial stages of sintering occur by a bulk diffusion mechanism, although the exact mechanism of this process is complex and not fully investigated.

3.5.1.1. Grain Growth in Porous Compacts

The rate of grain growth in crystals is often analysed by assuming that (i) the grain boundaries move towards their centre of curvature at a rate proportional to the grain diameter, and (ii) the grain boundary curvature is inversely proportional to the grain diameter Kingery and Francois (1965)(47) found that in UO_2 and Al_2O_3 systems, in contrast to migration of solid inclusions, pore migration takes place solely along grain boundaries and suggested that pores (during migration due to evaporation condensation, surface diffusion of volume diffusion) restrain grain boundaries and thereby control the pore grain geometry of the system. Nichols (48), however, disagrees with their findings and develops the arrangement to include the effect of vapour transport.

3.5.1.2. Effect of Inclusions upon Grain Growth during Sintering

With many exides (Al_2O_3; HfO_2; MgO and ZrO_2), grain growth may be inhibited by the addition of small metal inclusions and there is evidence that some compounds may have the same effect, diffusion or evaporation of the impurity influencing the grain growth of the matrix oxide (49), and it may be surmised that similar effects may hold true for other oxides.

3.5.2. Internal Strain

In ceramic materials formed by sintering, each grain is surrounded by randomly orientated neighbouring grains, all closely adhering at their boundaries. Every grain is therefore effectively damped by adjacent grains and, on cooling, a complex system is set up within the material.

Phase transitions occuring during cooling produce an even greater complexity of stresses within the material, the internal stresses produced in each grain depending on the constraining forces acting on that grain.

The presence of stresses within the material will therefore considerably affect the electrical properties of ferroelectric materials, the free energy function relating strain and polarization in these materials being given by Devonshire (1949) (50).

3.6. THERMODYNAMIC THEORY.

Many of the properties of ferroelectric materials, such as polarization and dielectric constant as well as their temperature field and pressure dependence can be interpreted by a thermodynamic model. Those properties which are dynamic in nature, e.g. switching, cannot however be represented in this way, the model being valid for equilibrium properties.

Devonshire (1949)(50) shows the differential dU of the internal energy of a body subject to external stresses and electric fields to be

$$dU = TdS - \sum_{i=1}^{3} X_i dx_i + E.dP \qquad 3.4$$

where s is the entropy and x_i and X_i the strain and stress components respectively. It is normal however to use G_g, the elastic Gibbs function expressed as a function of temperature stress and polarization, as the potential function and A as the Helmholtz free energy.

The function may be expanded for various particular conditions. For example, under conditions of zero stress, G can be expanded in terms of P^2 if the crystal has a centre of symmetry above the Curie point.

$$G = G_o + \tfrac{1}{2}\chi(P_a^2 + P_b^2 + P_c^2) + \tfrac{1}{4}\zeta(P_a^4 + P_b^4 + P_c^4)$$
$$+ \tfrac{1}{2}\lambda(P_a^2 . P_b^2 + P_c^2 . P_a^2 + P_b^2 . P_c^2) + \tfrac{1}{6}\zeta(P_a^6 + P_b^6 + P_c^6)$$
$$+ \tfrac{1}{6}\eta P_a^2 . P_b^2 . P_c^2 + \ldots, \qquad 3.5$$

where G_o is the free energy for zero polarisation.

Then assuming that the spontaneous polarisation lies in the c axis in the ferroelectric phase and that electric fields are only applied in this direction, Pa = Pb = 0. Thus from equation (3.5)

$$G = G_o + \tfrac{1}{2}\alpha P^2 + \tfrac{1}{4}\gamma P^4 + \tfrac{1}{6}\delta P^6 \qquad 3.6$$

where P is the polarization in the direction.

Differentiating with respect to P gives the electric field E acting on the ferroelectric in terms of the polarization P:-

$$\frac{\partial G}{\partial P} = E = \alpha P + \gamma P^3 + \delta P^5 \qquad 3.7$$

and differentiating again with respect to P, neglecting saturation effects and making P = 0, gives the relationship:

$$\chi = \frac{P}{E} = \frac{1}{\alpha} \qquad 3.8$$

Assuming α can be approximated to a linear function around the Curie Point

$$\alpha = \beta.(T - To) \qquad 3.9$$

δ and γ being considered constant.

Thus the dielectric stiffness $K = \frac{1}{\chi} = \beta.(T - To)$ 3.10

If the system is considered to have finite stress the free energy in terms of stresses and polarization is given by:-

$$\begin{aligned}
G_1 - G_{10} = {} & - 1/2 s_{11}.(X_a{}^2 + Y_b{}^2 + Z_c{}^2) - \\
& s_{12}(X_a Y_b + Y_b Z_c + Z_c X_a) - 1/2.s_{44}(X_b{}^2 + Y_c{}^2 + Z_a{}^2) \\
& + (Q_{11}X_a + Q_{12}Y_b + Q_{12}Z_c)P_a{}^2 + (Q_{12}X_a + Q_{11}Y_b + Q_{12}Z_c)P_b{}^2 \\
& + (Q_{12}X_a + Q_{12}Y_b + Q_{11}Z_c)P_c{}^2 + Q_{44}(X_b P_a P_b + Y_c P_b P_c \\
& + Z_a P_c P_c) + A(P_a{}^2 + P_b{}^2 + P_c{}^2) + B(P_a{}^4 + P_b{}^4 + P_c{}^4) \\
& + C(P_a{}^6 + P_b{}^6 + P_c{}^6) + D(P_a{}^2 + P_b{}^2 + P_b{}^2 P_c{}^2 + P_c{}^2 P_a{}^2 \\
& + G(P_a{}^2 P_b{}^4 + P_a{}^4 P_b{}^2 + P_b{}^2 P_c{}^4 + P_b{}^4 P_c{}^2 + P_c{}^2 P_a{}^4 + P_c{}^4 P_a{}^2)
\end{aligned}$$

X_a, Y_b, Z_c = normal stress components
X_b, Y_c, Z_a = sheer stress components
s_{11}, s_{12}, s_{44} = elastic compliances
P_a, P_b, P_c = components of polarization
Q_{11}, Q_{12}, Q_{44} = electrostrictive coefficients
A, B, C, D, G = coefficients of free energy function

The permittivity expressions are given by:-

$$\frac{4}{\epsilon_a} = \frac{4}{\epsilon_{aa}} = \frac{{}^2 G_1}{P_a{}^2}$$

$$\frac{4}{\epsilon_c} = \frac{4}{\epsilon_{cc}} = \frac{{}^2 G_1}{P_c{}^2}$$

Fpr spontaneous polarization

$$E_c = 0 = \frac{\partial G_1}{\partial P_c} \text{ and } P_a = P_b = 0, \; P_c = P_s \qquad 3.11$$

and it is therefore possible to calculate values for permittivities at any given values of stress within the crystal.

CHAPTER 4

4. APPARATUS AND TECHNIQUES

4.1. HIGH TEMPERATURE FURNACE CONTROLLER

A potentiometric transitrol process control unit by Ether Limited was used to control the operating cycle of an Amalgam Type CH.3 electrical furnace, having a maximum operating temperature of 1,550°C. It is a mechanically-programmed unit and its use facilitates the attainment of reproducible firing cycles.

4.1.1. Specification

The control unit will hold the temperature of the furnace constant or will move over any predetermined cycle to an accuracy of 0.5% of the maximum scale reading, cold-junction compensation circuits being employed in the measuring circuit. The absolute error will however be greater than this, as this error does not include the effects of thermocouple ageing.

4.1.2. Mode of Operation

The output voltage of the furnace Pt/Pt 13% Rh. thermocouple is fed into the controller where it is immediately filtered to reduce any a.c. signals to a negligible level. The signal is then fed into a transistor chopper. A measuring slide wire is supplied with a constant current from a temperature compensated stabilized source and is then shunted to give the predetermined required span. The measuring slide wire moving contact is positively connected to the measuring contact and the signal from this contact is fed into the chopper circuit and compared with the input signal. The resultant error is converted into an a.c. signal which is amplified by a four-stage amplifier. The amplified signal triggers a phase-sensitive detector which, in turn, operates an actuator driving the slide-wire contact and measuring pointer to a new position to eliminate the error.

4.1.2.1. Operation of the Controller

The controller is mechanically programmed, using cams graduated in time and temperature. They are cut to suit the required operating cycle and it is only necessary to start the synchronous driving motor to the cams to actuate the programme unit. The temperature of firing may be kept constant at any time in the cycle by switching the driving motor off for the required period. At the end of each cycle, or at a selected time or temperature, the controller will automatically switch off depending upon it's setting.

4.1.3. Emergency Precautions

A number of possibilities arise:-

(i) failure of the thermocouple
(ii) failure of the control unit
(iii) failure of the a.c. supply

The first possibility, failure of the thermocouple or associated compensating leads, is covered by the design of the controller. Should any such fault occur, the measuring arm and contact moves to the full-scale deflection position, thus passing the programmed setting and therefore automatically switching off the electrical feed to the furnace contactor. The furnace will then cool to room temperature or the h.f. supply will cut off.

Any failure of the controller which does not result in shutdown of the furnace, or at least holding of a steady temperature, must cause the furnace to exceed its maximum rated temperature in time and, for this reason, a gold fuse is placed inside the furnace. The fuse is protected by a porcelain sleeve and is connected in series with the furnace elements. It is designed to melt when a specified temperature is reached, thus preventing permanent damage to the fabric of furnace.

Failure of the a.c. supply shuts down the furnace, but the cycle is completed when the supply is restored.

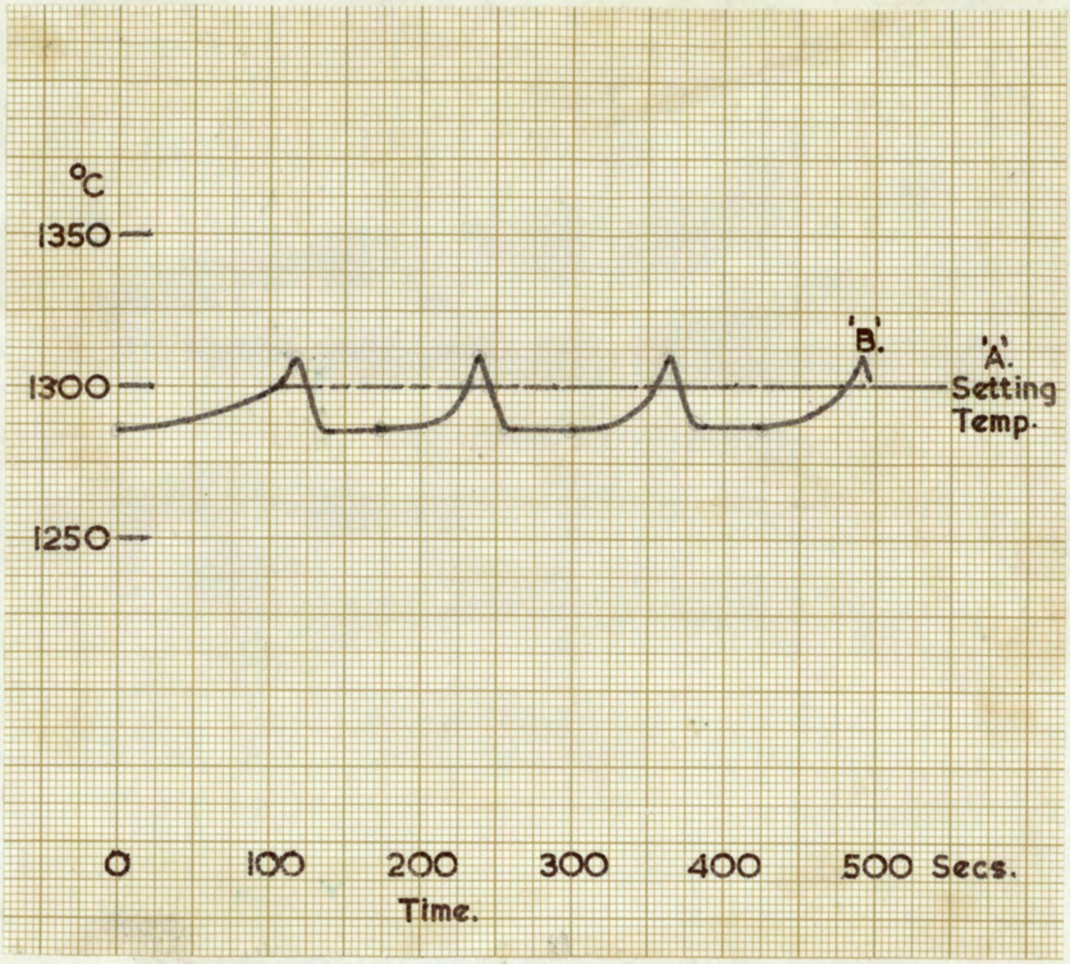

Figure 4.1. Performance of Temperature Controller. A. Programmed cycle.
B. Actual firing cycle.

4.2. FURNACE

4.2.1. Kiln

A standard laboratory Amalgam type CH.3 Electric Chamber furnace was used for firing the ceramic test pieces.

The furnace is electrically heated, using silicon carbide elements, and is capable of firing to a maximum temperature of 1,400°C. Automatic control by the programme control unit (4.1.) enables reproducible firing schedules to be carried out over long periods.

4.2.1.1. Testing

Tests were carried out to determine furnace behaviour at high temperatures and, for this purpose, platinum-rhodium thermocouples were placed in the furnace through small apertures bored through the furnace wall.

4.2.1.2. Results

(i) Temperature gradients were found to exist along the length of the furnaces at high temperatures:-

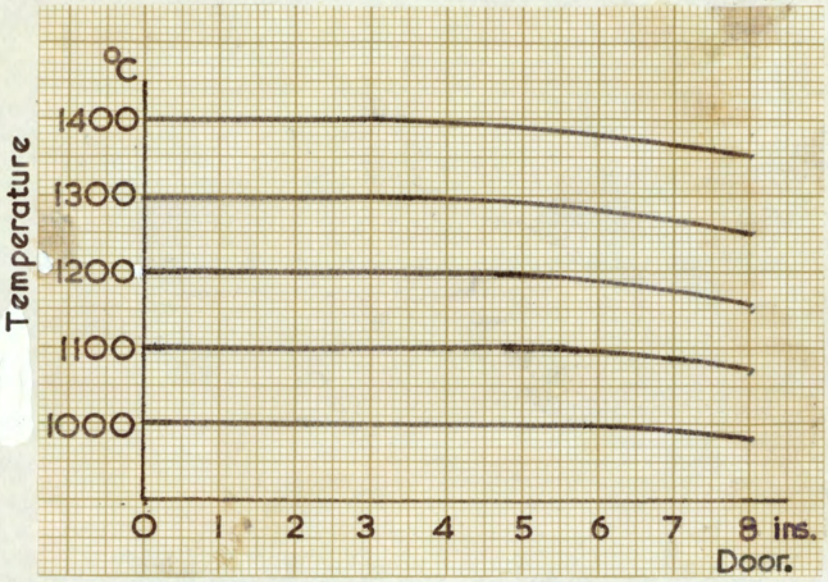

Figure 4.2. Temperature gradients along kiln length.

(ii) Slight overshoot (20°C.) occurred at maximum temperatures during automatic running.

4.2.1.3. Conclusions

To ensure a homogeneous environment for firing, all samples were placed within three inches of the back wall of the furnace.

In order to reduce overshoot, the thermal inertia of the furnace needed to be increased. Accordingly, a piece of zirconia plate was placed in the furnace to act as a heat sink.

4.3. PRESSES

4.3.1. Conventional Pressing

For conventional pressing operations, a hand operated L-30 hydraulic press (by Research and Industrial Instruments Company) having a capacity of 30 tons was used in conjunction with an X04 evacuable die by the same manufacturer.

The press had a daylight between platens of three to six inches depending upon the platen setting.

4.3.2. Hydraulic Pressing

For hydraulic pressing, a Dennison 50-ton hydraulic press was used.

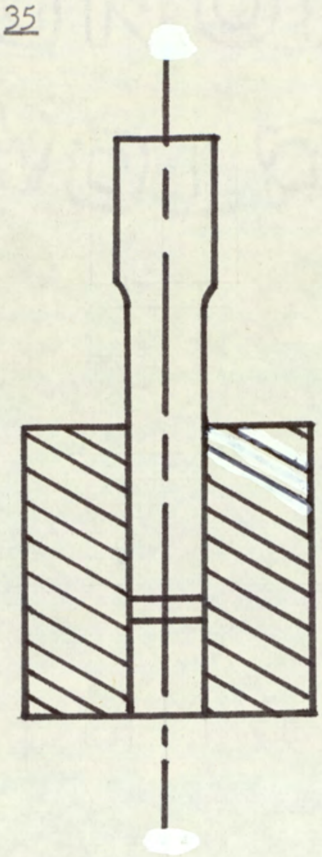

Scale:-Full Size.

Fig. 4.3. Mild Steel Die.

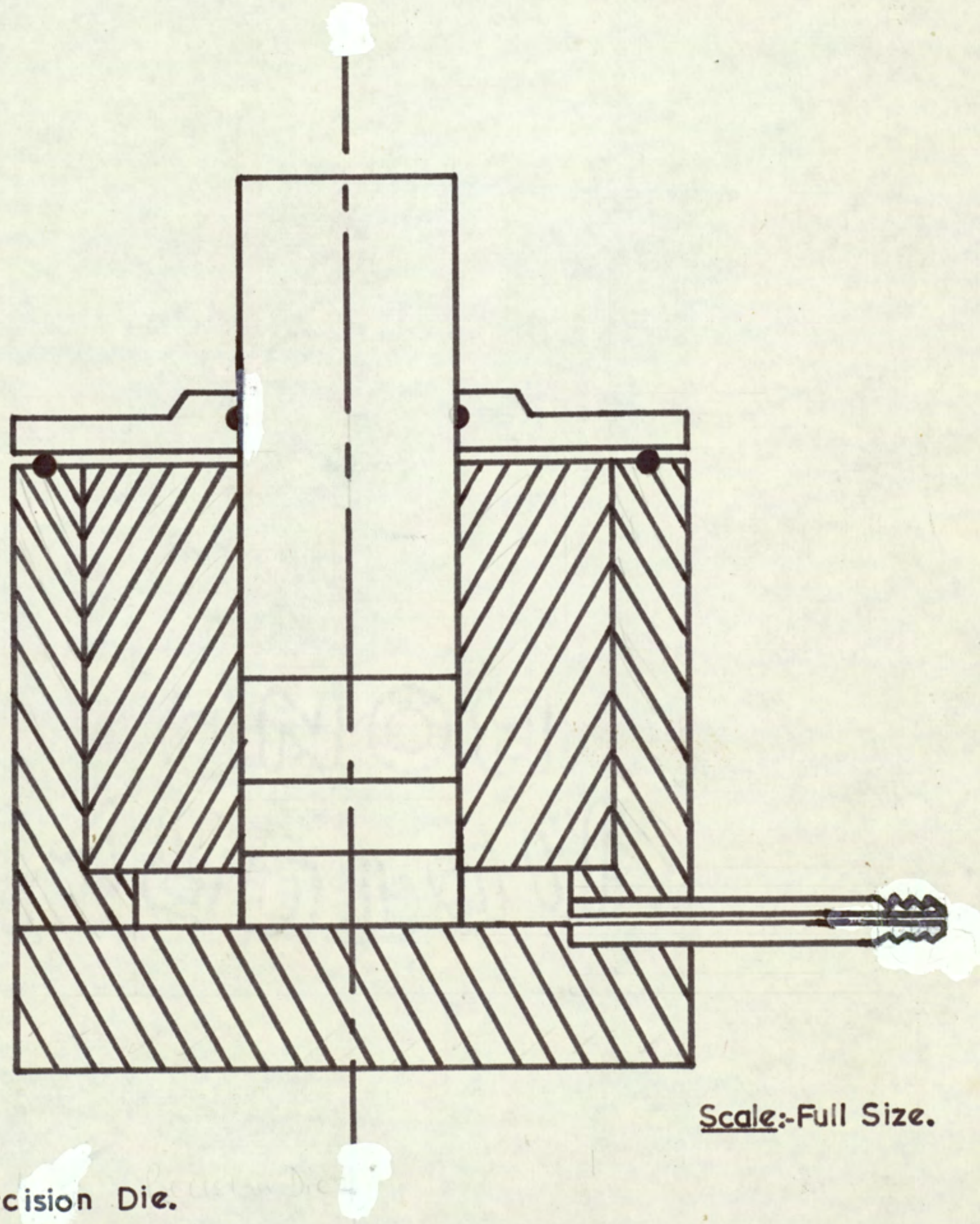

Scale:-Full Size.

Fig. 4.4. Precision Die.

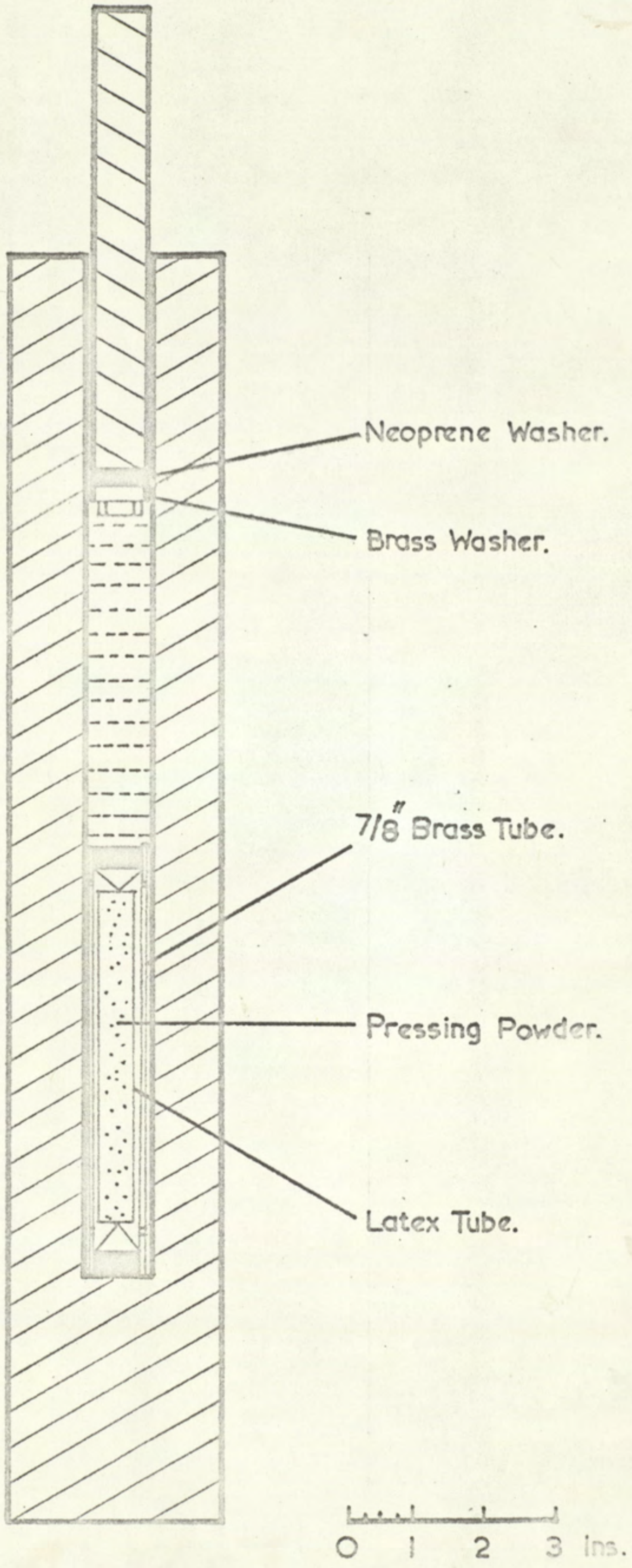

Fig. 4.5. Hydraulic Die

The press had five ranges of ram pressure: 0 - 1 - 5 - 10 - 25 - 50 tons. It has a daylight between platens of three feet.

4.4. DIES

4.4.1. Mild Steel Dies

Two identical dies were constructed using mild steel to the dimensions shown; (Fig.4.3). The die was hardened and the die faces were ground flat and mirror polished using metallurgical papers on revolving wheels. The interior face of the die was lapped smooth. The dies did, however, suffer from defects; it was difficult to produce satisfactory samples with either and the walls of both were eroded by the powders during pressing. (Plate 3.).

4.4.2. Precision Die

An X04 precision die made by Research and Industrial Instruments Company was made available for conventional pressing when the limitations of the previous dies became obvious (Fig.4.4).

The precision die had $1\frac{3}{8}$" diameter optically-flat and mirror-polished die faces. Provision is made for die evacuation during the pressing operation, but this facility was not used during the pressing operations as it was not considered necessary, a satisfactory product being obtained without it.

4.4.3. Hydraulic Die

A hydraulic die for use in the production of spinel powder rods for the tentative growing of spinel single crystals had been designed and constructed. It was suggested that similar rods of barium titanate powders might be produced by this method.

4.4.3.1. Construction

The die (Fig.4.5) was made from a solid 18 inch by 3 inch diameter mild steel billet.

A $16\frac{1}{2}$ inch x 1 inch diameter chamber was bored along its longitudinal axis and a 7 inch long x 1 inch diameter mild steel ram was made up to a tight fit. The ram was hardened and fitted with a $\frac{1}{4}$ inch thick x 1 inch diameter neoprene washer secured by $\frac{3}{8}$ inch whit. nut and washer.

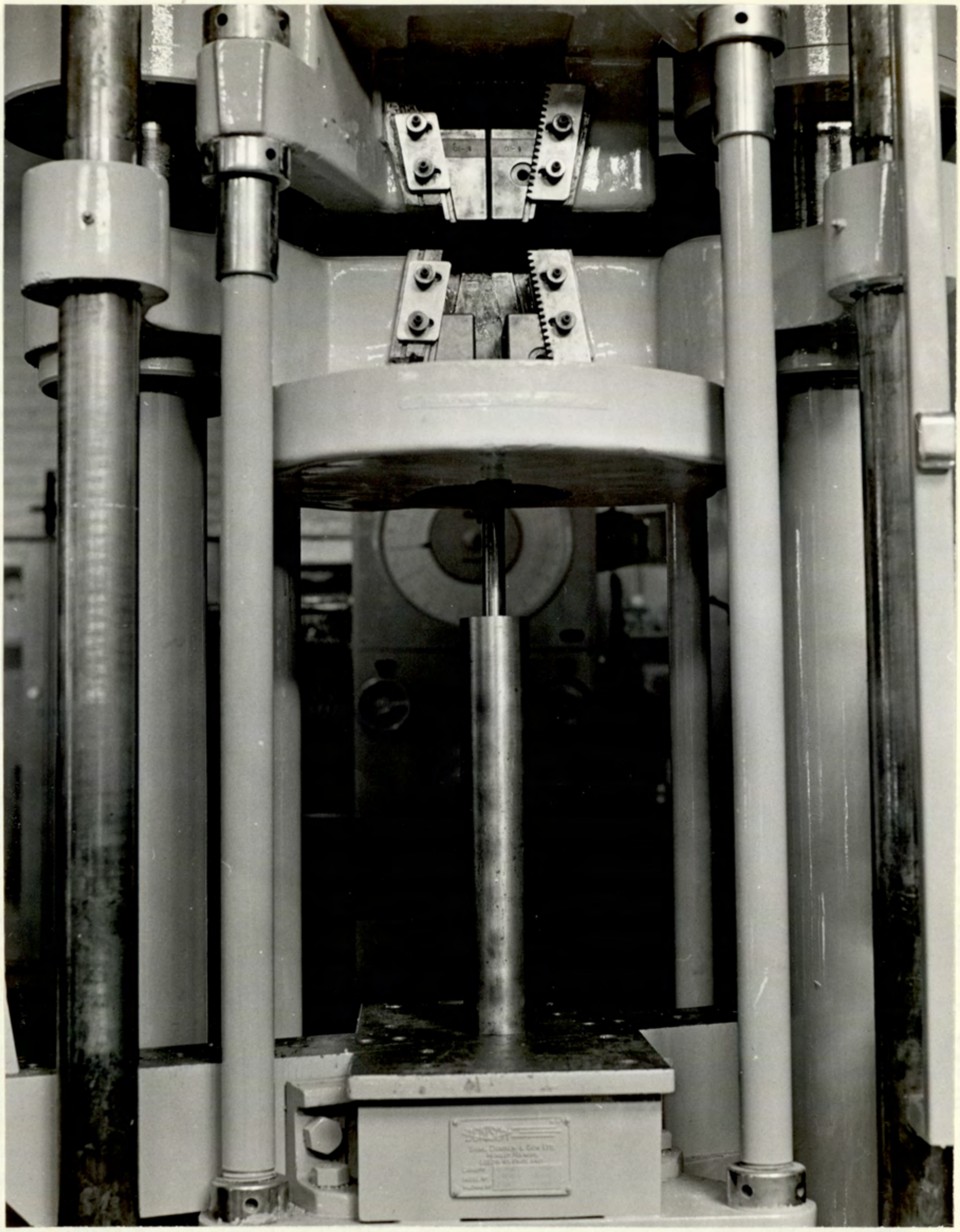

Plate 1. Hydraulic Die.

4.4.3.2. Testing

For test purposes, several samples of powder were placed in thin rubber tubing which was sealed and placed in the die chamber. The chamber was filled with water, predetermined pressures applied, held for ten seconds and released gradually.

The powder rod was extracted from the rubber tube and examined for cracking.

4.4.3.3. Results

Examination and subsequent firing did not reveal any abnormalities with any of the powders used. No binders were necessary. No pressure lines, strata or deformations could be detected in any powder specimens or in the fired product. Fired sample densities were always very high.

4.5. PREPARATION OF BARIUM TITANATE

4.5.1. GENERAL METHOD

4.5.1.1. Chemical Process

Generally barium titanate is formed by the calcination of an intimate mixture of barium carbonate and titanium dioxide, in stoicheiometric proportions. Essentially the reaction proceeds as follows:-

$$BaCO_3 + TiO_2 = BaTiO_3 + CO_2$$

but Templeton and Pask (23) describe the following intermediate reactions:-

(i) initially a small quantity of barium metatitanate is formed, the reaction becomes diffusion controlled and the reaction:-

$BaTiO_3 + BaCO_3 = Ba_2TiO_4 + CO_2$ proceeds.

The reaction continues until the amount of barium carbonate remaining is negligible (small amounts of $BaTi_3O_7$ and $BaTiO_9$ may form in addition during this reaction).

(ii) the proportion of barium titanate then increases until all Ba_2TiO_4 or TiO_2 is consumed:-

$$Ba_2TiO_4 + TiO_2 = 2BaTiO_3$$

4.5.1.2. Production Method

The two powders are dried, weighed out in proportion and intimately mixed in a ball mill. Small amounts of water are added at this stage to facilitate blending. The mixture is then calcined in platinum boats or refractory crucibles at temperatures ranging between 1,100°C. and 1,300°C. The reaction proceeds and can be observed by taking measurements of sample weight at set periods of time. When the reaction is complete, the calcined material is broken up and ball milled to reduce the material to a workable form.

4.5.2. DIGESTION OF BARIUM TITANATE IN OXALIC ACID

4.5.2.1. Barium titanate may be digested by oxalic acid at low temperatures:-

$$BaTiO_3 + 2(COOH)_2.2H_2O = BaTiO(C_2O_4)_2 + 2H_2O$$

Calcination of the product, barium titanyl oxalate, yields barium titanate:-

$$BaTiO(C_2O_4)_2 = BaTiO_3 + CO_2 + H_2O$$

the product being usually of finer crystal size than that described in paragraph 4.3.1.1.

4.5.2.2. A solution of oxalic acid is made up using 'Analar' oxalic acid and distilled water. A measured quantity of barium titanate is added to an excess of the oxalic acid solution. The mixture is placed in a water bath running at 90°C. and is left for 24 hours.

At the end of this time, the precipitated solid is removed from the solution and is washed with distilled water and dried. Calcination of the product at temperatures ranging from 400°C. to 1,000°C. follows, depending upon the end product required.

4.5.3. DOUBLE DECOMPOSITION OF POTASSIUM TITANIUM OXALATE AND BARIUM CHLORIDE

4.5.3.1. Chemical Process

If solutions of barium chloride and potassium titanium oxalate are added together, double decomposition occurs:-

$$BaCI_2 + K_2TiO(C_2O_4)_2 = BaTiO(C_2O_4)_2 + 2KCI$$

Barium titanium oxalate being precipitated from solution calcination of the product yields barium titanate.

$$BaTi(C_2O_4)_2 = BaTiO_3 + CO_2 + H_2O$$

4.5.3.2. Procedure

Solutions of barium chloride and potassium titanium oxalate are made up using pure 'Analar' reagent and distilled water. The solutions are mixed in approximate proportion and barium titanium oxalate is immediately precipitated as a white solid. The precipitate is filtered off, washed with distilled water and dried. Calcination is carried out as in 4.3.2.3.

4.5.4. Samples of barium titanate were produced by all three methods. There was, however, a considerable discrepancy found between the quality of several of the materials and samples of commercially available barium titanate were obtained for comparison.

4.5.4. Summary of Available Barium Titanate Powders

Material	Calcination Temp.	X-Ray Particle Size μ.	Purity	Quality
BaTioxalate.	1000 C	0.2.	Poor	Not Acceptable
$BaCO_3+TiO_2$	1000 C	>1.0.	Poor	Not Acceptable
Ultra Pure Grade.*	———	0.914	Very High	Very Good.
Commercial Grade.**	———	0.643	Good	Good.

*E.S.P.I. Inc. Los Angeles., **Steatite &Porcelain, Stourport on Severn, Worcs.

4.6. PREPARATION OF CERAMIC TEST SPECIMENS

Polycrystalline barium titanate test samples may be produced by any of the production methods in general use in the ceramic manufacturing industry, but it is considered preferable to use pressing methods for scientific work, as a more uniform product is assured, the fired sample density usually approaching the theoretical density of the material.

4.6.1. Preparation of Powder

Materials for use in ceramic must be kept pure to ensure consistent products and therefore all powders used were carefully handled to avoid cross contamination and contamination by outside sources. The powders must be stored in airtight containers and must only be transferred to dies or containers for pressing with clean nickel or plastic spatulas.

When binders are required, mixing must be carried out in clean glass equipment.

4.6.2. Pressing of Barium Titanate Samples

4.6.2.1. Pressing with Conventional Dies

Flat discs or shaped powder specimens may be pressed in conventional dies, but the samples produced usually contain inherent structural defects. These may take the form of stratification, dishing, cracking along stress lines, etc., depending upon the material used. The situation may be aleviated somewhat by the use of binders and precision dies, but considerable structure deformations are usually evident after firing. With $BaTiO_3$ powders, some difficulty is usually experienced in obtaining the right type and quantity of binder to suit a particular pressing force. The material will not press without binders by this method.

4.6.2.2. Hydraulic Pressing

The technique of hydraulically pressing powders is becoming well known in the technical ceramic industry. Samples produced by this method do not suffer from the abnormalities associated with conventionally-pressed samples, but are more expensive to produce.

In this technique the pressing powders are placed in flexible housings which are then carefully sealed to ensure that they are water tight.

The assembly is placed in a water-filled die and various pressures are applied for set periods of time.

On release of pressure, the assembly is opened and the compressed samples are removed. Samples of different powders for comparison may be pressed in the same die at the same time. No binder is necessary for the production of samples by this method, and the samples produced thus retain their relative purities and do not suffer from physical imperfections.

4.6.2.3. Experimental

A range of $BaTiO_3$ powder specimens were pressed in both types of die. An industrial wax was found to be a most useful binder in the case of

Plate 3. Pressed sample showing internal structural defects (no binder).

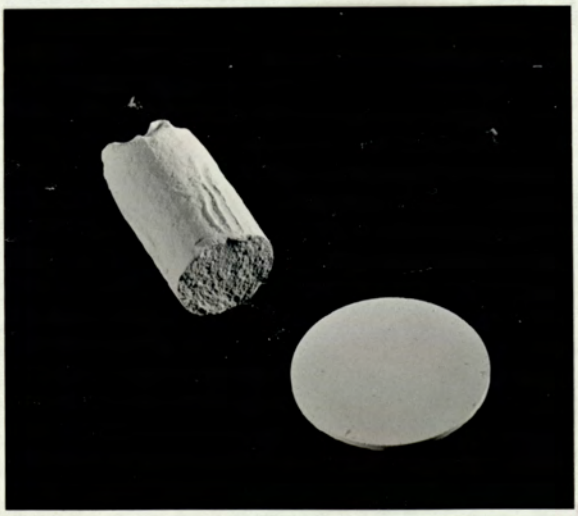

Plate 4. Left, hydraulically pressed sample (no binder) and right, disc specimen produced using X04 precision die (7% wax binder).

conventional pressings and it produced optimum results when added to the powders in the proportion of 7% by weight.

No difficulties were apparent with any of the available $BaTiO_3$ powders during hydrostatic pressing tests.

4.6.2.4. Conclusions

It was concluded from the experimental work that the samples produced by conventional pressing are suitable for most technical applications but, for detailed physical investigation, the hydraulically pressed material is far superior in every way.

4.6.3. Firing Procedures

Ceramic bodies are generally formed at temperatures exceeding 1,000°C. $BaTiO_3$ is no exception the inception of vitrification probably occurring slightly below 1,300°C.

Firing of $BaTiO_3$ for capacitor application is confined to the temperature region above this point but below 1,430°C. in normal atmospheres. This is due to the formation of the hexagonal polymorph at temperatures exceeding 1,430°C. The polymorph remains stable after cooling to room temperature under some conditions.

4.6.3.1. Investigation of Possible Firing Cycles

A series of test samples were fired over a range of firing cycles to investigate the effect of temperature gradients on the quality of the fired ceramic $BaTiO_3$. It quickly became apparent that the usual firing cycles adopted for the firing of ordinary ceramic bodies could be shortened without detriment to final fired quality of the samples. It was also found that, in order to obtain reproducible test specimens, tight control of the firing cycle was essential and that manual operation was not acceptable for this purpose.

The length of time at which the specimens were held at maximum temperature the 'soak' time was found to be of great importance in determining the physical properties of the fired material and this was considered to be a major point for investigation.

4.6.3.2. Conclusions

It was concluded that the firing schedules used for normal ceramic bodies could be shortened without detriment to the quality of the end product.

Two suitable firing schedules for $BaTiO_3$ specimens are shown below in Figure 4.6.

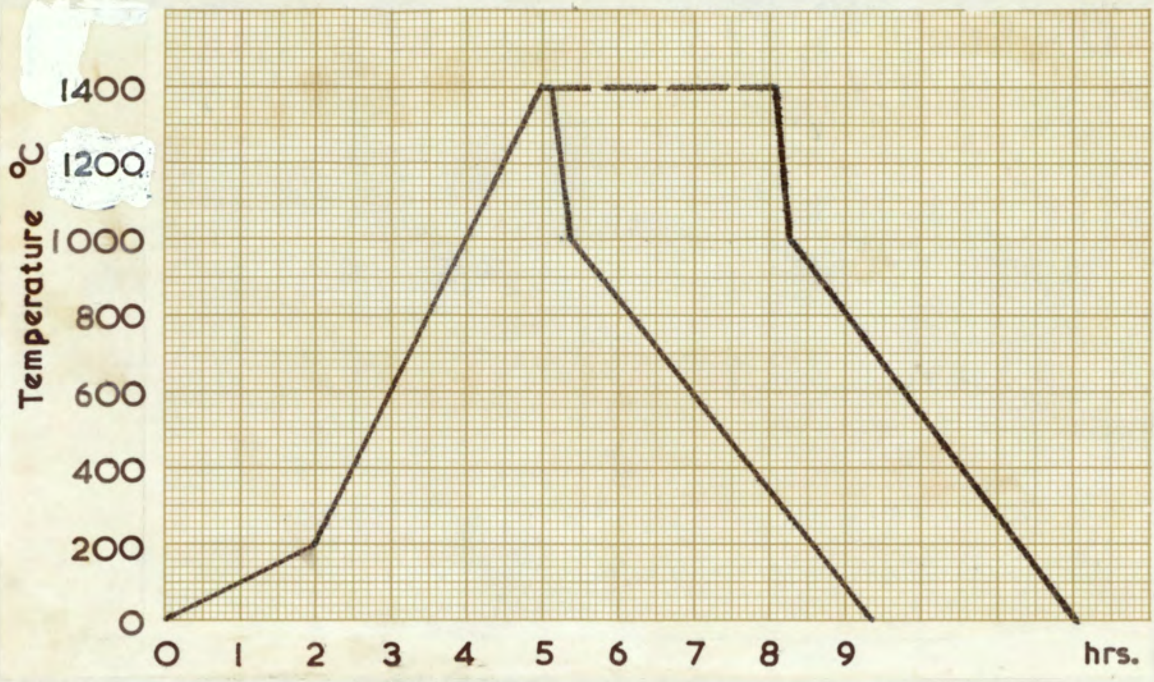

Figure 4.6. Time temperature schedules adopted for firing $BaTiO_3$ powder samples.

4.6.4. Finishing

The ceramic specimens produced in conventional dies require no further treatment before electrodes are applied, but the rods produced by hydrostatic means have to be cut into slices before satisfactory test specimens can be produced.

The actual rods produced had a somewhat irregular surface in many instances and some means of embedding or clamping the rods was found to be necessary to ensure that accurate parallel cuts could be made.

To achieve this, each rod was embedded in polyester resin. The rods were placed centrally in plastic tubes of $\frac{3}{4}$" diameter and a quick-setting polyester resin mixture was poured in until the tube was full. The tubes were placed in an oven at 60°C. for several hours to cure the resin.

On setting, the embedded rods were removed from the tubes and using a diamond impregnated cutting wheel each specimen was cut into as many slices of approximately 1 m m thickness as was possible. Each slice was washed with distilled water and dried in the oven. Measurements were taken with a micrometer to ensure that the faces of each slice were parallel.

On completion, all specimens having structural defects were removed, thereby ensuring that the test specimens used were of as high quality as was possible.

4.7. A COMPARISON OF ELECTRODE MATERIALS FOR TEST PURPOSES

In order to make accurate electrical measurements with ceramic samples it is of the utmost importance to have electrodes which are in intimate contact with the ceramic. Any intermediate layer of oxidised material or air will cause large errors in measured quantities. It is also of importance to utilize electrodes which do not deteriorate at test temperatures or which cause secondary effects which mask the properties of the material under investigation.

A study of electrode materials for use with ferrite and titanate ceramics at room temperature has been made by Flaschen and Van Uitert (52) who showed that electrode to surface barrier layers may be set up with certain electrodes, in particular fired-on platinum and silver pastes. The smallest effects were found in In-Hg.amalgam, graphite and aquadag.

Later Sauer and Flaschen (42) concluded that metals evaporated onto 'n' type semiconducting ceramic imparted high resistance to the material which was independent of electrode material.

Sussman and Ern (53) extended the work by measuring the temperature and frequency dependance of resistivity and dielectric constant on a typical 'n' type semiconducting ceramic material (reduced $Ba._{0.7}\ Sr._{3}O_{3}$). Films of silver, gold, aluminium, indium and indium-gallium alloy were all shown to exhibit normal d.c. resistivity behaviour between 70° and 400°K. No anomalous behaviour was observed at the Curie Point of the material (35°C.).

All samples having evaporated electrodes showed similar contact effects, with strong relaxation of apparent resistivity and dielectric constant.

4.7.1. High Vacuum Metal Deposition

A Genevac E.C.12 metal coating unit was used to deposit metal electrodes on the surface of ceramic test pieces.

4.7.1.1. Operation

The ceramic specimens were placed inside the high vacuum chamber of the coating unit, immediately above a tungsten boat containing a small quantity of gold wire or foil. Each specimen rested in a metal support, which also acted as a mask enabling a circular electrode to be applied to within approximately 1/16th inch of the edge of each sample. The unit was evacuated to 3×10^{-4} torr by means of rotary and mercury diffusion pumps and the filament was heated electrically until the gold melted.

On melting, the gold evaporated and the metal vapour coated the adjacent exposed areas with a thin layer of metal. The process was repeated to coat the opposite faces of the samples.

4.7.2. Examination of Electrode-Ceramic Interface

Samples of the coated ceramic were examined with an electron microprobe analyser to determine the thickness of the plated electrode and to examine the metal-ceramic interface. In the samples examined, the electrode layer was found to have a thickness of 16 μ, the metal vapour having penetrated all open pores in the ceramic free surface. In some cases, metal vapour had penetrated to a depth of 3 μ from the mean surface.

4.7.3. Conclusions

It was concluded that the electrodes were in intimate contact with the ceramic and therefore provided good electrical contact. Electrodes of this type are seen to have good electrical and mechanical properties.

4.7.4. High Temperature Electrode Test

A quantity of similar industrial samples of doped barium titanate were used for the test. Evaporated metal electrodes were applied to both sides of the samples, batches of five samples being coated with the same metal at the same time. The electrodes used were of $\frac{3}{8}$ inch diameter, the industrial samples having a diameter of $\frac{1}{2}$ inch. One batch of samples were painted with D.A.G. conducting paint. The samples were subjected to repeated cycling from -70°C. to 200°C., electrical measurements being made at room temperature between cycles,

After each cycle the electrodes were examined for damage.

4.7.5. Results and Conclusions

Electrode	Melting Pt.^{o}C.	Cycle		
		1	2	3
Cr	1,830	R	R	-
Cu	1,084	C	O.R.	-
Au	1,063	C	C	C
Pb		I	O.R.	-
Ag	960	R	O.R.	-
Su		C	C	C
D.A.G. paint	-	E	C	C

C - Consistant results in each sample
O - Surface oxidized, bad electrical contact
R - Reduction in electrode area due to evaporation and oxidation
I - Inconsistant results
E - Elevated result

Figure 4.7. Summary-Electrode materials for ceramic specimens

Examination of electrodes and comparison of the dielectric measurements immediately gave indication of the most suitable electrode materials. Early reduction in the amount of material forming the electrodes was observed with Cr and Ag electrodes, whilst Cu gave poor electrode contact in the second and third cycle due to surface oxidation. D.A.G. conductive paint gave anomolous electrical results in the initial cycle, but consistant results in the second and third indicated that a film of solvent was still perhaps present initially at the electrode-ceramic interface.

The metals remaining (gold and tin) gave consistant results throughout the test. However gold was chosen as the better electrode material, as it does not tarnish even at high temperatures and gives a somewhat better surface finish. D.A.G. conductive paint was omitted as were other conducting paints and pastes, because they are difficult to apply satisfactorily.

4.8. DIELECTRIC MEASUREMENTS

4.8.1. Sample Holder

To ensure that all dielectric measurements are made under identical

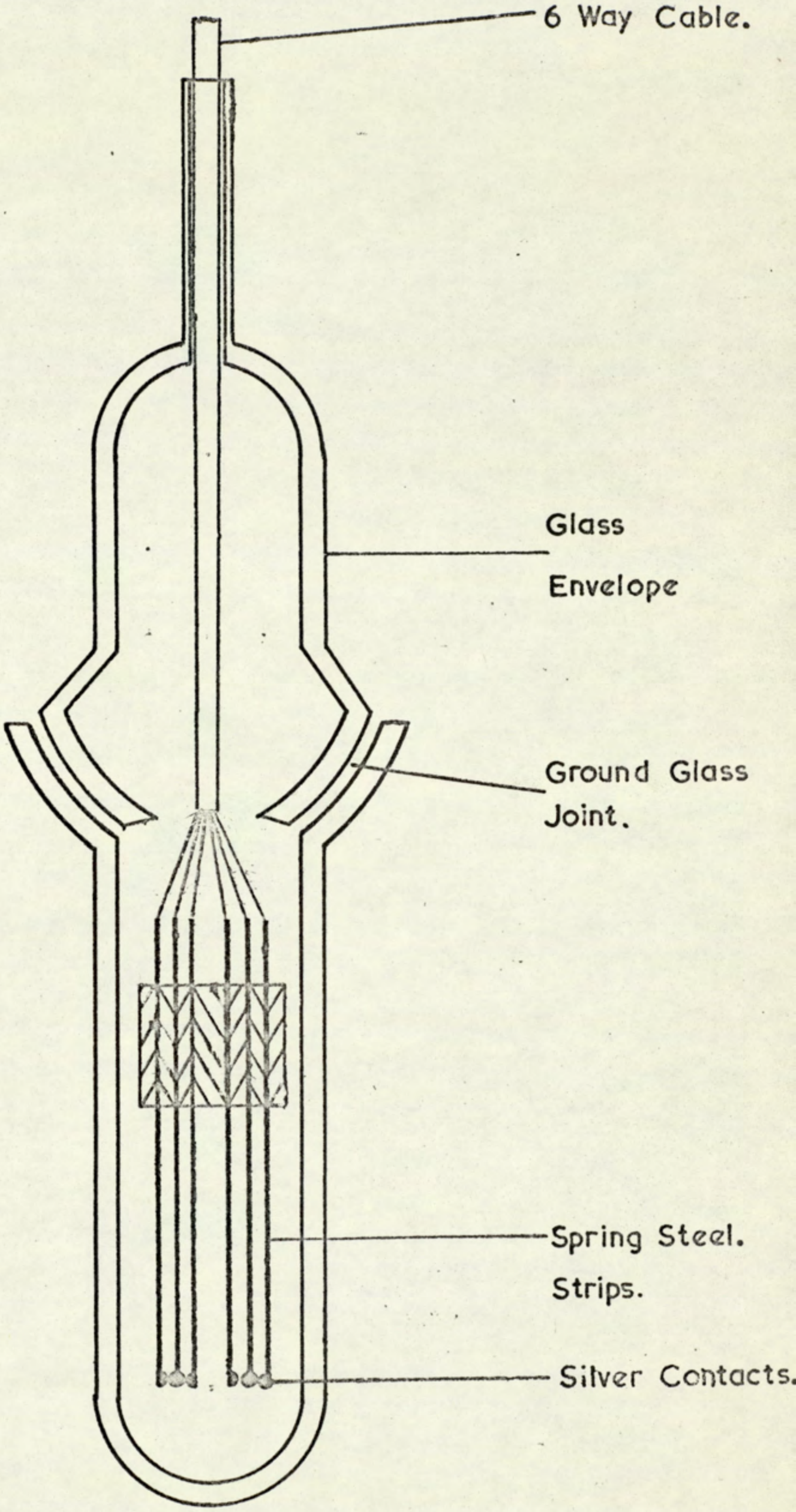

Fig 4.7a. Sample Holder.

electrical conditions specimens under test are placed in a sample holder. The sample holder used throughout this project is shown in Figure 7(a).

4.8.1.1. Construction

The sample holder was constructed using six spring contacts arranged such that four separate samples could be accomodated at one time. Each double pair of electrodes was connected to a four way switch at the remote end and a common wire was run from the other two to the other pole of the switch. The holder was totally enclosed in a glass sheath. A thermocouple was arranged to be in intimate contact with the centre sample

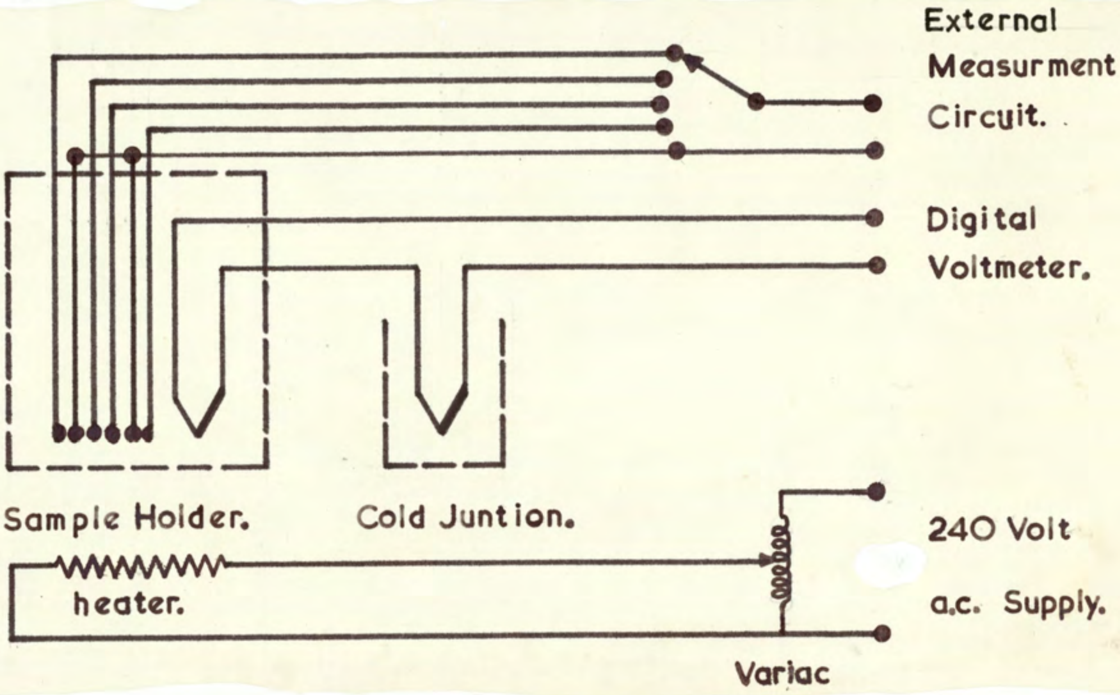

Figure 4.8. Dielectric measurements schematic circuit.

4.8.1.2. Capacitance Measurements

Capacitance measurements were made by the substitution method. Initially, the capacitance of the leads and the sample holder with an air gap between the electrodes were measured (C_1). A second reading was then taken with the sample in place (C_2).

Therefore the true capacitance of the sample = $(C_2 - C_1)$

To determine the error due to stray capacitance, measurements of capacitance were taken at room temperature by connecting capacitors both directly across the bridge and in the sample holder.

4.8.1.3. Results

Using a 1000 pF capacitor, no finite stray capacitances could be detected. However, the capacitance of the leads was found to be appreciable, as the length of cable, 1 m. long, was needed to gain access to the heated chamber of the oven. The capacitance of each pair of leads was 1:- 34pF; 2:- 35pF; 3:- 34pF; 4:- 34pF.

4.8.2. Controlled Temperature Devices

In order to measure temperature-dependent dielectric properties above room temperature, a controlled oven was used to heat the samples over the range (20° - 150°C.). A cryostat was designed and constructed for measurements below that temperature.

4.8.2.1. Cryostat

The cryostat was designed to provide a controlled environment for low-temperature measurements. Solid carbon dioxide was used as the cooling agent, with methyl alcohol as a wetting agent. A small carbon resistor (1005L) was used as a heat source when a variation in temperature was required. The apparatus was found to be useful over the range - 75° to 10°C., equilibrium conditions in the sample holder being easily maintained by variation of the supply to the carbon resistor (Figure 4.9)

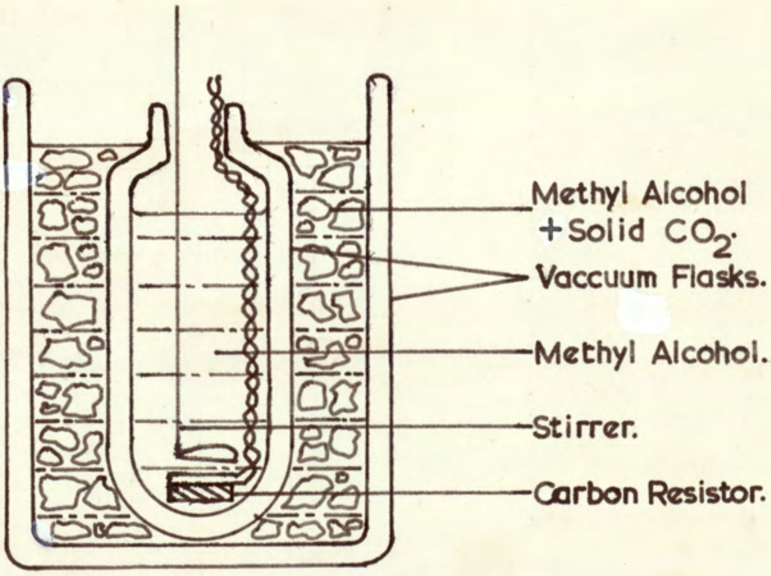

Figure 4.9. Cryostat for low temperature dielectric measurements.

4.8.2.2. Oven

A Haerau (250°C.Max.) laboratory oven was tightly controlled using a 10A variac. Access to the heated chamber was provided by a vent in the roof of the oven. Dielectric measurements were taken only when thermal equilibrium conditioned prevailed.

4.8.3.1. Temperature Measurement

Temperature measurements were made with copper constantin thermocouples using melting ice as the cold junction. The emf generated by the thermocouples was measured with a digital voltmeter. The thermocouples were standardised using boiling distilled water, due regard being paid to atmospheric pressure at that time.

4.8.4. Low Stress Capacitance Bridge

A Marconi 0.1% Universal bridge type T.F.13134 was used for the measurement of capacitance and loss factor at low electrical stresses.

4.8.4.1. Specification

The bridge will measure capacitance values from 0.1$_p$F 110 F in seven ranges, the accuracy of measurement dependent upon the range used:-

1100$_p$F and 11 F ranges inclusive basic error (0.1%)
110$_p$F and 110 F ranges basic error 0.1% of reading

Loss factor may be measured over four ranges to the following accuracies:-

(i) Q. 0 - 3)
) 10% of reading 3% of full scale value
D. 0.005 - 0.031)

(ii) Q. 0.5 - 31.0 5% of reading 0.5% of full scale value
D. 0.005 - 3.0 5% of reading

$$Q = \frac{1}{D}$$

4.8.5. High Stress Capacitance Bridge

Marks et al. (1956) (55) describe a modified Sawyer-Tower bridge for the recording of dielectric hysteresis loops for measurement purposes:-

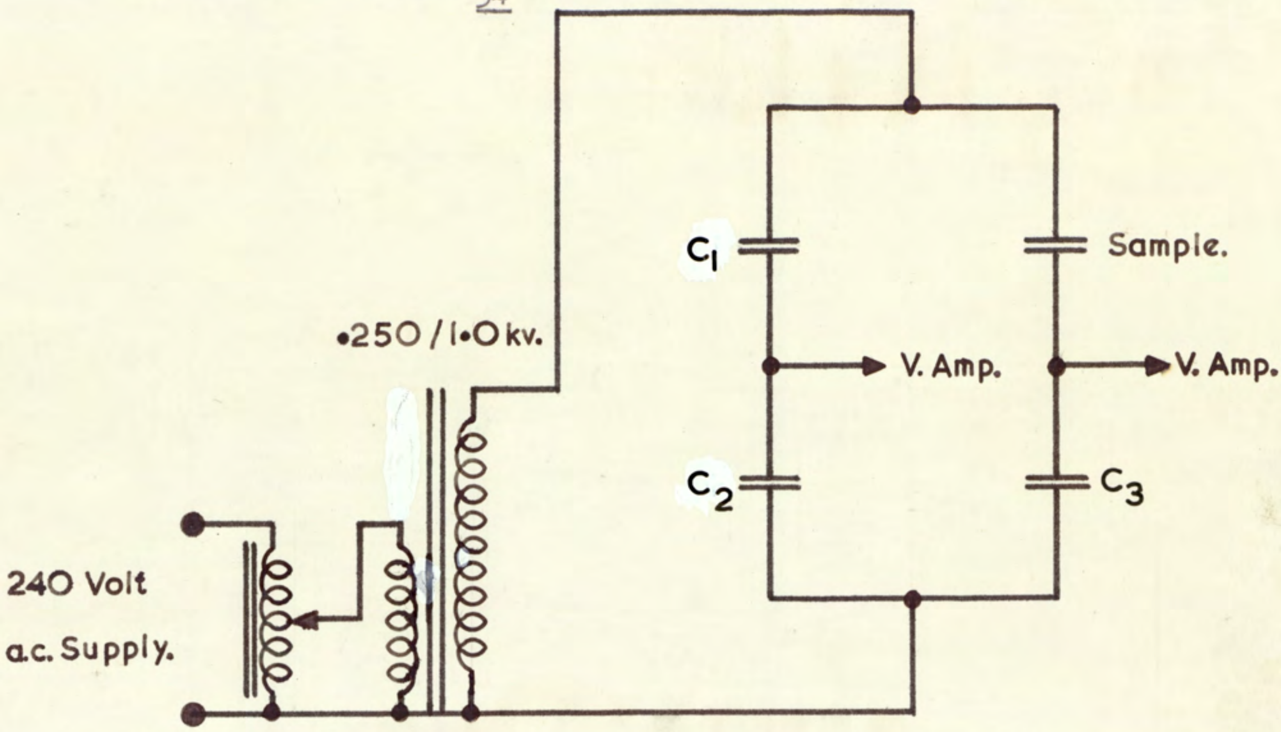

Figure 4. Modified Sawyer-Tower circuit for the recording of dielectric hysteresis loops

The co-ordinates of the display oscilloscope are easily calibrated using this form of modified bridge as:-

(i) $E = \frac{C_2 V_2}{C_1 t}$ if $C_2 \gg C_1$

where E is the voltage applied to the specimen,

and (ii) $P = \frac{C_3 V_3}{A}$

since $V_3 = \frac{1}{C_3}\int i \ dt.$

and $P = \frac{1}{A}\int i \, dt.$

4.8.5.1. Calibration

The modified circuit is shown in Figure 4.10. the co-ordinates of the display oscilloscope being calibrated from capacitance measurements of the components and their physical dimensions.

$$E = V_H \, (0.863) \times 10^6 \text{ v/m.}$$

and $P = V_V \, (4.852) \times 10^{-2}$ Coulombs/m^2

The overall permittivity at any point on the displayed hysteresis loop is given by the relationship

$$\epsilon_n = 1 + 4\pi.\frac{P}{E}$$

and the energy loss per cycle is represented by the area enclosed by the loop.

4.8.5.2. Experimental

The hysteresis loops obtained using this bridge were recorded using a Tektronix 564 storage oscilloscope and a series 125 oscilloscope camera. Measurements were made either directly from the screen using the storage facility or from photographic prints of the oscilloscope traces. Both methods were found to be equally satisfactory in practice.

4.8.6. Measurement of Switching Transients

The normal circuit for the measurement of switching transients is given in Chapter 3 (Figure 3.3).

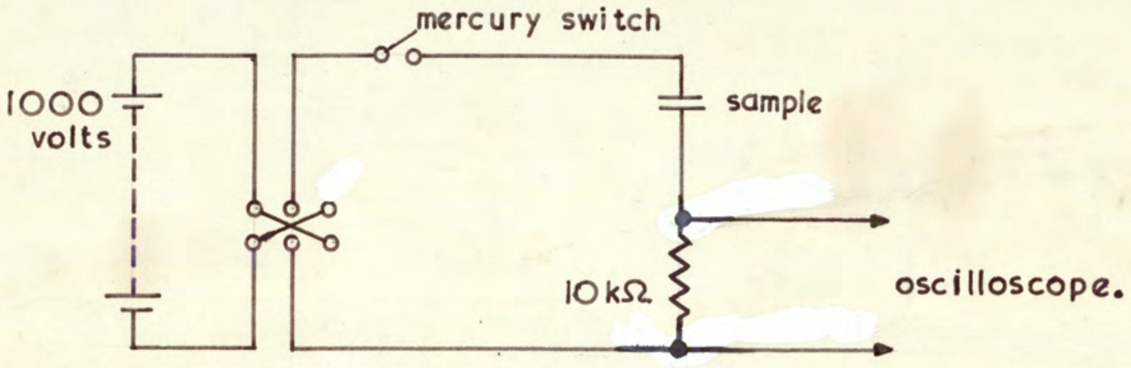

Figure 4.11. Circuit for the recording of switching transients in polycrystalline $BaTiO_3$.

The current transients were recorded for measurement either with the storage facility of the oscilloscope or with a Polaroid camera attachment.

4.8.7. Measurement of Resistivity

The relationship between resistivity and temperature in $BaTiO_3$ is non-linear as is the relationship between applied field and current, Busch et al.(1948) (56) Heywang (1961) (1963) (57) (58).

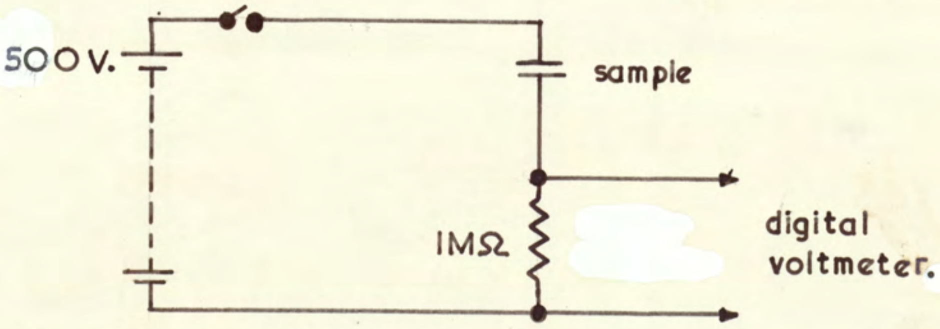

Figure 4.12. Circuit for the measurement of resistivity in ceramic specimens

4.8.7.1. Experimental

Using a digital voltmeter, precision galvanometer and a standard resistor, the resistivities of some of the test samples were measured over a range of temperature. The relationship between applied voltage and current was also established.

4.9. PHYSICAL ANALYSIS

4.9.1. X-Ray Crystallographic Analysis

When a beam of x-rays is incident upon a single infinite perfect crystal of some particular substance, the beam is scattered by the microscopic physical components of the substance. The refracted intensity of the beam may be measured with a suitable detector, the intensity maximum occurring as a very sharp peak.

In real single crystals, however, the total and maximum intensities of the refracted beam are dependant upon the state of perfection of the crystal, and in polycrystalline samples the x-ray intensity curve exhibits broadening due to the defect crystal structure of the material. By suitable techniques the particle size and strain within the material may be estimated.

4.9.1.1. Determination of Particle Size

If a single crystal is to be analysed, it is convenient to consider that the crystal is composed of a 'mosaic' of blocks of unit cells of perfect register and that imperfections are represented by slight misorientation of the mosaic blocks.

If such a system is applied to a polycrystalline sample analysis then, provided that each mosaic block is considered to be one particle of powder, then the intensity peak hight is given by:-

$$I = I_0 . p^2 . q^2 . \sin^2 \phi . \qquad \text{where } \phi = \frac{2\pi}{\lambda} \cdot p.d.\cos\theta .$$

If the angular width of the intensity characteristic at half the net peak intensity, i.e. $\frac{\text{Peak intensity - background}}{2}$, is used as a measure of broadening, then the value of ϕ corresponds to 1·4.

X-ray techniques enable crystallite size to be estimated in polycrystalline materials. The results may differ from those obtained by other methods,as crystals are usually formed from several crystallites optically indistinguishable from each other.

4.9.1.2. Experimental

Using a Phillips PW1010 x-ray generator and Type PW1050/25 goniometer, measurements of crystal size w re made using one specimen from each batch of test samples.

Ni filtered Cr radiation was used for the measurements, the observed angle being 59.2° (2θ). Each individual measurement was taken over a period of ten seconds.

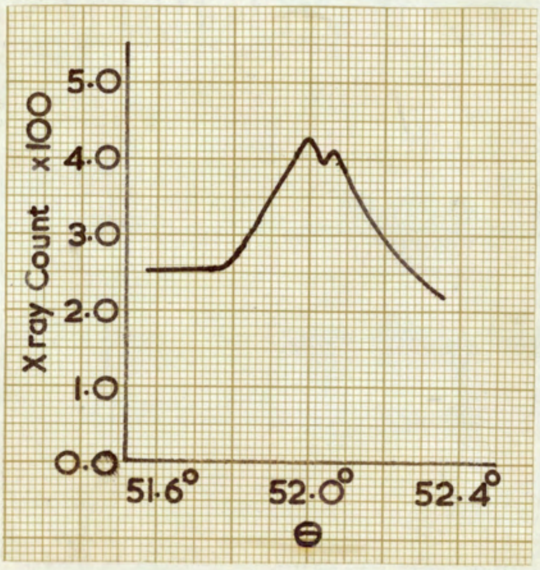

Figure 4.13. Typical X-ray characteristic specimen HEI

4.9.2. Electron Microprobe Analysis

The use of the Electron Microprobe Analyser for the non-destructive chemical analysis of ceramic specimens is well known.

4.9.2.1. Mode of Operation

A narrow (1 or 2 microns) beam of electrons is accelerated along an evacuated column by an electric field and is focussed upon a specimen of some particular material requiring analysis. On striking the material,the characteristic x-ray radiation of the material is emitted and this is passed through a crystal spectrometer where the amplitude and angle of the radiation is recorded (Figure 4.13). If the electron beam is made to scan the specimen and the x-ray intensity at some convenient angle is continuously monitored, a characteristic is produced which is proportional to the quantity of the observed element along the scanned length.

4.9.2.2. Sensitivity and Accuracy

Measurements made with electron probe analysers have a normal accuracy of 1%, but with care this may be reduced to 0.1%.

With ceramic specimens, satisfactory analysis of small areas of diameter 1 or 2 microns is achieved, although any pore present in the specimen will influence the x-ray intensity measurement within 1 or 2 microns of its edge.

The apparatus will detect and measure diffused impurities, will define areas of attack and the nature of the agent, but will not define the crystalline properties of the material.

4.9.2.3. Experimental

In the initial stages of the project, the fired purity of the ceramic samples was investigated. Small specimens of the material were cut and polished on metallurgical wheels. A thin layer of carbon was deposited on each exposed section to ensure good electrical conductivity and measurements were made to establish the type and mechanism of deposition of any impurity content present in the specimens.

4.9.2.4. Results

Large quantities of impurities were found in many of the early samples.

All the samples produced by conventional pressing technique were noticed to pick up material from the sides of the die. Electron microbe analysis of the faces of sample which had been subjected to most contact with the die revealed a thin film of iron impurity of no great depth on the surface of the sample. Quantities of zirconia which had diffused into the samples from the supporting batts were also identified. (Figure 4.14 and Figure 4.15).

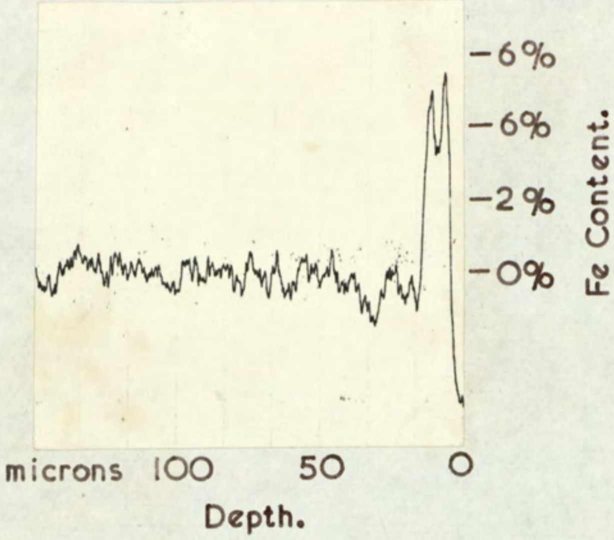

Figure 4.14. Typical iron impurity at the surface of ceramic $BaTiO_3$ specimens produced by conventional pressing technique.

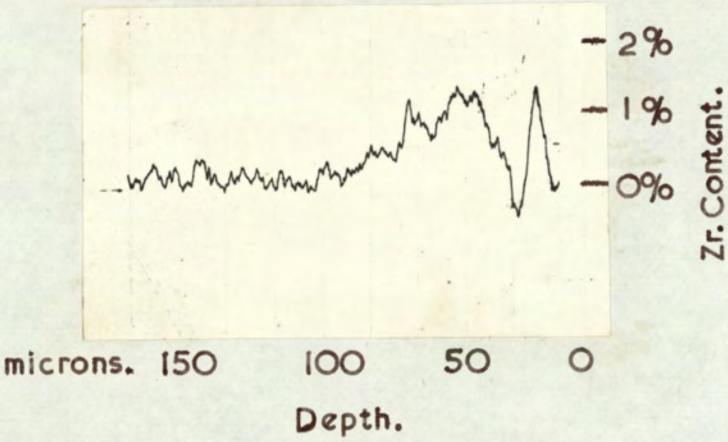

Figure 4.15. Typical Zr. impurity diffused into $BaTiO_3$ samples during firing on zirconia batts.

Later, the physical properties of the metal electrode film were investigated The thickness of the electrode films and the depth to which the metal vapour had penetrated the ceramic were measured.

4.9.3. Optical Methods

4.9.3.1. Preparation of Polished Specimens

Samples for observation were prepared by conventional metallurgical technique. The ceramic specimens were embedded in a polyester resin. Although use of this type of resin is not really satisfactory, due to the high degree of mismatch in the strength of the two materials, its use may be acceptable if the porosity of the test piece is low (60), as it was in this case.

Surfaces for examination were lapped flat with graded metallurgical papers using water as a lubricant. Final polishing using 'Dialap' diamond paste spread on rotating polishing pads and 'Microfin' fluid as lubricant produced samples suitable for high-power optical observation.

Each sample was polished in a circular motion, enough microfin fluid lubricant being added to just dampen the diamond paste. At intervals, the samples were mounted on glass slides and placed in a Metals Research Image Analyser (4.9.3.4.) to determine the percentage porosity of the sample. When this figure remained constant over several polishings it was assumed that any apparent porosity due to 'tear out' of the material during some of the coarser polishing steps had been removed.

4.9.3.2. Etching

After the final polishing stage, the samples were prepared for optical examination by etching in concentrated HCl. for eight minutes. The samples were then washed and dried and the structure of the material was examined using both an image analyser and a conventional microscope.

The etching process was found to successfully reveal the crystal structure of all the test specimens produced.

4.9.3.3. Microscope

Polished etched specimens were observed with a Vickers Metallurgical microscope. The instrument had magnifications of x 50, x 100, x 500, x 1,000, depending upon setting. Photomicrographs were taken with the aid of a camera attachment.

4.9.3.4. Image Analysis

The structure of each polished sample was examined and analysed using a Metals Research 'Quantimet' Image Analysing Computor. The instrument can determine porosity and volume fraction in single or multiphase ceramic systems.

4.9.3.4.1. Mode of Operation

In this apparatus the image of a microscope is projected onto the screen of a television camera. The electrical output from the camera is fed into a television monitor, where the image is displayed, and into a detection unit, where the signals emanating from distinct features are selected from the rest of the signal.

The output from the detector unit consists of pulses from the distinct features which may be displayed simultaneously with the image. A computor unit measures the parameters of the detected features.

4.9.3.4.2. Measurement

The areas of detected features may be calibrated absolutely, or may be expressed as percentages of the blank frame area.

Various shades of grey are distinguished, allowing separate measurement for each of as many as six distinct phases under favourable circumstances.

Accuracies:- Meter ranges 0-100 0.3% f.s.d.

Area measurement to below 0.003%.

4.9.4. Electron Microscope

A Phillips 'Stereoscan' scanning electron microscope was used to observe both the polished and unpolished surfaces of several of the ceramic test pieces produced.

4.9.4.1. Sample Preparation

Specimens for observations were mounted on small metal sample holders using a quick setting adhesive. Each sample was then coated with a very thin film of gold, using the high vacuum metal deposition described previously. A small amount of Dag conducting paint was then applied to the edge of the sample to ensure good electrical contact with the metal sample holder.

4.9.4.2. Operation

The samples on their holders were then placed in the microscope and the unit was pumped down to its operating pressure. Each specimen was then observed at various magnifications and any points of interest investigated. Electron micrographs were then taken using a camera attachment.

CHAPTER 5

5. EXPERIMENTAL WORK

5.1. Production of Barium Titanate

Barium titanate for experimental use is usually prepared by two methods:- (i) calcination of an intimate mixture of $BaCO_3$ and TiO_2 in correct proportion and (ii) calcination of $BaTi(COOH)_2$.

5.1.1. Calcination of $BaCO_3$ and TiO_2

In order to produce a reasonable quantity of barium titanate for pressing powders, calcination of $BaCO_3$ and TiO_2 mixtures was attempted early in the project. Quantities of reagent-grade (Analar) materials were dried to constant weight, weighed out and mixed in a vibrating pot mill. After several hours the mixture of powders was taken from the pot mill and transferred into silica crucibles (with lids), using clean metal spatulas. It was noticed that the powders tended to cake during mixing, the grinding balls becoming covered with the material.

The crucibles containing the mixture of powders were transferred to the kiln, where they were calcined for varying temperatures and times. On cooling, the calcined material was removed from the crucibles. Some considerable reduction in volume of the powder was always noticed and in most cases the silica crucibles had been attacked, in many cases the attack being severe.

The resulting compounds were somewhat hard, yellow brown materials, which required grinding in a mortar and pestle to reduce them to powders. Intermediate sieving, using sieves of standard mesh, and regrinding usually served to produce a fairly satisfactory end product suitable for the pressing of test specimens.

5.1.2. Calcination of $BaTi(COOH)_2$

In an effort to produce powder samples having higher purities than those already produced, a quantity of barium titanium oxalate was prepared by precipitation from solution. Solutions of Analar potassium titanium oxalate $K_2Ti(COOH)_2$ and barium carbonate $BaCO_3$ were made up using distilled water. A slight excess of $BaCO_3$ solution was added to the $K_2Ti(COOH)$

solution and a white material $BaTi(COOH)_2$ was precipitated. The precipitate was filtered off, washed in distilled water and dried in an oven at 60°C.

The precipitate was transferred to silica crucibles and calcined at 1,000°C. The resulting compound was also found to attack the silica crucibles and a platinum crucible was obtained in order that this source of impurity could be eliminated.

The powders were calcined in the platinum crucible. The resultant powders were yellow brown powders but at the point of contact of the crucible a distinct pink colouration was observed. The powders produced at low calcination temperatures crumbled easily,but those produced at high temperatures were hard and required grinding to produce satisfactory pressing powder.

5.2. PRODUCTION OF $BaTiO_3$ TEST PIECES

5.2.1. Pressing

5.2.1.1. Conventional Pressing

Test samples were made by pressing the powder specimens produced above in a mild steel die (Section 4.4.1.). Many of the samples were found to contain flaws, the defects taking the form of statification or sheer lines at 45° to the direction of applied pressure.

To overcome these difficulties,various types of binder were tried. Earlier work in the department had shown that materials such as water and stearic acid were unsuitable for this purpose,but a pure wax (melting point 60°C) was eventually found to produce good pressed specimens. Approximately 5% of wax by weight was used to obtain optimum results.

In many cases the powders were found to scour the die, iron impurities being noticeable on the edges of the test pieces. This was later confirmed by X-ray analysis, Section (4.9.2.4.).

It was evident that some improvement in the standard of the pressed specimens was required and a precision idustrial die was obtained. The quality of the test pieces produced immediately improved and the die was used in all subsequent pressing operations.

5.2.1.2. Hydrostatic Pressing

The conventionally pressed samples could not be considered to be homogeneous in nature, due to their inherent structural defects and samples of powders were pressed hydrostatically to obtain a more uniform product. The pressing powders were placed in a thin latex tube and this was sealed and placed inside a water-filled die. Varying pressures were applied, usually for set periods of ten seconds, and when the tube was removed from the die, pressed powder rods six inches long and ½" in diameter were found to have been formed.

The rods were found to be very dense and homogeneous, each breaking evenly across its diameter on application of moderate pressure and this was taken as an indication that no stress lines or stratification existed, or were at least very small with this type of pressed material. No difficulty was experienced with this method in pressing any of the powders produced.

5.2.1.3. Production of Pressed Samples for Test Purposes

Using both the methods described above, a range of pressed powder samples of specimens were produced for subsequent firing. Pressing powders produced in the laboratory and powders obtained from industrial sources were subjected to pressing forces ranging from 5 to 15 tons. When the conventional dies were used, great difficulty was experienced in obtaining pressed samples from each type of powder for a particular pressure and binder content. However, no difficulty was experienced with any powder during hydrostatic pressing operations.

5.2.2. Firing

Reproducible ceramic $BaTiO_3$ specimens may be produced by firing pressed powder specimens at high temperatures under tightly controlled conditions.

Rase and Roy (24) indicate that the optimum firing temperatures for $BaTiO_3$ bodies lies in the range 1,320° - 1,460°C. Tests to establish the validity of this statement indicated that this was indeed the case although the lower point was found to be slightly less than that stated.

In order to obtain reproducable test specimens however it is also successfully used for this purpose. The sheets protected the samples from both the batts and from spall falling from the furnace linings. $BaTiO_3$ in its ceramic form was not found to react with platinum metal.

5.2.2.1. Firing Schedules

Due to the usual bulky size and inhomogenity of ceramic pieces firing schedules are kept fairly long and seldom involve steep time-temperature gradients. This state of affairs does not normally exist where small quantities of pure pressed powders are concerned and (except for the early part of the firing cycle where binders, if used, are burnt off) higher temperature gradients may be tolerated without cracking or distortion taking place.

Numerous firing cycles were investigated to obtain two schedules which would allow $BaTiO_3$ powders to be successfully fired over both a range of temperatures for a certain constant period at maximum temperature and a range of firing periods at constant maximum temperature.

In the two schedules eventually adopted, the temperature gradients to and from the maximum points were made identical. A period of five minutes was allowed for the 'soak' period in cycle A, as this was found to be minimum time necessary for the whole of each sample to attain the maximum furnace temperature. The temperature maximum in cycle B was chosen as 1,300°C., the temperature at which vitrification occurred in all the samples investigated.

Cycle A.

0 - 200 °C at 100 °C/hr.
200 - 1400 °C at 400 °C/hr. Variable Peak Temperature, 5 minute soak.
1400 - 1000 °C at 800 °C/hr.
1000 - 0 °C at 250 °C/hr.

Cycle B.

0 - 200 °C at 100 °C/hr.
200 - 1300 °C at 400 °C/hr.
1300 °C variable soak period 0 to 6 hours.
1300 - 1000 °C at 800 °C/hr.
1000 - 0 °C at 250 °C/hr.

Figure 5.1. Firing schedules for $BaTiO_3$ pressed powder specimens.

In addition, in order to produce reproducable specimens, it was foun
necessary to (i) tightly control the firing temperature-time cycle of the furnace and (ii) reduce the amount of impurities diffusing into the samples during the firing cycle to a negligible amount.

Manual operation of the furnace was quickly found to be unacceptable for control of perposes and a programmed potentiometric comparator control unit was utilized to operate the furnace during firing. The unit was mechanically programmed, using shaped cams, and the output of a Pt-PtRh thermocouple placed in the chamber of the furnace was used as a measure of firing temperature.

The device was found to be excellent in operation but in some cases, particularly those in which large quantities of pressed specimens were fired together, some variation in quality was noticed between those samples fired at the far end of the furnace chamber and those at the end nearest the door.

It was presumed that temperature gradients existed along the length of the kiln and that these were responsible for the variations in fired quality. To test this theory, a number of small holes were drilled through the furnace walls along its length and thermocouples were inserted into the chamber.

Temperature gradients (see Figure 4.2) were found to exist along the length of the kiln during firing, although the effect was only severe over the half of the chamber nearest to the door. In all subsequent firings, the pressed powder samples were therefore fired at the far end of the chamber, usually within three inches of the back wall. The measuring thermocouple (in its protective sheath) was permanently placed at the centre of this area and the centre sample of each batch was arranged to be within ⅛" - ¼" of its tip at the start of each firing cycle.

It was during these test runs that the remarkable affinity of $BaTiO_3$ for most refractory materials was noticed, the material readily forming solid solutions with a large number of compounds. In an effort to reduce this effect, use was made of zirconia (ZrO_2) covered refractory batts, the normal industrial technique, but some reduction in this coating was noticed after firings. Several samples were investigated using an Electron Microprobe Analyser and diffused zirconia impurities were positively identified some 50µ. from the plane of contact. Eventually, Pt sheets were

[redacted]

For Conventional and Hydraulic Pressing

Material	Pressing Tons	Max.Temp. °C.	Cycle	Soak Period Mins.
1.2	5	1,300	A	5
1.2	7.5	1,300	A	5
1.2	10.0	1,300	A	5
1.2	12.5	1,300	A	5
1.2	15.0	1,300	A	5
1.2	5	1,200	A	5
1.2	5	1,250	A	5
1.2	5	1,300	A	5
1.2	5	1,350	A	5
1.2	5	1,400	A	5
1.2	5	1,300	B	5
1.2	5	1,300	B	30
1.2	5	1,300	B	60
1.2	5	1,300	B	120
1.2	5	1,300	B	180
1.2	5	1,300	B	360

Sample 1 - Industrial sample (Steatite Ltd.)
" 2 - Very high purity sample (E.S.P.I.Ltd.)

Figure 5.1. Summary of firing runs

5.2.2.2. Firing Runs

A complete range of $BaTiO_3$ test pieces were produced by firing sets of the pressed powder specimens, made earlier, over the two firing cycles A and B (Figure5.1).

For each firing,the four sets of pressed sample were placed together between platinum sheets. Each separate batch of samples consisted of two sets of ten conventionally pressed powder samples and two hydrostatically-pressed powder rods.

At no time during the firing period were any of differing sets of samples allowed to come into contact with one another,and after each firing cycle the platinum sheet was cleaned off and soaked in concentrated HCl.

5.2.2.3. Finishing Procedure

On completion of firing,all warped or cracked specimens were rejected. The rods were placed in plastic moulds and a polyester resin was poured over them. The moulds were transferred to an oven set at 60°C. and were left to cure.

On setting,the embedded rods were removed from the moulds and were cut into slices of approximately 1 mm. thickness using a water-cooled diamond impregnated cutting wheel. The thickness of each slice was measured with a micrometer to ensure that the faces were parallel and any suspect specimens were rejected. Each slice was then washed in distilled water and dried in the oven. The surface finish was found to be good.

5.3. APPLICATION OF ELECTRODES

There are many materials available which may be used as electrodes with ceramic bodies but,for most experimental purposes,evaporated electrodes, fired on metal electrodes or conducting paints are generally preferred.

In order to determine which type of material was most suitable for the purposes of the project,a trial of various electrodes was made (see section 4. The initial selection of materials was made on the basis of ease of application, availability and working temperature range,but the final choice depended upon the electrical behaviour of the electrodes over repeated cycling of the specimen through the entire temperature range expected.

To test specific electrode behaviour, doped $BaTiO_3$ test pieces, in batches of five, were coated with various electrode materials and were cycled from -70°C. to 200°C. and back for five complete cycles. Dielectric measurements were made at the end of each cycle and each specimen was examined for damage. Evaporated metal, in particular gold, was found to be both physically and electrically superior to all other types of electrode material, the metal vapour penetrating all open pores in the ceramic surface during coating, thereby ensuring good electrical contact.

Gold electrodes of this type were used throughout the project. No unforeseen difficulties occurred during this time.

5.4. ELECTRICAL MEASUREMENTS

The electrical properties of five samples from each batch of test specimens were measured over the temperature range -70° to 150°C. The results were averaged over the five samples in each set to obtain figures representative of the batch as a whole.

Measurements in the lower temperature range (-70° to 20°C.) were made with the sample holder placed in a cryostat (Section 4.8.2), the samples themselves being immersed in methyl alcohol. The cryostat temperature was controlled by the small heating resistor and individual measurements were taken only when thermal equilibrium had been reached, this usually occurring approximately five minutes from the time of alteration of the supply to the resistor, the methyl alcohol being stirred at intervals.

To obtain readings in the upper portion of the range, the sample holder and its glass envelope was simply placed in a heat controlled oven (Section 4.8.2.2. No liquid medium was used to surround the samples because silicone oil, one of the few suitable high temperature materials available for this purpose, was found to lift off the evaporated metal electrodes at high temperatures. As before, for a particular temperature setting, measurements were only taken when thermal equilibrium had been reached in the sample holder.

5.4.1. Measurement of Low Stress Relative Permittivity

The low stress capacitance of each sample was measured over the stated temperature range using a 0.1% Marconi Universal bridge. Graphs of sample capacitance against thickness were plotted for each set of readings and the average relative permittivity was calculated in each case.

5.4.2. Measurement of High Stress Relative Permittivity

Hysteresis loops were displayed on a C.R.O. using a modified Sawyer Tower Circuit (Section 4.8.5). The traces obtained were recorded on either Polaroid film or the trace storage facility of the oscilloscope.

The co-ordinates of the oscilloscope were calibrated from the circuit parameters and the necessary measurements for the calculation of permittivity were taken from the traces.

Measurements were taken over the complete range of temperature.

5.4.3. The Display of Switching Transients and the Measurement of Resistivity

The current transient due to the application of a d.c. voltage to a ferroelectric material may be observed using the circuit shown in Figure 4.8.6. Using a somewhat higher series resistance, the resistivity of the sample may be calculated from voltage measurements taken when steady-state conditions have been reached in the circuit.

For the purpose of the project, a 10kΩ resistor was used for the observation of switching transients in the test samples produced. D.C. voltages were applied to the samples, both a positive and negative wave being used for each step. The amplitude of the current transient and the time which it took to reach its steady state value were measured and the corresponding graphical relationships drawn.

To measure the resistivity of each sample, the 10kΩ resistor was replaced witha 1MΩ standard resistor and the process repeated. Measurements of supply and resistor voltage were taken at steady conditions using a digital voltmeter.

The value of resistivity for each sample was calculated and the results were averaged for each batch of specimens.

5.5. PHYSICAL ANALYSIS

In order to determine the mechanisms of grain growth in polycrystalline $BaTiO_3$ it was necessary to observe the structure of representative samples from each batch of fired test specimens.

5.5.1. Density

The absolute density of each test piece was determined either by the direct measurement of sample dimensions and weight or, in the cases where this was not possible, by the technique of water displacement. The results were averaged to obtain a representative figure for each separate batch of fired samples.

5.5.2. Porosity

Porosity plays an important part in the structural changes which take place in ceramic bodies during firing and, in order to elucidate the mechanisms of the changes which occur in $BaTiO_3$ ceramics, it was found necessary to examine the pore structure of each representative sample in detail.

Each sample was prepared for microscopic investigation by lapping flat specific areas of the material with metallurgical wheels. Each face was given a final polish with diamond paste and the specimen was mounted on a glass slide.

Then using an Image Analyser, the pore size, shape and area were measured for various regions of each polished face, the frequency of occurence of specific pore sizes being noted for each particular case.

5.5.3. Crystal Structure

The crystal structure of ceramic bodies is easily revealed by observing polished etched specimens of the materials with an optical microscope. In the case of polycrystalline $BaTiO_3$, the most satisfactory etchant was found by trial and error to be concentrated HCl.

In order to show the crystal structure of the individual test pieces, the specimens prepared for porosity measurements were placed in a beaker containing enough concentrated HCl to cover them completely. They were then left to etch for 8 minutes and at the end of this time were removed from the acid, washed in distilled water and dried.

Each specimen was mounted on a glass slide and placed under a microscope for structural examination.

Measurement of particular structures were taken directly from the monitor screen of the Image Analyser used for the porosity measurements. The crystal structure of most samples were clearly observed, the domain configurations present in the large crystals being clearly visible.

5.4.4. X-ray Crystallography

An attempt was made to measure the size of constituent crystallites of the hydrostatically pressed specimens using x radiation.

The specimens were placed in an x-ray goniometer and, using Ni filtered Cr radiation the intensity and angle of various particular refracted x-ray beams were measured.

From these measurements, it was possible to identify each specimen as tetragonal $BaTiO_3$ at room temperature and give some measure of the average crystallite size in each case.

5.4.5. Electron Microscopy

Several of the etched specimens were observed with a reflection electron microscope.

Samples with pronounced domain structure were observed and an attempt was made to locate antiparallel c domains in sample H.E.16, which had previously been subjected to a switching pulse of 126 volts for two minutes.

5.4.6. Spectrographic Analysis

The pressing powders and two hydraulically-pressed samples were subjected to spectrographic analysis to determine their respective impurity contents. (see Appendix 4).

The fired samples were first ground to a fine powder. These powders and the original materials were then individually mixed with very pure graphite paste and placed in separate graphite tubes.

The usual process of spectrographic analysis ensued and qualitative and quantitative estimations of the respective impurity contents were made.

CHAPTER 6

6. STRUCTURAL STUDIES

The structural study detailed here for $BaTiO_3$ ceramics was made using polished etched specimens taken from the batches of fired test pieces later used for electrical measurement.

It was immediately noticed that the pores existing within the material could be classified into four groups according to size:-

(i) large pores(50-80 microns diameter)scattered at random through the material

(ii) medium sized pores(approximately 25 microns diameter)scattered at random through the material

(iii) small pores(8-16 microns in diameter).

(iv) micropores(2-4 microns in diameter).

Pores in groups (iii) and (iv) can be randomly distributed throughout the material,but are usually subjected to ordering processes.

No such classification of individual crystals or groups of crystals was possible.

6.1. VARIATION OF PRESSING FORCE

6.1.1. Hydrostatically Pressed Pure Grade Material

6.1.1.1. Overall Density

The fired density of the pure grade samples rose linearly from 4.71 gm/ml at 5.0 tons force to 5.36 gm/ml at 15.0 tons force (Figure 6.1).

6.1.1.2. Pore Structure

Initially, a small number of pores from groups 1 and 2 were seen to be scattered at random through the material. A large number of spherical concentrations of group 3 pores were also observed at regular intervals. The concentrations ranged from 8.0 to 30 microns in diameter. Microporosity (group 4) was scattered at random through the remaining material,although several small spherical concentrations were noticed in some areas.

As the pressing force increased,the numbers of group 1 and 2 pores decreased rapidly,none being observed in samples formed by forces greater than 12.5 tons. The concentrations of group 3 pores,however,grew in size and eventually covered the whole of the centre area of the material.

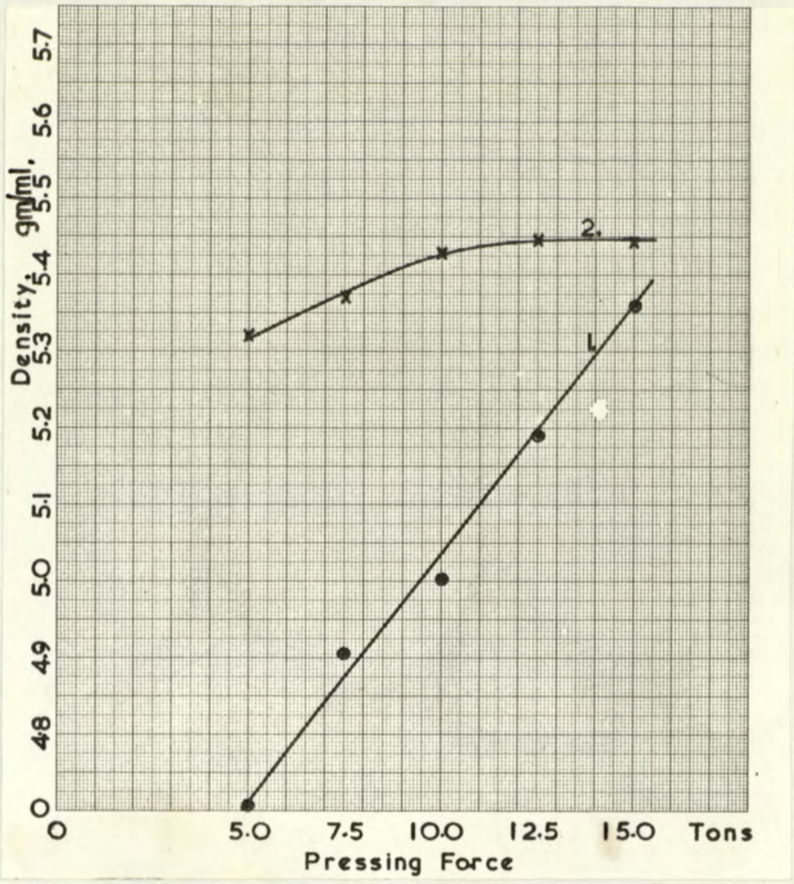

Fig 6.1. Density v Pressing Force. 1 Pure Grade.
2 Commercial Grade.

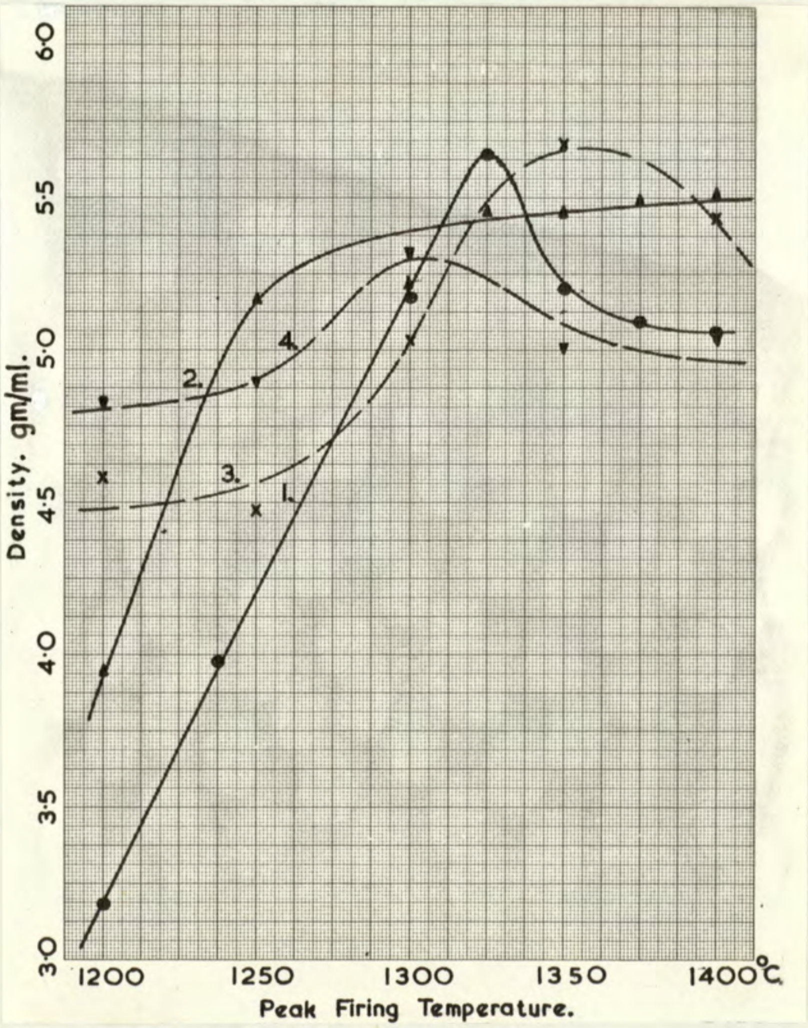

Fig 6.2. Density v Firing Temperature. 1 P.Grade (H).
2 C.Grade(H); 3 P.Grade (C). 4 C.Grade (C).

a. 5 tons.f.

b 7·5 tons.f.

c. 10 tons.f.

d. 12·5 tons.f.

e. 15 tons.f.

Photomicrographs 1.

Material Pure Grade. (H).

Firing Constant 1300 C 5 mins.

Subject Pore Structure with increasing pressing force.
(x160)

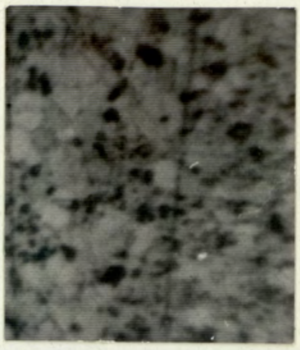

a. 5 tons.f.

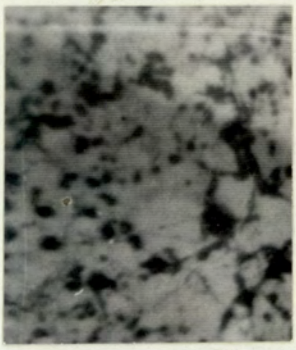

b 7·5 tons.f.

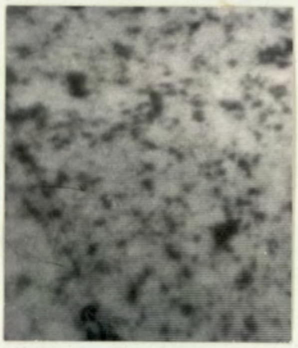

c. 10 tons.f.

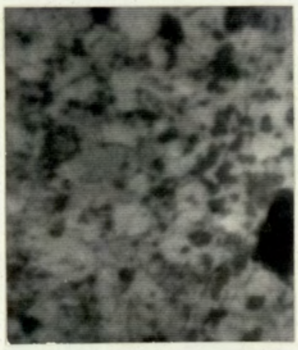

d. 12·5 tons.f.

e. 15 tons.f.

Photomicrographs 2 .
Material Pure Grade (H).
Firing Constant 1300 C 5 mins.
Subject Crystal Structure with increasing pressing force.
(x590)

The boundaries of the pore concentrations were always very distinct, percentage porosity changing abruptly from 11-15% outside the concentrations to 20% immediately inside. No change in porosity was detected across the diameter of any concentration investigated although in many cases a group 1 or 2 pore formed the geometric centre of the group.

(See photomicrographs 1(a) - (e)).

6.1.1.3. Crystal Structure

The individual crystals forming the material were seen to be regular in size and shape. Many of the crystals were twinned having a characteristic butterfly shape.

Bonding between adjacent crystals took two forms:

(i) bonding between the corner or minor flat of one crystal and the major flat of another

or (ii) bonding between major flats

The first, bonding by thin sinter bridges, was found to be most prevalent at lower compaction pressures. When the pressure was raised the proportion of bonds across major flats increased and large dense crystal masses were formed.

(See photomicrographs 2(a) - (e)).

6.1.2. Hydrostatically Pressed Commercial Grade Material

6.1.2.1. Density

The fired density of the commercial grade material rose linearlly with increasing pressure, but at 10.0 tons force the rate of increase slackened rapidly and a maximum density of 5.44 gm/ml was reached at 12.5 tons. No increase in density could be achieved beyond this point.

(See Figure 6.1).

6.1.2.2. Pore Structure

A number of group 1 pores were present in the material and were spaced at intervals of 100-220 microns. Concentrations of group 3 pores also occurred, but each was centred on one of the many inclusions present in the material. The inclusions were oblong or cusplike in shape and usually had a group 1 pore associated with one particular side of their mass. The volume fraction of porosity inside the concentrations was found to be in the range 30-35%.

a. 5 tons.f.

b 7·5 tons.f.

c. 10 tons.f.

d. 12·5 tons.f.

e. 15 tons.f.

Photomicrographs 3 ,

Material Commercial Grade.(H).

Firing Constant 1300 C 5 mins.

Subject Pore Structure with increasing pressing force.
(x160)

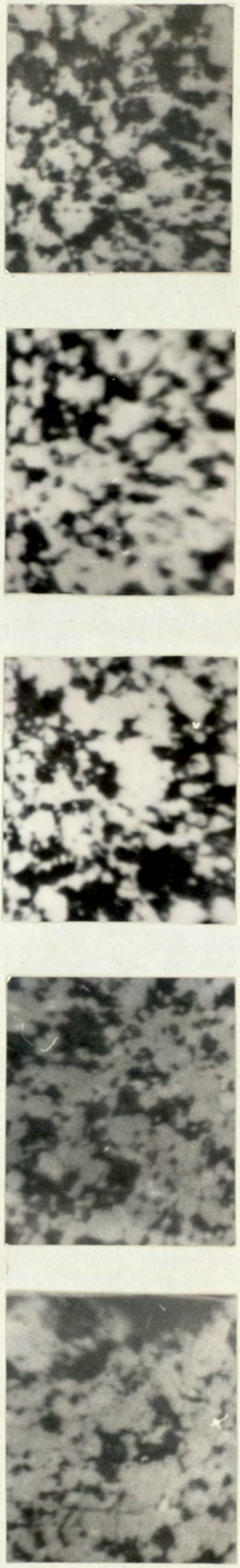

a. 5 tons.f.

b 7·5 tons.f.

c. 10 tons.f.

d. 12·5 tons.f.

e. 15 tons.f.

Photomicrographs 4.

Material Commercial Grade (H).

Firing Constant 1300 C 5 mins.

Subject Crystal Structure with increasing pressing force.
(x590)

With increasing force,the pore concentrations were seen to enlarge and eventually join together and fill the whole central area of the material.

(See photomicrographs 3(a) - (e)).

6.1.2.3. Crystal Structure

Initially,the material is composed of a mass of well defined crystals (3-4 microns in diameter)but occasionally numbers of small crystals were observed also.

In most cases intercrystal bonding was effected by the formation of narrow sinter bridges,but a small number of crystals in groups of 2-10 were found to have bonded across their major flats. As the pressing force was raised,there was an increasing tendancy for more groups of crystals to join together to form very dense areas and the proportion of sinter bridges present fell off rapidly.

Eventually,numbers of crystals of varying sizes began to join in groups and large crystal masses were formed.

(See photomicrographs 4(a) - (e)).

6.2. VARIATION IN FIRING TEMPERATURE

6.2.1. Hydrostatically Pressed Pure Grade Material

6.2.1.1. Density

The density of the fired specimens rose slowly at first,but at firing temperatures between 1,250° and 1,300°C. (the onset of vitrification) the rate of densification increased quickly and a maximum value of 5.65 gm/ml was reached at a firing temperature of 1,355°C. Above this point,the value of fired density fell away rapidly.

(See Figure 6.2).

6.2.1.2. Pore Structure

The samples fired below 1,300°C could not be polished satisfactorily for complete optical examination, the material being in a somewhat powdery state. It was possible,however, to make a partial study of the samples fired at 1,250°C. A number of group 1 and 2 pores were scattered at random throughout the samples; no concentrations of pores were distinguished. A

a. 1300°C. centre.

b. 1350°C. centre.

c. 1350°C. surface.

d. 1400°C. centre.

e. 1400°C. surface.

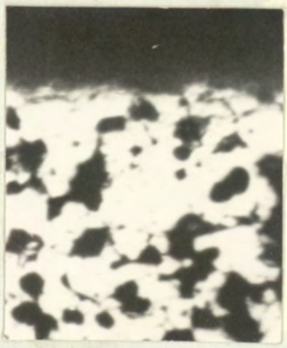

Photomicrographs. 5
Material Pure grade (H)
Firing Varying Temperature, Constant time
Subject Pore structure (x160)

light-coloured area was observed at the surface of the specimens.

On firing the material at or above 1,300°C, the pores within the material partially regrouped, the group 3 pores forming spherical concentrations 30-80 microns in diameter.

The pores forming the concentrations were very regular in size and of circular shape. The boundaries of the spheres were very distinct, the pore volume fraction changing abruptly from approximately 20% outside the spheres to 31% immediately inside them.

With increasing firing temperature, the pore concentrations and the pores within them grew in size until finally, with samples fired at 1,400°C., the central mass of each specimen was filled with pores 8-20 microns in diameter, the proportion of microporosity (group 4) within the material having become virtually negligible.

The external surfaces of the samples had, in the meantime, become increasingly dense with increasing firing temperature.

(See photomicrographs 5(a) - (e)).

6.2.1.3. Crystal Structure

No crystal structure was observed with samples fired below 1,300°C, although a distinct white area was observed at the surface of the specimens.

At firing temperatures of 1,300°C, the crystal structure of the material had developed sufficient for optical observation. The individual crystals within the material were regular in size and shape; a large proportion of the crystals were bonded together by thin sinter bridges. Large single isolated crystals (8 microns in diameter) were occasionally observed within the structure.

With increasing temperature, the structure of the material changed rapidly. The sinter bridges generally enlarged, eventually becoming the major faces of the individual crystals. Large crystal masses (12-21 microns in diameter) were formed, some microporosity (group 4) becoming trapped at the crystal boundaries.

The dense masses at the external surfaces were found to consist of large individual crystals and these grew disportionately with increasing firing

a. 1300°C. centre.

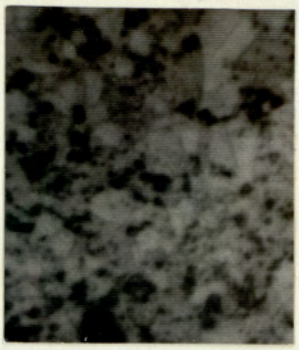

b. 1350°C. centre.

c. 1350°C. surface.

d. 1400°C. centre.

e. 1400°C. surface.

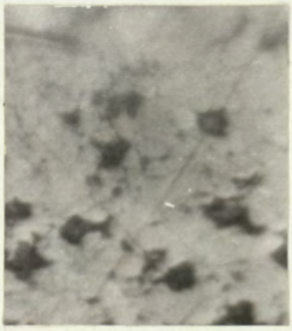

Photomicrographs. 6

Material Pure grade (H)

Firing Varying Temperature, Constant Time.

Subject Crystal structure. (x590)

temperature most becoming very large later, the boundaries of their constituent crystals vanishing completely. A number of these crystals contained large pores (group 3) but the microporosity (group 4) had disappeared completely.

Finally, although many of the crystals were still growing regularly and were now approximately 18 microns in diameter, there was an increasing tendency for adjacent crystal to coalesce and disproportionate grain growth was occurring throughout the mass of the material.

Many complex 'a' domain structures now became visible within the larger crystals and crystal masses and, in some cases, individual domains were seen to extend over 11 or more original crystals a total length of 86 microns. In every case, the width of the 'a' domains was found to be 1 micron.

(See photomicrographs 6(a) - (e)).

6.2.2. Hydrostatically Pressed Commercial Grade Material

6.2.2.1. Density

The material densified slowly at first, but above firing temperatures of 1,250°C the rate increased rapidly reaching a maximum of 5.31 gm/ml for a firing temperature just above 1,300°C. The fired density then dropped rapidly beyond this point.

(See Figure 6.2).

6.2.2.2. Pore Structure

The pore structure of the commercial-grade material differed somewhat from that of the pure material. As before, vitrification occurred somewhere between 1,250° and 1,300°C, but concentration of group 3 pores was now centred on the inclusions present in the material. The concentrations were not therefore so regular in size and shape as those present in the pure-grade material.

A dense surface layer began to form at the exterior surfaces of the samples. The porosity in this region was found to be reduced to 11% by volume.

As the firing temperature was increased, the pore concentrations increased in size and areas of the surface layer became even more dense.

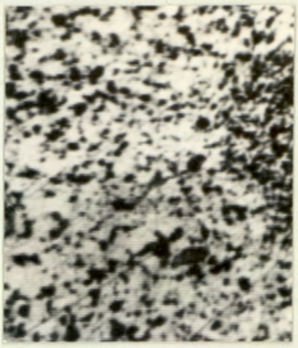

a. 1300°C. centre.

b. 1350°C. centre.

c. 1350°C. surface.

d. 1400°C. centre.

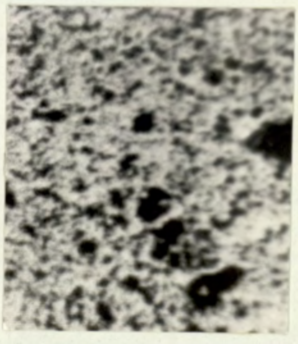

e. 1400°C. surface.

Photomicrographs.	7
Material	Commercial grade (H)
Firing	Varying Temperature, Constant Time.
Subject	Pore Structure. (x160)

a. 1300°C. centre.

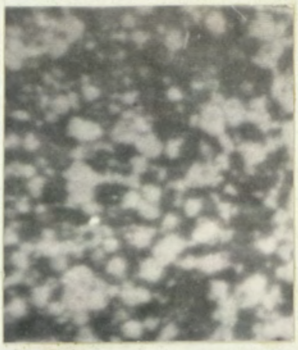

b. 1350°C. centre.

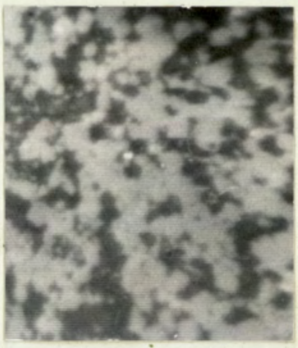

c. 1350°C. surface.

d. 1400°C. centre.

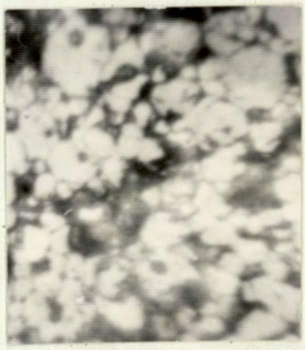

e. 1400°C. surface.

Photomicrographs. 8
Material Commercial grade (H)
Firing Varying temperature, Constant time.
Subject Crystal Structure. (x590)

Eventually the pore concentrations covered the whole of the central area, except in the area immediately next to the surface layer(where the structure was extremely disjointed). Microporosity (group 4) within the central area was considerably reduced.

(See photomicrographs 7(a) - (e)).

6.2.2.3. Crystal Structure

The crystal structure of the material developed just below 1,300°C. firing temperature. Crystals within the material were seen to be of regular shape,but varied in size and the majority were joined to each other by means of thin sinter bridges.

As the firing temperature was raised,disproportionate crystal growth occurred at the surface of the specimens and complex 'a' domain structures were observed within individual crystals.

Crystals in the interior of the specimens showed an increasing tendency to coalesce and form large dense masses,but a large quantity of microporosity remained at the crystal boundaries during this process and large homogeneous crystals did not form in quantity.

(See photomicrographs 8(a) - (e)).

6.2.3. Conventionally Pressed Pure Grade Material

6.2.3.1. Density

The values of fired density are seen to increase linearly with increasing firing temperature until a maximum value of 5.63 gm/ml is reached at a firing temperature of 1,325°C. Above this temperature the value of density drops away rapidly,but at higher temperatures this rate of fall slackens considerably.

(See Figure 6.2).

6.2.3.2. Pore Structure

Vitrification occurs between 1,250° and 1,300°C. Some very large pores (group 1) are present,but many are distorted, assuming eliptical form. A number of pore concentrations form from large groups of group 3 and 4 pores. Some surface densification is apparent.

As the firing temperature was increased,the concentrations of group 3

a. 1300°C (i) centre.

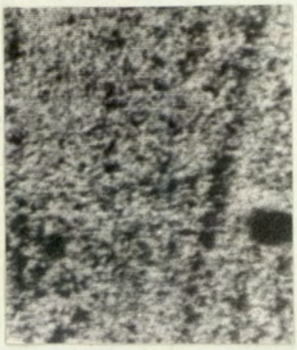

b. 1325°C (i) centre

(ii) surface.

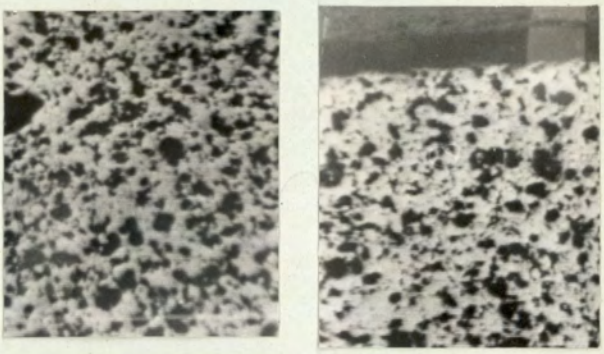

c. 1350°C (i) centre.

(ii) surface.

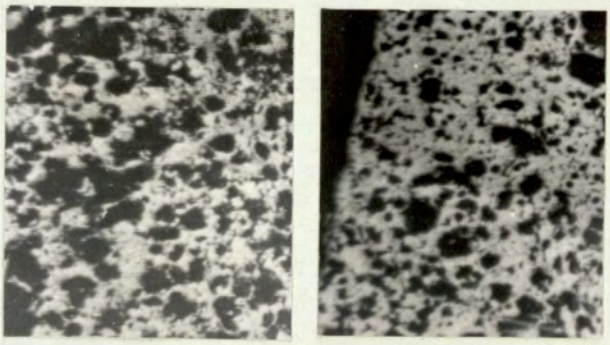

d. 1375°C (i) centre.

(ii) surface.

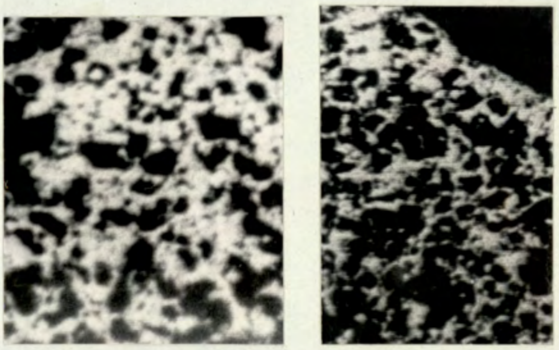

e. 1400°C (i) centre.

(ii) surface.

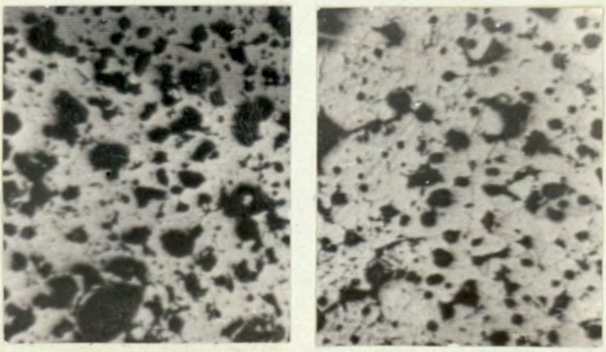

Photomicrographs. 9 .

Material. Pure grade (C)

Firing. Varying Temperature.

Subject. Pore Structure. (x160)

a. 1300°C (i) centre.
(x295)

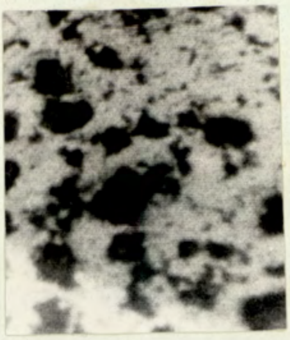

b. 1325°C (i) centre
(ii) surface.

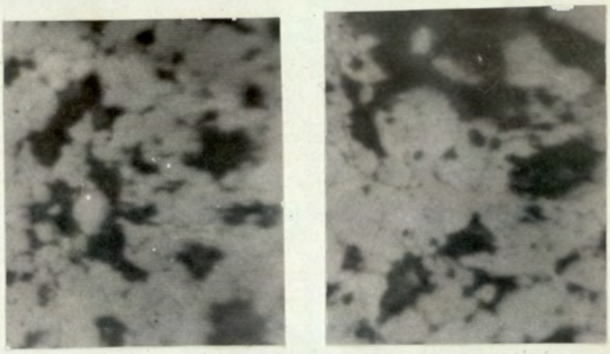

c. 1350°C (i) centre.
(ii) surface.

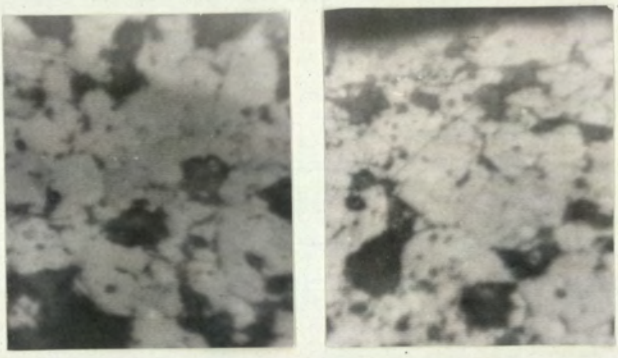

d. 1375°C (i) centre.
(ii) surface.

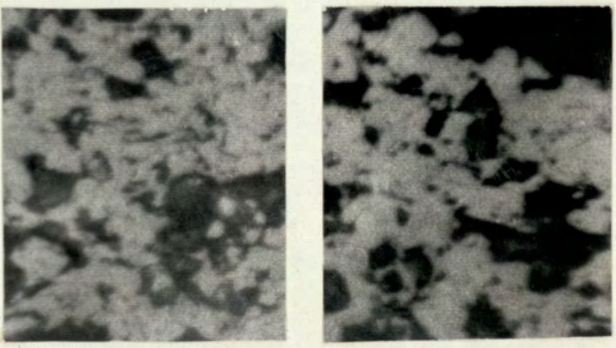

e. 1400°C (i) centre.
(ii) surface.

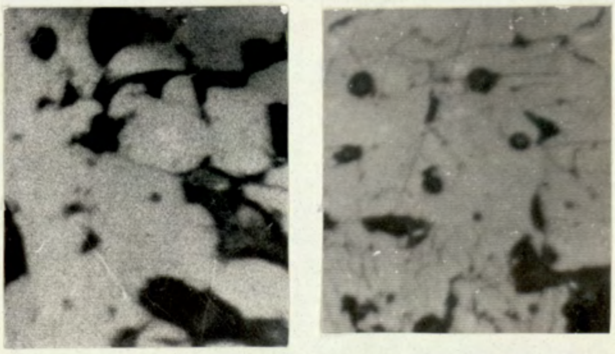

Photomicrographs. 10
Material. Pure grade (C)
Firing. Varying Temperature.
Subject. Crystal Structure. (x590)

pores grew in size and gradually joined with each other.

Finally, the central area of the samples was completely filled with group 3 pores and microporosity (group 4) was negligible in quantity.

(See photomicrographs 9(a) - (e)).

6.2.3.3. Crystal Structure

Crystals in the central mass of the material fired to 1,300°C were regular in size and were bonded by means of small sinter bridges. Small groups of two or three crystals were occasionally found within the matrix and, as the firing temperature increased these groups increased in number and size.

The crystals forming at the surface are seen to be growing disproportionately with respect to those at the centre.

All the larger crystals within the material fired at 1,400°C were found to exhibit complex 'a' domain structure.

(See photomicrographs 10(a) - (f)).

6.2.4. Conventionally Pressed Commercial Grade Material

6.2.4.1. Density

The fired density of material increases quickly with increasing firing temperature. Between 1,250°C. and 1,300°C, the rate of increase in density slackens and the characteristic proceeds at a reduced rate, the density reaching a value of 5.5 gm/ml at 1,400°C.

(See Figure 6.2).

6.2.4.2.

Vitrification was seen to occur at approximately 1,250°C, when small isolated groups of crystals were seen to bond together and form a definite structure. The pores present in the material at that time belonged to groups 1 and 2.

As the temperature was increased, large numbers of group 4 pores became apparent. These moved towards the inclusions in the material, forming large irregular masses.

When the temperature had reached 1,350°C, 50% of these pores had coalesced to form group 3 pores, many of which grouped immediately behind a dense surface

a. 1300°C (i) centre.

b. 1325°C (i) centre

(ii) surface.

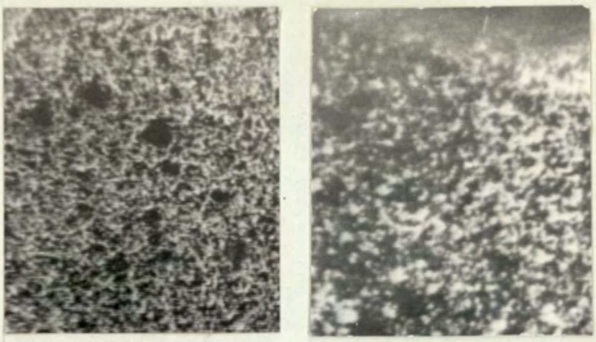

c. 1350°C (i) centre.

(ii) surface.

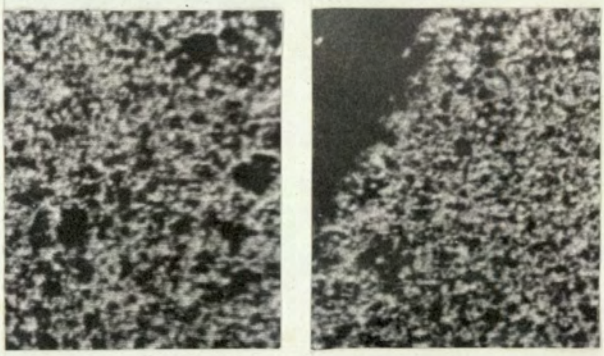

d. 1375°C (i) centre.

(ii) surface.

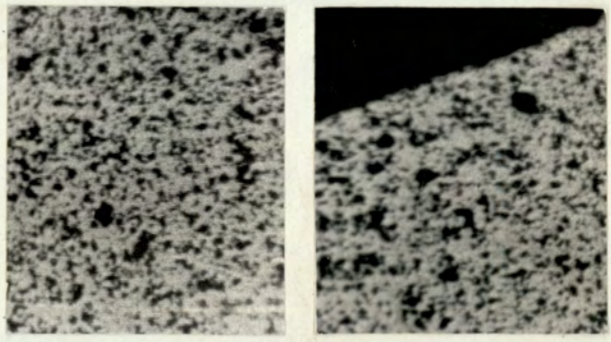

e. 1400°C (i) centre.

(ii) surface.

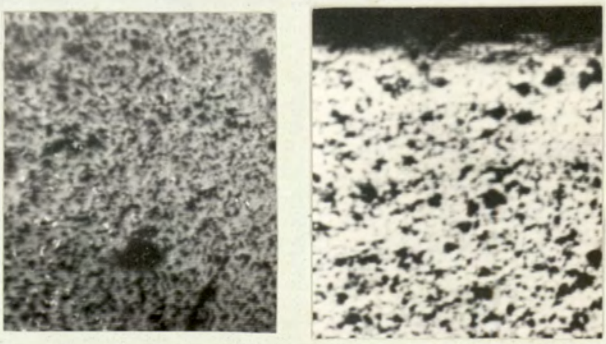

Photomicrographs. 11 .

Material. Commercial grade (C)

Firing. Varying Temperature.

Subject. Pore Structure. (x160)

a. 1300°C (i) centre.

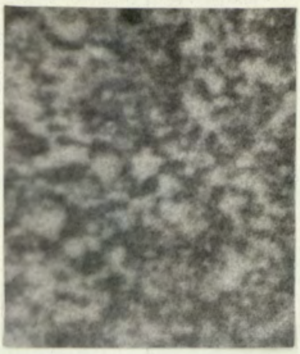

b. 1325°C (i) centre
(ii) surface.

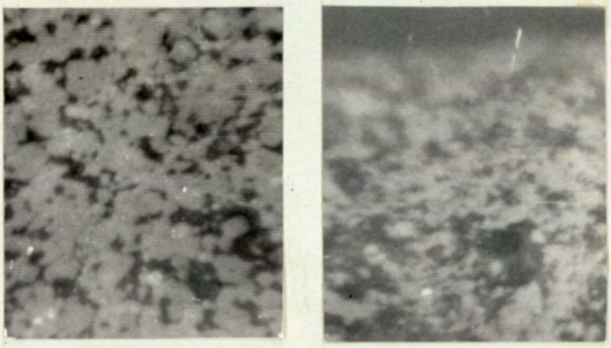

c. 1350°C (i) centre.
(ii) surface.

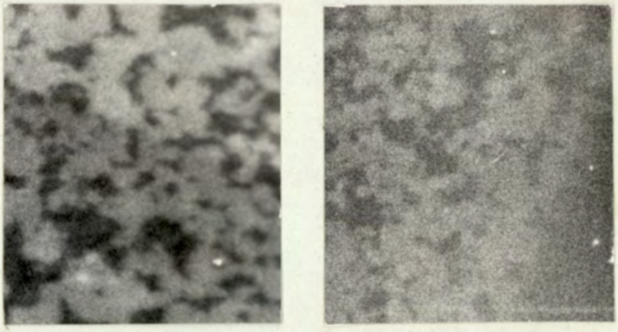

d. 1375°C (i) centre.
(ii) surface.

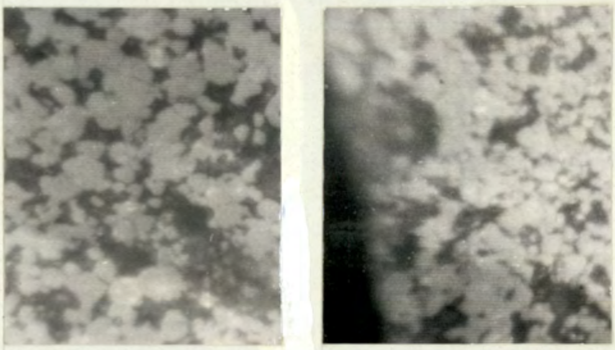

e. 1400°C (i) centre.
(ii) surface.

Photomicrographs. 12.
Material. Commercial grade (C)
Firing. Varying Temperature.
Subject. Crystal Structure. (x590)

layer which had been forming as the temperature increased. The crystal structure in the area of the pores became extremely distorted for some depth into the sample.

Further increase in temperature served only to increase the numbers of group 3 pores and decrease the group 4 pores and at 1,400°C, the change was almost complete, the whole central mass of the material being filled with group 3 pores.

(See photomicrographs 11(a) - (f)).

6.2.4.3. Crystal Structure

Small isolated groups of crystals were seen to form in the material fired to 1,250°C. On raising the firing temperature to 1,300°C, the complete mass of material vitrified and the structure was readily observed after etching.

The groups of crystals within the matrix were small (4 microns) and had the common double form, adjacent crystals bonding together with thin sinter bridges.

Increasing temperature was seen to increase the tendency for groups of crystals to form together into dense masses. Densification of the external surface layers was also becoming apparent at this point and secondary crystallization was observed in this area.

Later large crystal masses began to form from crystals of varying size and, in many cases complex domain patterns were clearly visible within these regions, the (a) domains forming across the visible grain boundaries.

At these temperatures, disproportionate grain growth within the surface layers became increasingly apparent.

(See photomicrographs 12(a) - (f)).

6.3. VARIATION IN FIRING TIME

6.3.1. Hydrostatically Pressed Pure Grade Material

6.3.1.1. Density

The density of the material rose quickly with increasing firing time and a maximum of 5.47 gm/ml was reached after one hour and ten minutes.

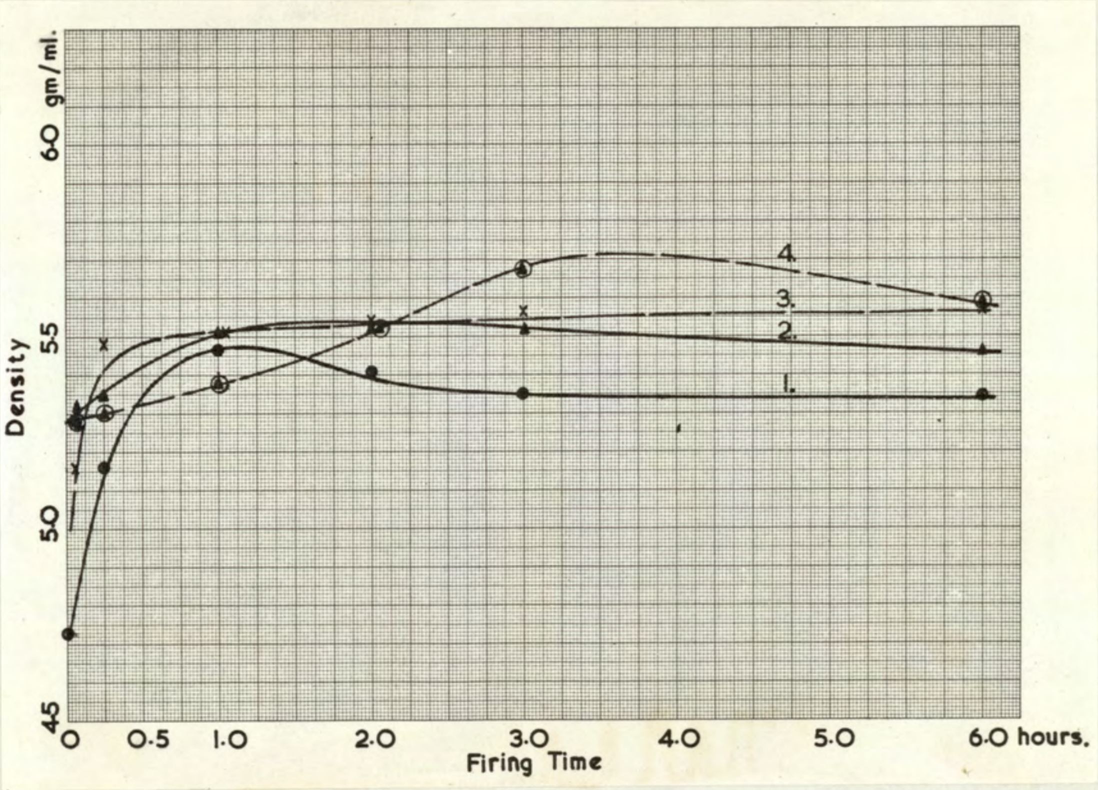

Fig 6.3. Density v Firing Time.

1 Pure Grade (H).
2 Commercial Grade (H).
3 Pure Grade (C).
4 Commercial Grade (C).

a. 5 mins. (i) centre.

b. 1 hr. (i) centre.

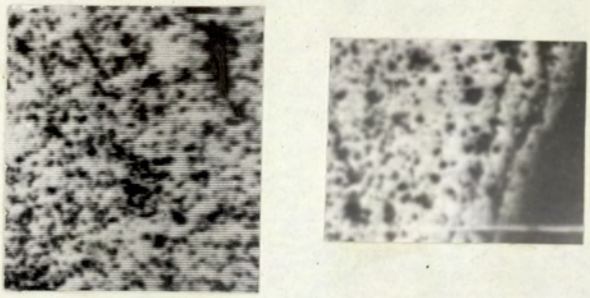

c. 2 hr. (i) centre.

(ii) surface.

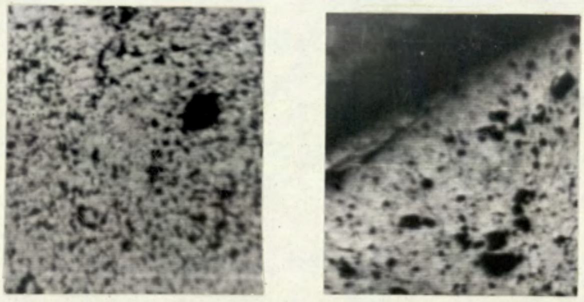

d. 3hr. (i) centre.

(ii) surface.

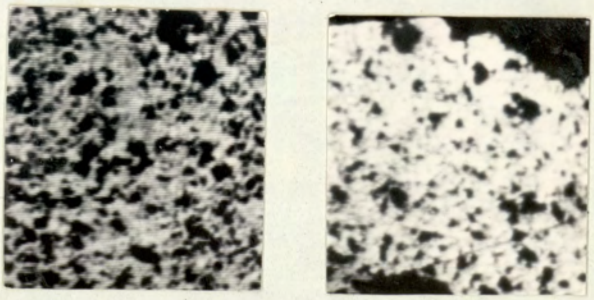

e. 6hr. (i) centre.

(ii) surface.

Photomicrographs 13.

Material. Pure Grade (H).

Firing. Varying Time.

Subject. Pore Structure, (x160).

The fired density values then fell slightly and after three hours total firing time, assumed a constant value of 5.4 gm/ml.

(See Figure 6.3)

6.3.1.2. Pore Structure

The samples fired for the shortest periods of time were found to contain numerous pore concentrations of the type already described and a small number of group 1 and 2 pores.

As the firing period was extended, the group 4 porosity lying between individual pore concentrations was found to have reduced in quantity and the pore concentrations to have increased in size, (from 8-30 microns diameter to 560-900 microns diameter).

Inevitably many of the concentrations then merged into one another and bands of pore concentrations 280-2,200 microns wide formed throughout the material. The band density was found to be constant at 35%, the constituent pores ranging from 14 to 28 microns in diameter.

The surface was found to have densified with increasing time and, after a firing period of six hours, the densified layer was found to have a thickness of between 100 and 140 microns and a volume percentage porosity of 11%. As in the case of materials fired in the higher temperature regions, the area immediately behind the surface layer was extremely disformed the percentage porosity reaching the value of the band structures.

(See photomicrographs 13(a) - (f)).

6.3.1.3. Crystal Structure

Initially, the individual crystals were regular in size and shape and were mutual bonded, except in a few isolated groups, by thin sinter bridges.

As the firing time increased, the crystals near the surface or in the immediate area of large pores began to grow in size and many more groups of crystals began to bond together to form dense masses, (10-15 microns in diameter) within the central area of the material. At this point (one hour) many of the individual grains still present in most of the specimens were still visible.

However, there was an increasing tendency for more larger groups to form from the individual grains and, after six hours, a large number of crystal

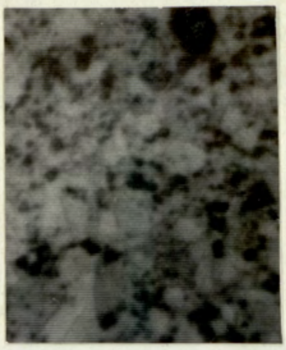

a. 5 mins. (i) centre.

b. 1 hr. (i) centre.

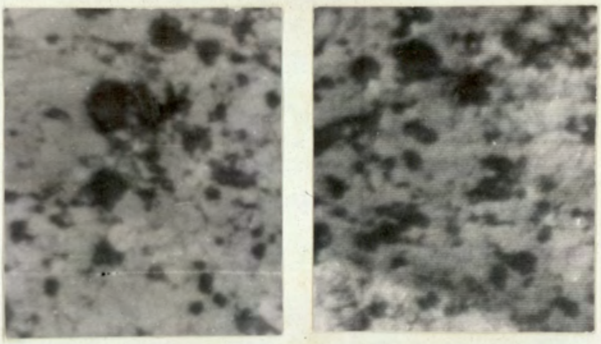

c. 2 hr. (i) centre.

(ii) surface.

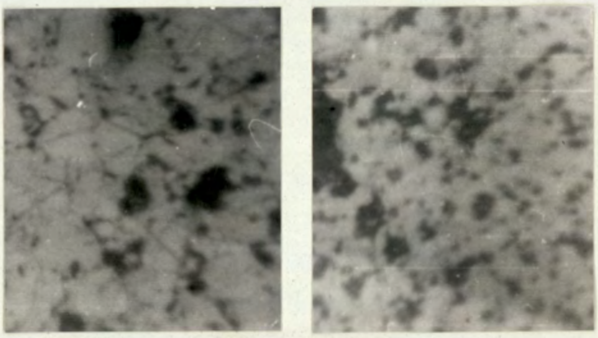

d. 3hr. (i) centre.

(ii) surface.

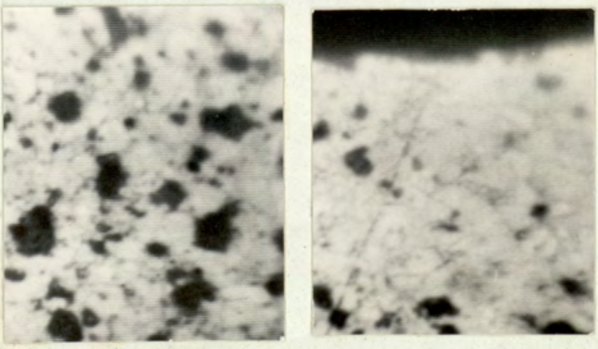

e. 6hr. (i) centre.

(ii) surface.

Photomicrographs 14.

Material. Pure grade (H)

Firing. Varying Time.

Subject. Crystal Structure (x590)

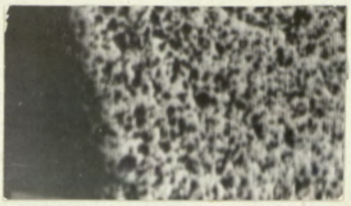

a. 5 mins. (i) centre.

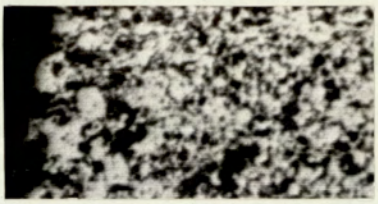

b. 1 hr. (i) centre..

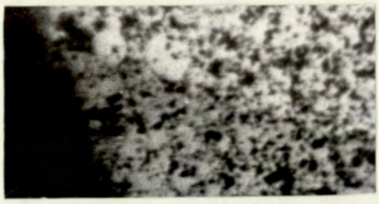

c. 2 hr. (i) centre.

(ii) surface.

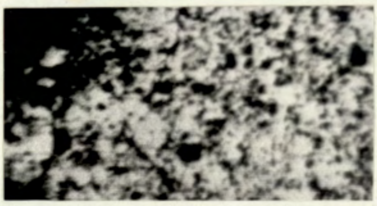

d. 3hr. (i) centre.

(ii) surface.

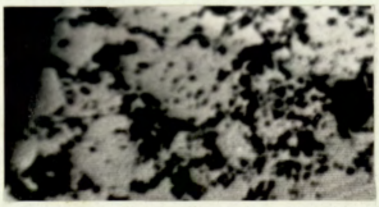

e. 6hr. (i) centre.

(ii) surface.

Photomicrographs15.
Material. Commercial Grade (H).
Firing. Varying Time.
Subject. Pore Structure (x160).

masses (20-30 microns in diameter) had formed.

The dense surface layer contained many very large crystals and complex domain structures were usually observed within these crystals.

(See photomicrographs 14(a) - (f)).

6.3.2. Hydrostatically Pressed Commercial Grade Powder

6.3.2.1. Density

The density of the material rose quickly with increasing firing time and a maximum of 5.54 was reached after 1½ hours. The fired density of the samples then fell slowly with increasing firing time, reaching a value of 5.46 gm/ml after six hours.

(See Figure 6.3).

6.3.2.2. Pore Structure

A number of large group 1 pores spaced at intervals of 100-200 microns were present within the material. Concentrations of group 3 pores occurred in quantity also, these being centred on the inclusions present within the material.

With increasing firing time, the pore concentrations enlarged and eventually filled much of the central mass of the samples.

A dense surface layer began to form after one hour firing time and as the firing time was increased, this layer increased in depth.

The boundary of the layer was a distinct pore concentrations forming immediately behind the densified area. The pore volume fraction was constant at 11% within the layer.

Finally, many of the group 3 pore concentrations began to coalesce at their centres, the proportion of group 1 and 2 pores increasing appreciably. In some cases, small concentrations (28 microns in diameter) of these larger pores occurred.

(See photomicrographs 15(a) - (f)).

6.3.2.3. Crystal Structure

The material was composed of a mass of well defined crystals (3-4 microns in diameter), but occasionally numbers of smaller crystals were seen also.

a 5 mins. (i) centre.

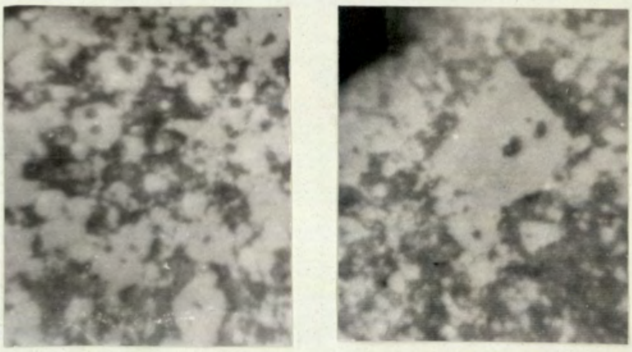

b. 1 hr. (i) centre.

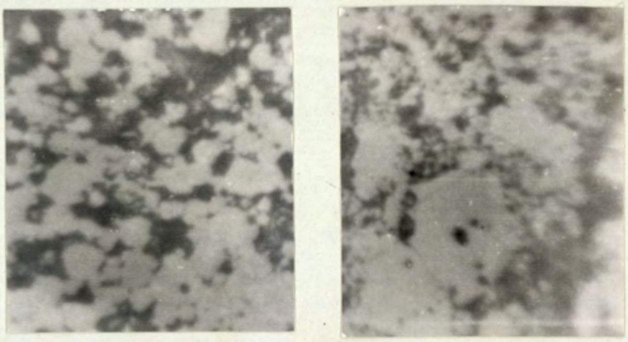

c. 2 hr. (i) centre.
(ii) surface.

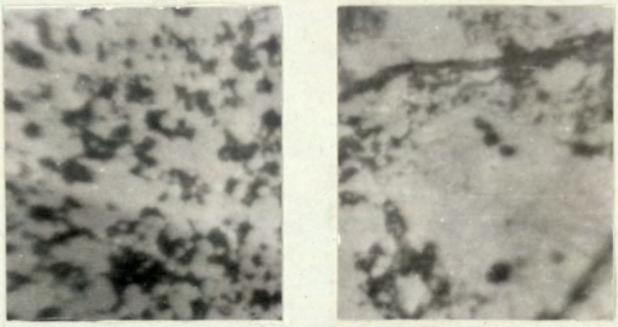

d. 3hr. (i) centre.
(ii) surface.

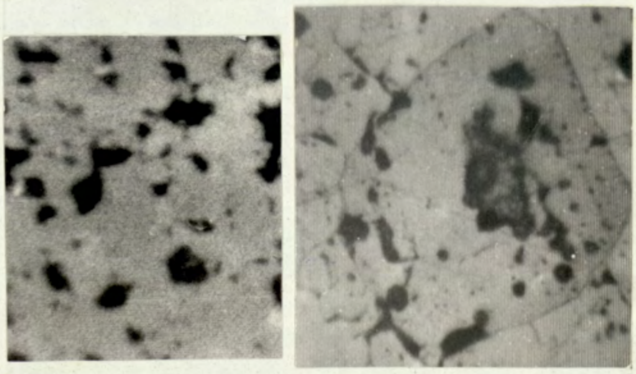

e. 6hr. (i) centre.
(ii) surface.

Photomicrographs 16.
Material. Commercial Grade. (H).
Firing. Varying Time.
Subject. Crystal Structure. (x590)

a 5 mins. (i) centre.

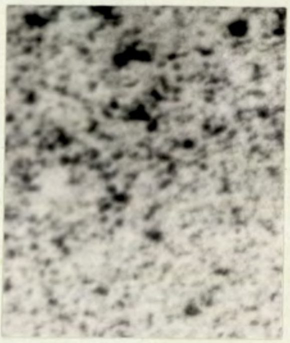

b. 1 hr. (i) centre.

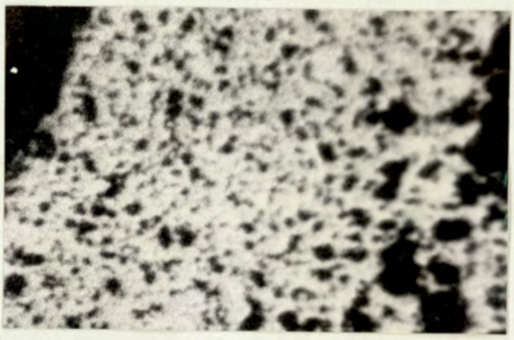

c. 2 hr. (i) centre.

(ii) surface.

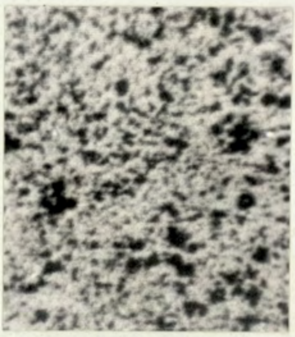

d. 3hr. (i) centre.

(ii) surface.

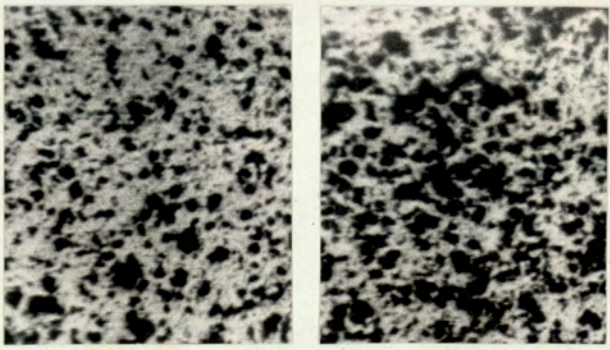

e. 6hr. (i) centre.

(ii) surface.

Photomicrographs17.

Material. Pure grade (C)

Firing. Varying Time.

Subject. Pore Structure (x160)

Normal intercrystal bonding was seen to take the form of thin sinter bridges, only a small proportion of crystals being bonded across their major faces.

With increasing firing time, large groups of 10-30 individual crystals began to form both at the surface and within the samples, the surface groups forming much more quickly than those at the centre (after one hour at the surface and two hours at the centre).

In all cases, the individual crystals within the groups were visible until all microporosity within the groups had disappeared. At first, the larger crystals showed normal butterfly configuration, but later a more complex (a) domain structure began to appear, particularly in those crystals at the surface of the samples.

Finally, most of the central and all of the surface layers were made up from large individual crystals showing complex (a) domain structure. The domain structure was apparently arranged at random as no preferential domain orientation was observed.

(See photomicrographs 16(a) - (f)).

6.3.3. Conventionally Pressed Pure Grade Material

6.3.3.1. Density

The fired density of the samples was found to rise quickly from 5.16 gm/ml at five minutes firing time to a constant value of 5.56 gm/ml after two hours.

(See Figure 6.3).

6.3.3.2. Pore Structure

As with samples pressed hydrostatically, the material contained concentrations of group 3 and 4 pores, but in addition many very large irregular group 1 pores were present.

With increasing firing time the pore concentrations increased in size and a number of group 1 and 2 pores formed. Many of these larger pores formed in rings of varying diameter, which eventually joined and formed extremely large group 1 pores.

Very dense areas were seen to form at the major surfaces of the samples and it was usual for a large number of small pores to form immediately behind these layers.

(See photomicrographs 17(a) - (f)).

a. 5 mins. (i) centre.

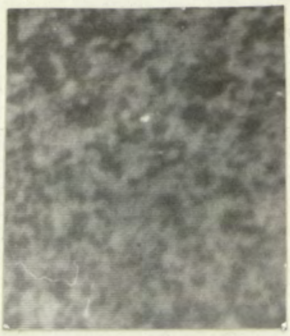

b. 1 hr. (i) centre.

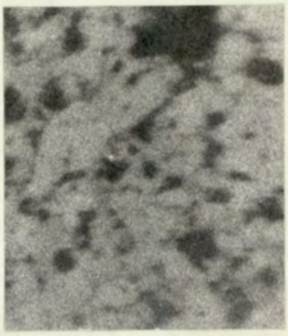

c. 2 hr. (i) centre.

(ii) surface.

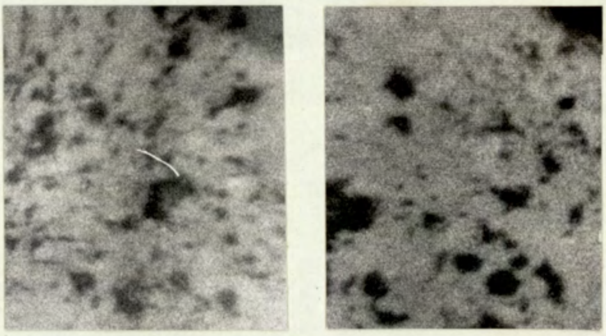

d. 3hr. (i) centre.

(ii) surface.

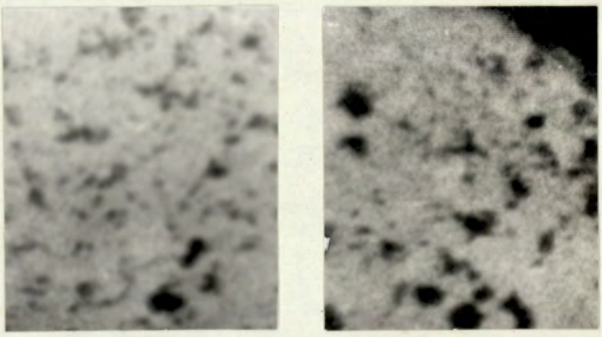

e. 6hr. (i) centre.

(ii) surface.

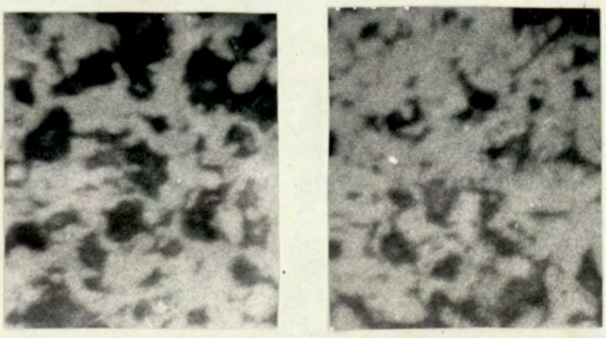

Photomicrographs 18.
Material. Pure Grade (C)
Firing. Varying Time.
Subject. Crystal Structure (x590)

6.3.3.3. Crystal Structure

The individual crystals within the material were of regular size and shape. Small groups of two or three crystals were occasionally found within the matrix and as the firing time increased, the number and size of these groups increased.

The groups of crystals within the surface layers of the samples grew disproportionately with time, some very large individual crystals being formed after two hours firing time.

Eventually, many large dense crystal masses were formed within the centre of the specimens. The constituent crystals of these masses retained their identity until all microporosity within the groups had disappeared.

Complex (a) domain structures were observed within these groups and within the crystals in the surface layers.

(See photomicrographs 18(a) - (f)).

6.3.4. Conventionally Pressed Commercial Grade Material

6.3.4.1. Density

The fired density of the samples rose slowly from an initial value of 5.28 gm/ml (for a five minute firing) to a maximum of 5.72 gm/ml (for a 3½ hour firing). The density then fell away slowly to a value of 5.58 (after six hours firing time).

(See Figure 6.3).

6.3.4.2. Pore Structure

Specimens fired for short periods were found to contain not only a number of concentrations of group 4 pores and a few group 1,2 and 3 pores, as before, but also a few very large irregular group 1 pores at specific areas within the material.

These particular pores were found to be sited at areas of differential compaction (i.e. at 45° to the major axees of the sample or parallel to the major surfaces) and sometimes extended for considerable distances (0.5m.m.).

With increasing firing time the pore concentrations grew in size, some joining together to form large irregular masses.

Later, many of the concentrations coalesced to form group 1 and 2 pores set in circles of varying diameter. The proportion of group 2 and 3 pores

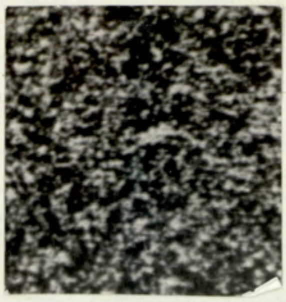

a. 5 mins. (i) centre.

b. 1 hr. (i) centre.

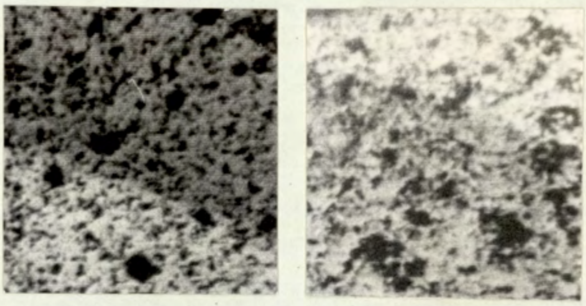

c. 2 hr. (i) centre.
(ii) surface.

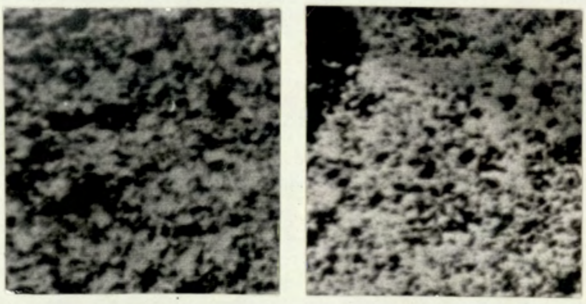

d. 3hr. (i) centre.
(ii) surface.

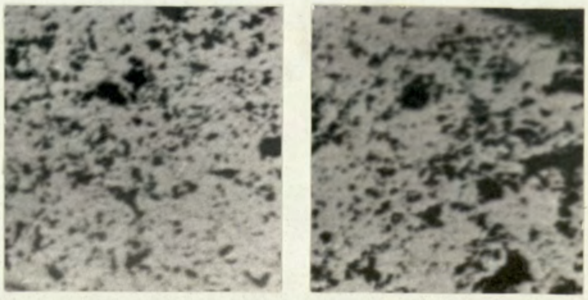

e. 6hr. (i) centre.
(ii) surface.

Photomicrographs 19.
Material. Commercial Grade (C)
Firing. Varying Time.
Subject. Pore Structure (x160)

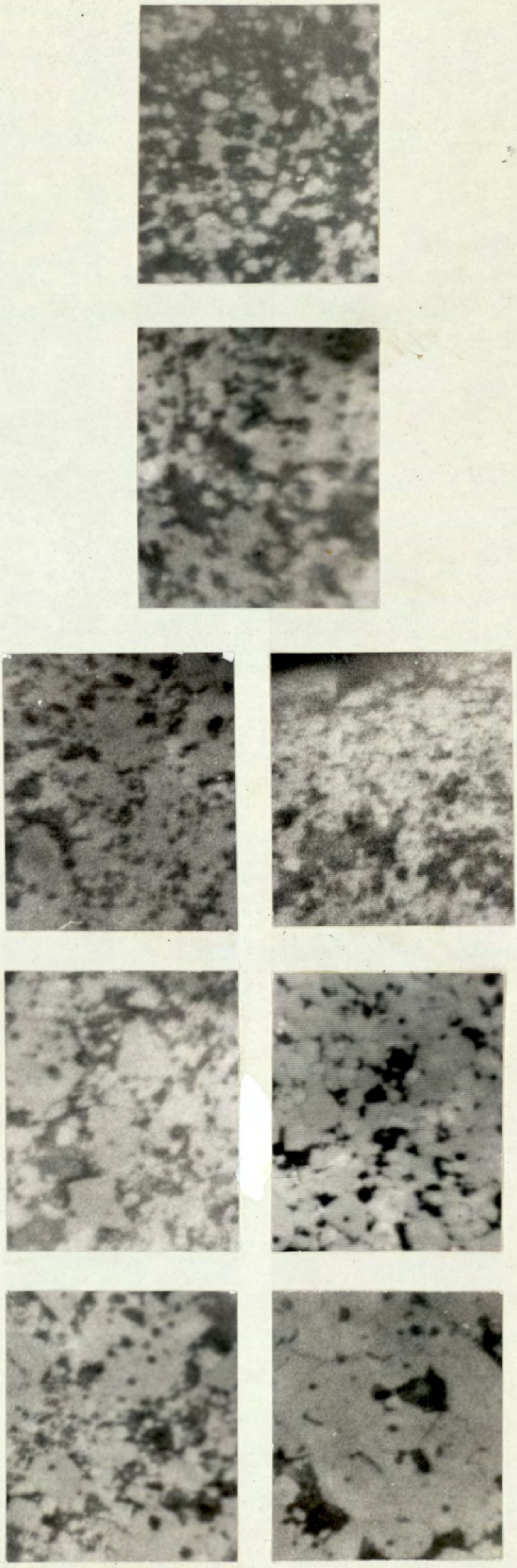

a. 5 mins. (i) centre.

b. 1 hr. (i) centre.

c. 2 hr. (i) centre.
(ii) surface.

d. 3hr. (i) centre.
(ii) surface.

e. 6hr. (i) centre.
(ii) surface.

Photomicrographs[20].

Material. Commercial grade(C)

Firing. Varying Time.

Subject. Crystal Structure (x590)

gradually increased, whilst the group 4 pores in the areas between concentration reduced in numbers.

At the surface of the samples the material became very dense, the thickness of the layer increasing with increasing firing time.

(See photomicrographs 19(a) - (f)).

6.3.4.3. Crystal Structure

The crystals within the material were seen to be composed of crystals (3-4 microns in diameter) of regular size and shape. There were also some crystals of smaller size present.

Many of the crystals were bonded together by means of thin sinter bridges, but small groups of crystals were also present in some areas.

As the firing time increased, more crystals bonded together in groups and, gradually interlinked chains of crystals (bonded across their major faces) formed throughout the central mass of the material.

Gradually, more groups of crystals began to form and the surface layers of the samples were found to be composed of very large crystals.

The crystal structure in the area behind the surface layer deteriorated rapidly, but in the central area the crystals forming the matrix were of regular size.

Finally, many very large dense crystalline areas were formed from masses of distinct crystals but, generally, the crystals were still of regular shape although of increased size.

Complex (a) domain structures were observed within the larger crystal masses, especially in those crystals within the surface layer. The smaller regular crystals were of the usual twinned butterfly shape.

(See photomicrographs 20(a) - (f)).

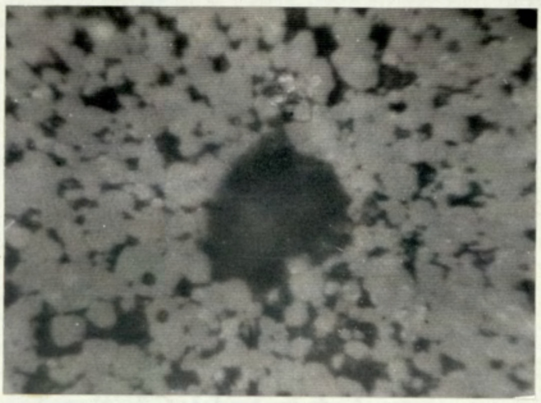

Photomicrograph 21. Pore Detail Sample No.HC14. (x590).

Photomicrograph 22. Crystal Structure Sample No.G. (x590).
Fired at 1300 °C 30 mins

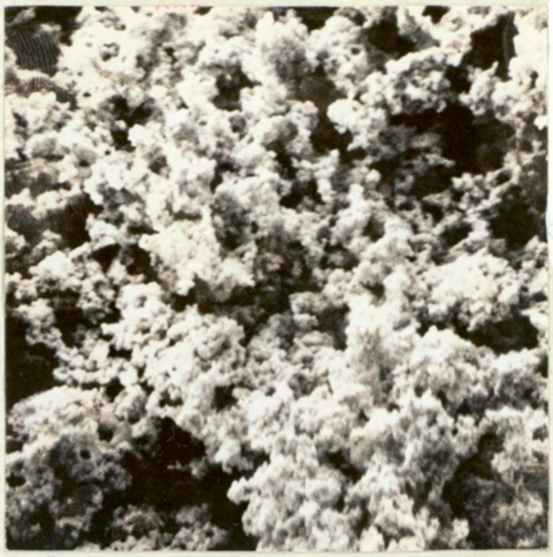

Electronmicrograph 1. Pure Powder. (x 1875).

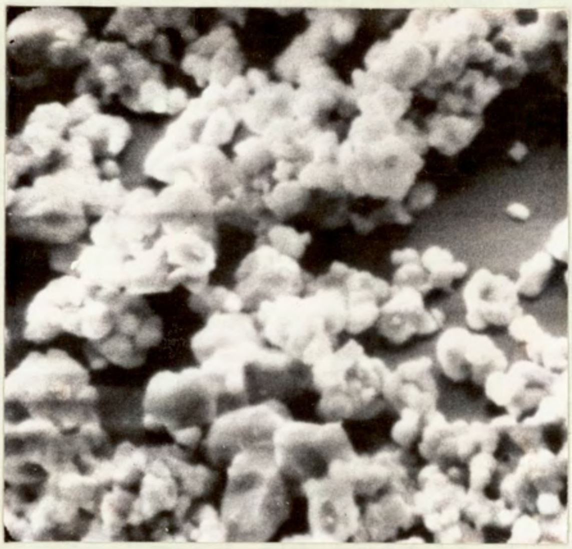

Electronmicrograph 2. Commercial Grade Powder. (x 5440).

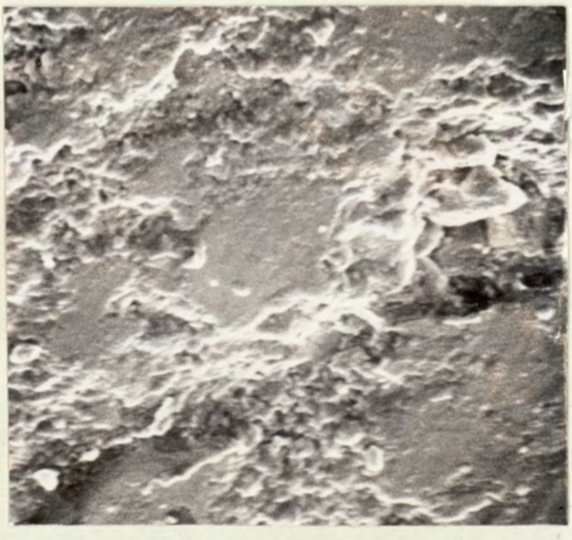

Electronmicrograph 3. Cut Surface Hydrostatically Pressed Specimen HE16. (x 1875).

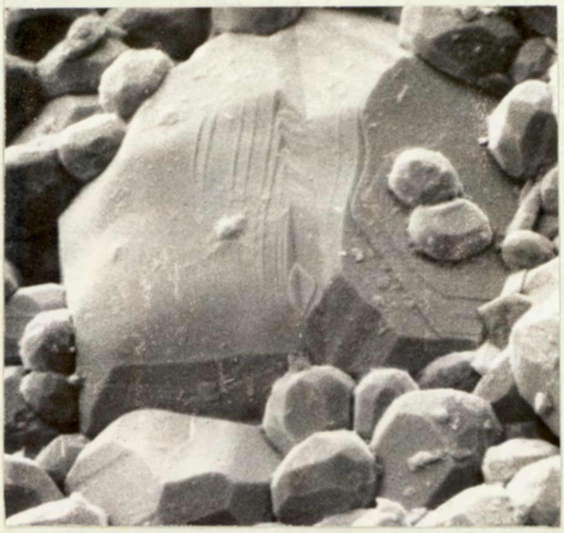

Electronmicrograph 4. SurfaceDetail Conventionally Pressed Specimen C.E.16. (x2325).

Electronmicrograph 5.Pore Structure Polished Surface Specimen HE16. (x1120).

Electronmicrograph 6.Pore Detail Sample HE16. (x5565).

Electronmicrograph 7. Crystal Structure Sample HE16. (x5500).

Electronmicrograph 8. Crystal Structure Sample HE16. Switched
120 V. d.c. 2 mins. (x5320).

CHAPTER 7

7. X-RAY STRUCTURAL STUDY

The size of the constituent crystallites within the samples was determined by x-ray diffraction technique. All the samples investigated were positively identified as the tetragonal polymorph of $BaTiO_3$. It was not, however, possible to make a study of the whole range of test pieces produced because of structural defects (warping, etc.) in the conventionally pressed samples, and measurements were therefore confined to the hydrostatically pressed specimens.

7.1. VARIATION IN PRESSING FORCE

7.1.1. Pure Grade Material

The crystallite size of these specimens was found to remain constant (at 0.206 microns) over almost the entire pressing range, only rising slightly when maximum force was applied.

(See Figure 7.1).

7.1.2. Commercial Grade Material

In contrast to the pure material, the commercial-grade specimens showed an initial decrease in crystallite size with increasing pressing force. Above 8 tons f, however, this tendency reversed and the crystallite size of the specimens rose quickly, reaching 0.370 microns at 15 tons applied force.

(See Figure 7.1).

7.2. VARIATION IN FIRING TEMPERATURE

7.2.1. Pure Grade Material

Between firing temperatures of 1,200°C and 1,250°C, the size of the constituent crystallites fell rapidly with increasing firing temperature, but beyond this region the rate of decrease slackened and an almost constant size was recorded for those materials fired above 1,350°C.

7.2.2. Commercial Grade Material

At first, the size of the constituent crystallites of the material fell quickly with increasing firing temperature (1,300°A per 100°C), but above 1,300°C the rate of decrease slackened considerably, and a crystallite size of 0.3250 microns was recorded for the test pieces fired at 1,400°C.

(See Figure 7.2).

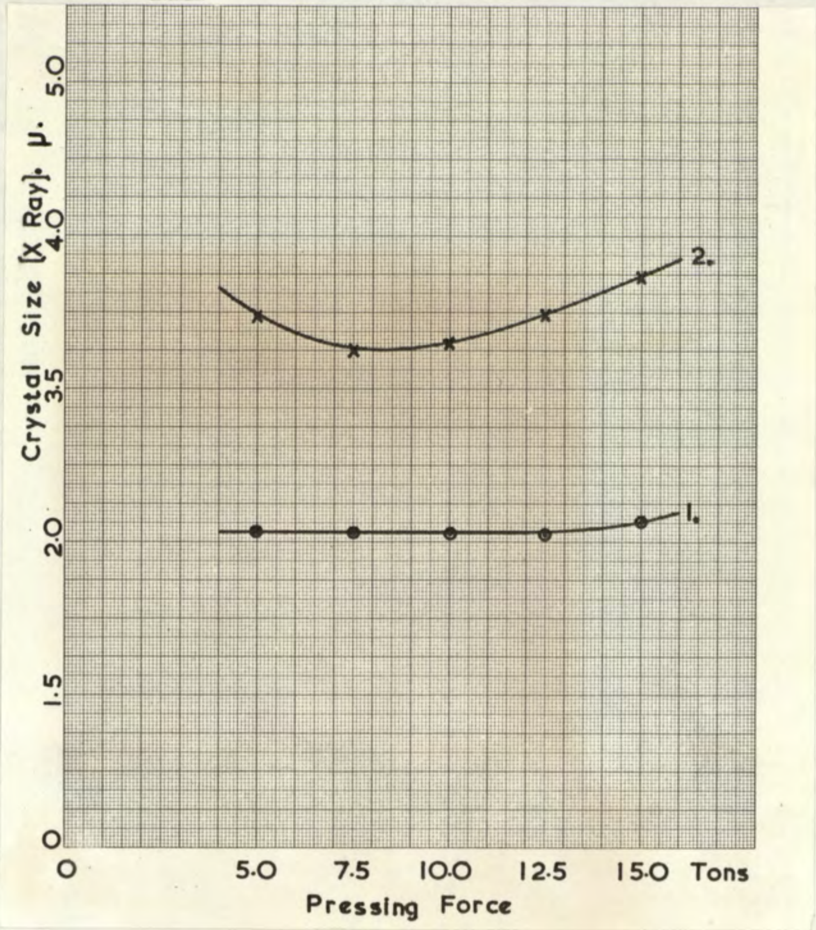

Fig 7.1. Crystal Size v Pressing Force. 1 Pure Grade.
2 Commercial Grade.

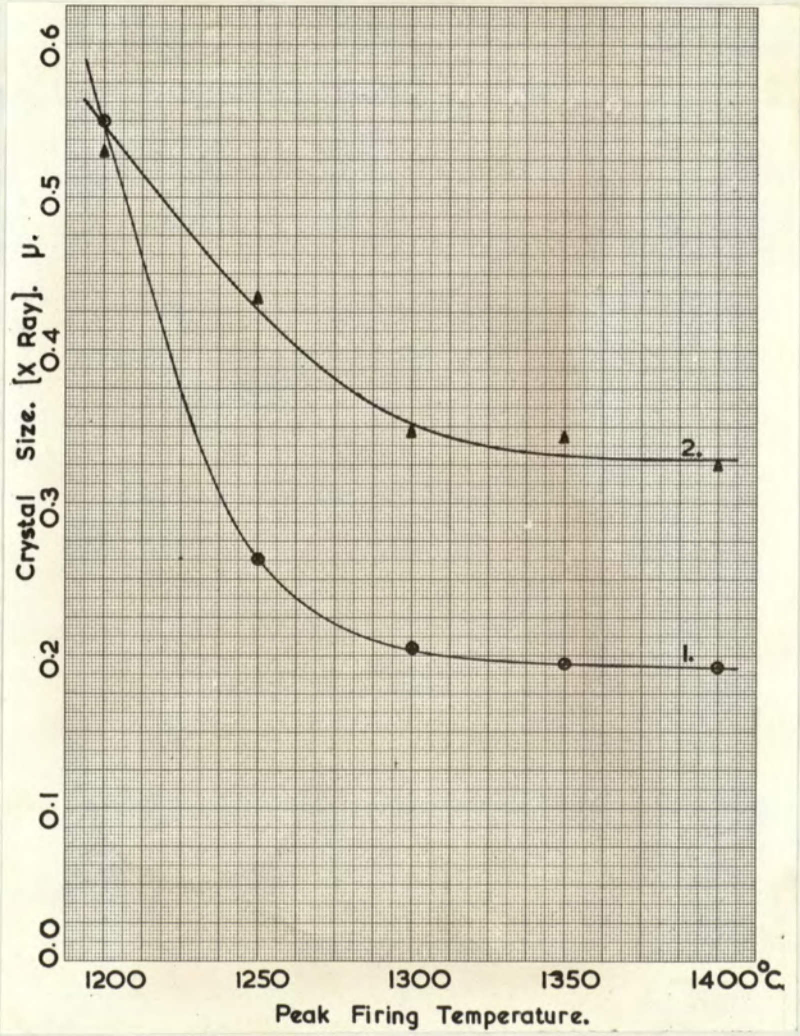

Fig 7.2. Crystal Size v Firing Temperature. 1 Pure Grade.
2 Commercial Grade.

7.3. VARIATION IN FIRING TIME

7.3.1. Pure Grade Material

Initially, the average size of the constituent crystallites was slightly above 0.2 microns. When the firing time was increased, the crystallite size rose slowly to a maximum of 0.33 microns for samples fired for a period of 2 hours 15 minutes. The crystallite size then began to decrease slowly and a constant value of 0.307 microns was reached for materials fired for periods longer than 4 hours.

(See Figure 7.3).

7.3.2. Commercial Grade Material

The size of the constituent crystallites of the commercial grade material remained constant at 0.348 microns for most of the firing range. It was only later (after 3 hours firing time) that any substantial change occurred, the particle size increasing to 0.402 microns.

(See Figure 7.3).

Figure 7.3. Crystal Size v. Firing Time. 1. Pure Grade. 2. Commercial Grade.

CHAPTER 8

8. DIELECTRIC STUDIES

The dielectric measurements recorded during the project were made over the temperature range -70° to 140°C. A specific characteristic for relative permittivity with varying temperature was observed for each batch of test pieces, but each took the general form of the corresponding characteristic for single crystal $BaTiO_3$. (Figure 2.2).

For the purposes of this project, the room temperature electrical properties were of primary interest and are recorded below. The variation of electrical properties in the region of the Curie Point were, however, also of great interest, as they are dependant upon crystal texture, and these are recorded separately (Chapter 9).

Specimen permittivity-temperature characteristics are shown in Figure 8.1.

8.1. VARIATION IN PRESSING FORCE

8.1.1. Hydrostatically Pressed Pure Grade Material

8.1.1.1. Relative Permittivity

The relative permittivity of specimens pressed at 5.0 tons was low (1077), but immediately above this point the value doubled (to 2150). Subsequent increase in pressing force produced a linear increase in relative permittivity at the rate of 110 per ton f.

(See Figure 8.2).

8.1.1.2. Resistivity

The resistivity of the test pieces decreased slowly with increasing pressing force, until a minimum point of $1.27 \times 10^6 \Omega m$ was reached at a point corresponding to an applied force of 11 tons f.

The value of resistivity then increased and reached a value of $6.7 \times 10^6 \Omega m$.

(See Figure 8.3).

8.1.2. Hydrostatically Pressed Commercial Grade Material

8.1.2.1. Relative Permittivity

At first the relative permittivity of the test pieces rose quickly with increasing pressing force, but later declined slowly after reaching a maximum

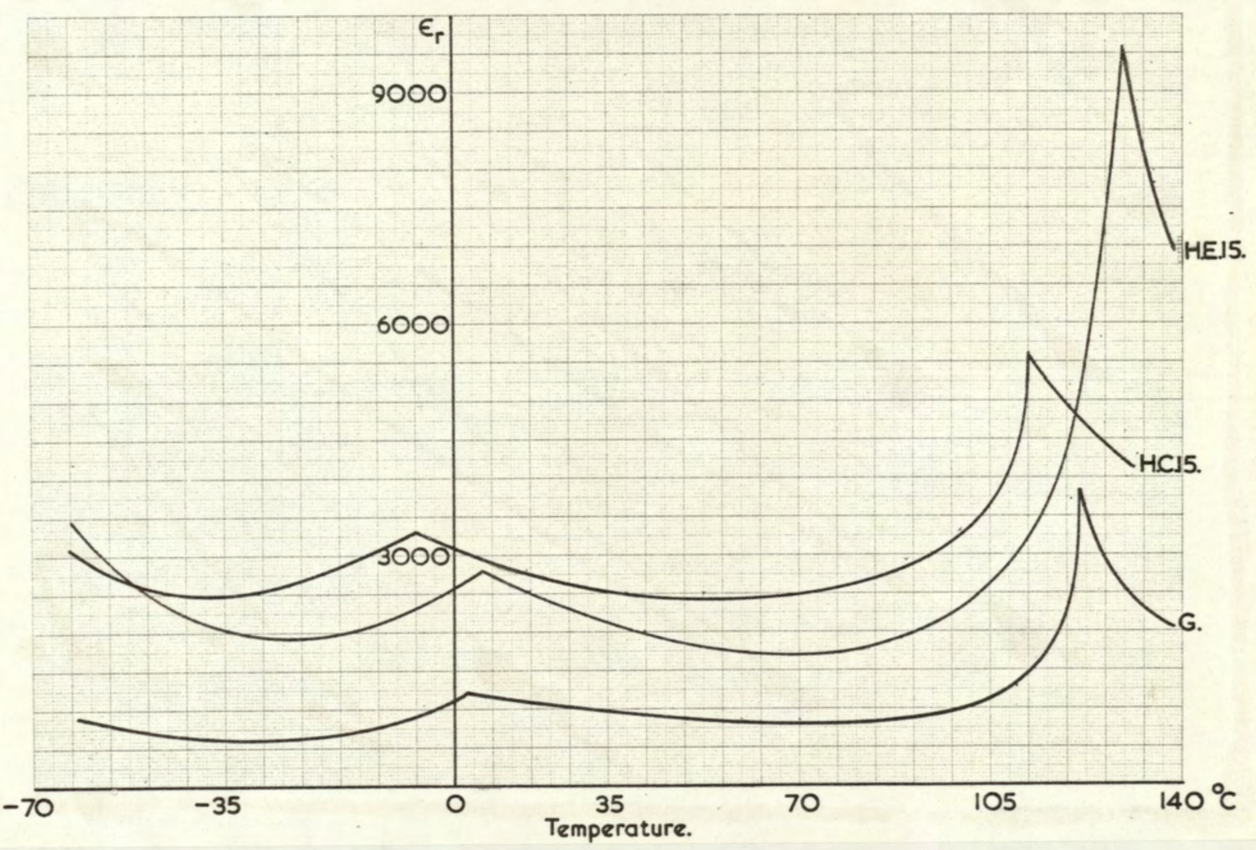

Fig 8.1. Typical Temperature-Permittivity Characteristics
Sample G. Coarse Grained 1300°C 1/2 hour.
Sample HE15 Pure Grade 1300°C 3 hours.
Sample HC15 Comm. Grade 1300°C 3 hours.

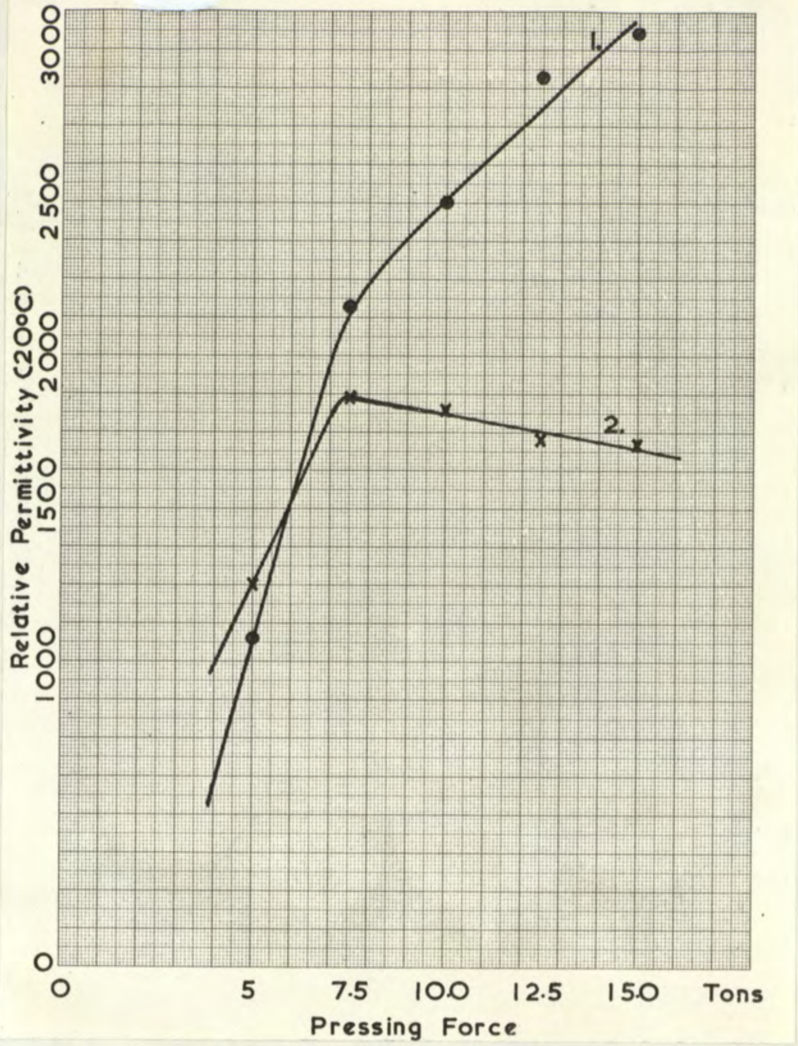

Fig. 8.2. ϵ_r v Pressing Force. 1 Pure Grade; 2 Commercial Grade.

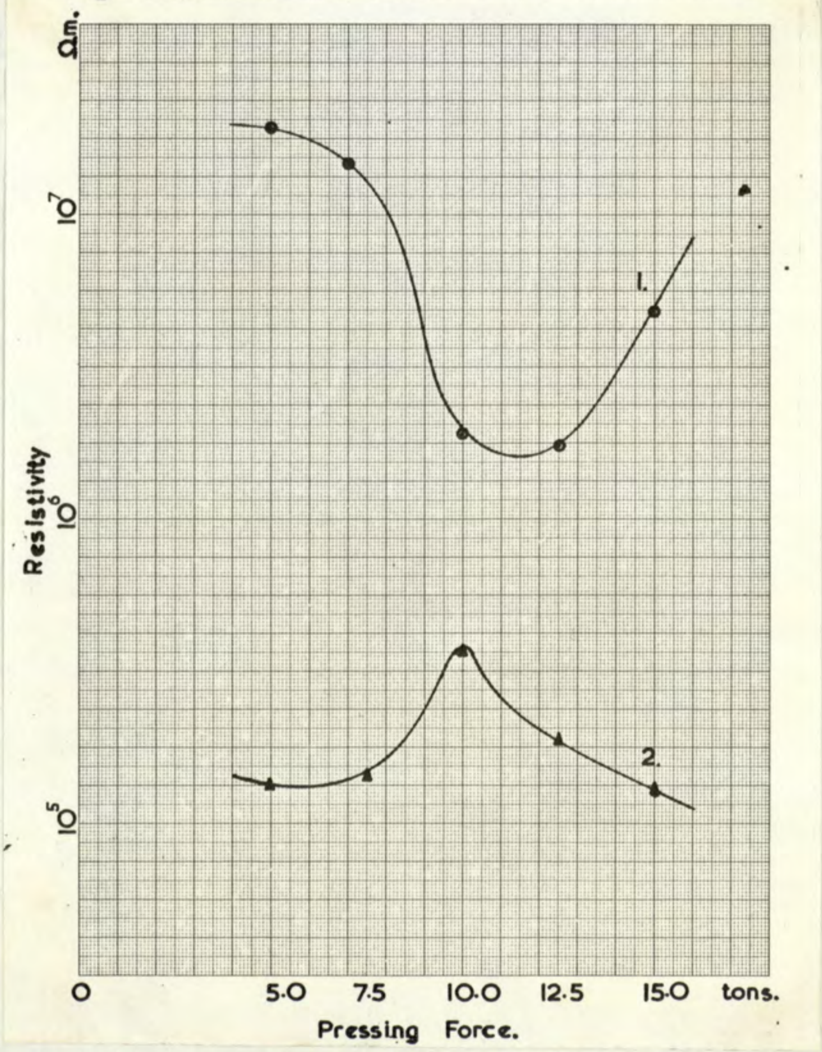

Fig 8.3. Resistivity v Pressing Force; 1 Pure Grade 2 Commercial Grade.

of 1,950 for a pressing force of 9.0 tons.

The material assumed a virtually constant value (1,714) at forces above 12.5 tons.

(See Figure 8.2).

8.1.2.2. Resistivity

The resistivity of the test pieces increased slowly with increasing pressing force, eventually reaching a maximum of $6.1 \times 10^5 \Omega m$ at a position corresponding to an applied force of 9 tons f. The characteristic then showed a decrease in resistivity with increasing force, the value of resistivity for samples pressed at maximum force (15 tons f.) being $9.1 \times 10^4 \Omega m$.

(See Figure 8.3).

8.2 VARIATION IN FIRING TEMPERATURE

8.2.1. Hydrostatically Pressed Pure Grade Material

8.2.1.1. Relative Permittivity

With increasing firing time, the relative permittivity of the hydrostatically pressed samples rose linearly at the rate of 690 per 100°C increase, and reached a maximum value of 1,747 for samples fired at 1,400°C.

(See Figure 8.4)

8.2.1.2. Resistivity

The resistivity of the material rose slightly with increasing firing temperature over the first 50°C of the characteristic. The curve then assumed a constant value of $2.5 \times 10^7 \Omega m$ for the remainder of the firing temperature range.

(See Figure 8.5)

8.2.2. Hydrostatically Pressed Commercial Grade Material

8.2.2.1. Relative Permittivity

Initially, as with the hydrostatically pressed pure grade material, the relative permittivity of the test pieces rose linearly with increasing firing temperature, but at the slightly reduced rate of 633 per 100°C increase. Above 1,350°C the value of relative permittivity increased very rapidly, reaching 1850 for material fired at 1,400°C.

(See Figure 8.4).

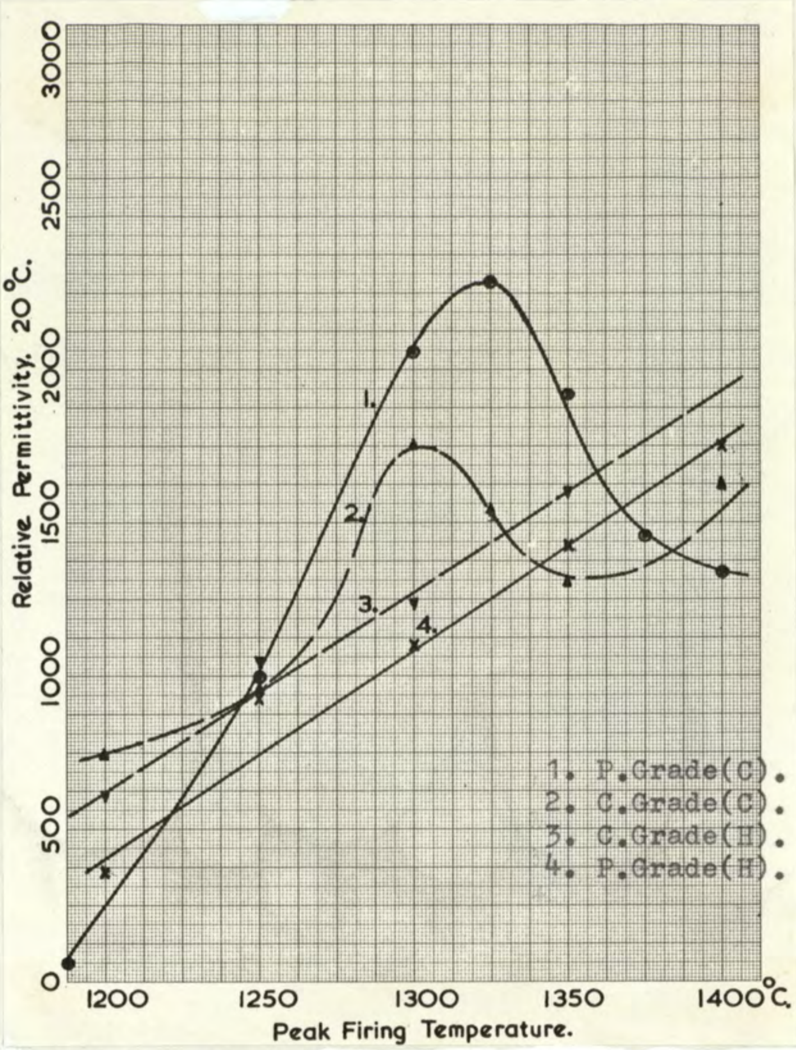

Fig 8.4. ϵ_r v Firing Temp.

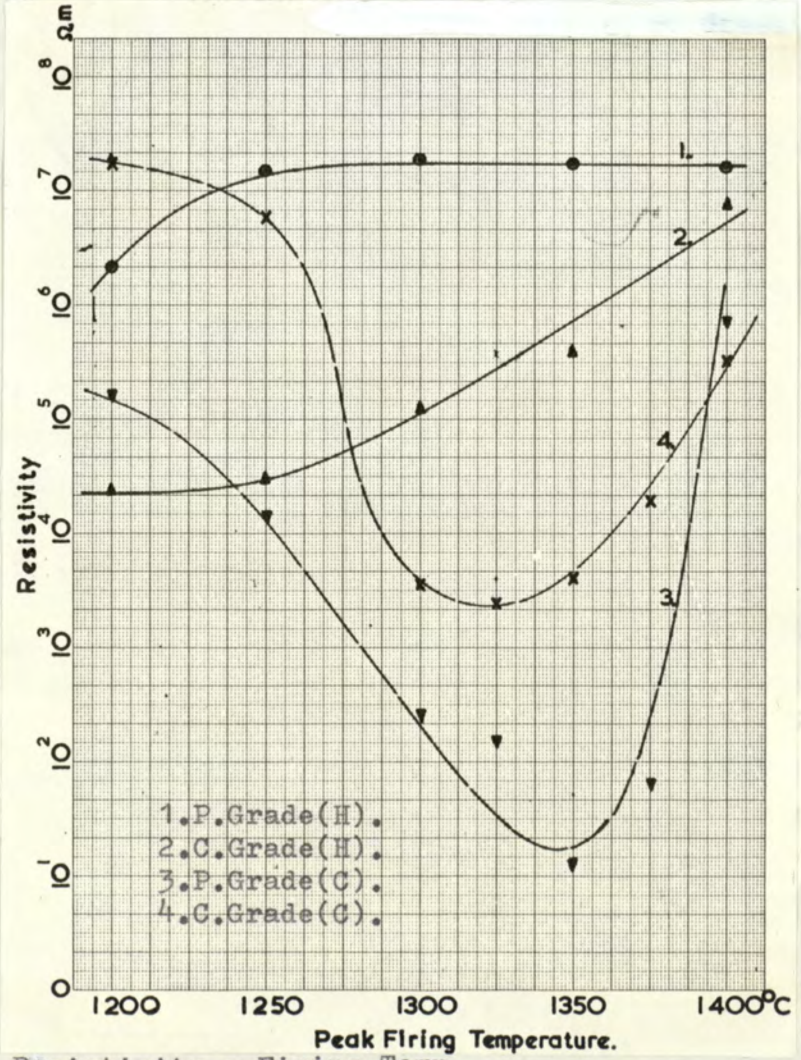

Fig 8.5. Resistivity v Firing Temp.

8.2.2.2. Resistivity

At first, the resistivity of the material rose slowly with increasing firing time, but above a firing temperature of 1,250 the rate of rise increased and the value of sample resistivity rose at the rate of 200Ωm per 100°C increase until a value of 2.73 x 10^6Ωm was obtained for test samples fired at 1,400°C.

(See Figure 8.5)

8.2.3. Conventionally Pressed Pure Grade Material

8.2.3.1. Relative Permittivity

The value of relative permittivity for these test specimens rose from a very low value for the materials fired at lower temperatures to a high peak (2,283) for materials fired at 1,325°C. The relative permittivity of materials fired at higher temperatures decreased rapidly with increasing firing temperature, falling to 1,340 for test pieces fired at 1,400°C.

(See Figure 8.4).

8.2.3.2. Resistivity

The resistivity of the samples dropped rapidly with increasing firing temperature and a definite minimum point was reached with material fired at 1,350°C.

Further increase in firing temperature produced a rise in sample resistivity, the observed value for materials fired at 1,400°C. being 5.2 x 10^5Ωm.

(See Figure 8.5).

8.2.4. Conventionally Pressed Commercial Grade Material

8.2.4.1. Relative Permittivity

The relative permittivity of the commercial grade specimens rose quickly from a relatively low value (728 for test pieces fired at 1,200°C) to a peak value of 1,800 for material fired slightly above 1,300°C. The measured value of relative permittivity then fell away quite rapidly with increasing firing temperature, but recovered quickly above 1,350°C, approaching the previous peak value at 1,400°C.

(See Figure 8.4).

8.2.4.2. Resistivity

The value of sample resistivity dropped as with the pure material, to a definite minimum as the firing temperature was increased.

The minimum point occurred slightly earlier however (at 1,3250°C) and the magnitude of the measured value was somewhat higher at $5.2 \times 10^5 \Omega m$.

(See Figure 8.5)

8.3. VARIATION IN FIRING TIME

8.3.1. Hydrostatically Pressed Pure Grade Material

8.3.1.1. Relative Permittivity

Initially, the relative permittivity of the pure grade materials increased very rapidly with increasing firing time, the rate of increase for the first hour being in the region of 2,000 per hour. The rate of increase then slackened considerably and a maximum value of 3,500 was apparent with materials fired for 1¾ hours.

The magnitude of the measured permittivities then fell away with further increase in firing time, the test pieces fired for the longest period (6 hours) having a permittivity of 2,134.

(See Figure 8.6).

8.3.1.2. Resistivity

The resistivity of the pure-grade hydrostatically-pressed material was found to decrease very rapidly in the materials formed within the first 2½ hours of firing at constant temperature. The value of resistivity fell at the rate of $5.0 \times 10^7 \Omega m$ per hour over this period, reaching a minimum value of $2 \times 10^5 \Omega m$ after 2½ hours.

When the length of firing was increased beyond this point, the gradient of the characteristic changed abruptly, the material resistivity then increasing rapidly (at the rate of $10^3 \Omega m$ per hour) and reaching a value of 5.521×10^3 for material fired for a period of 6 hours.

(See Figure 8.7).

Fig 8.6. ϵ_r v Firing Time. 1 P.Grade (H); 2 C.Grade (H); 3 P.Grade (C); 4 C.Grade (C).

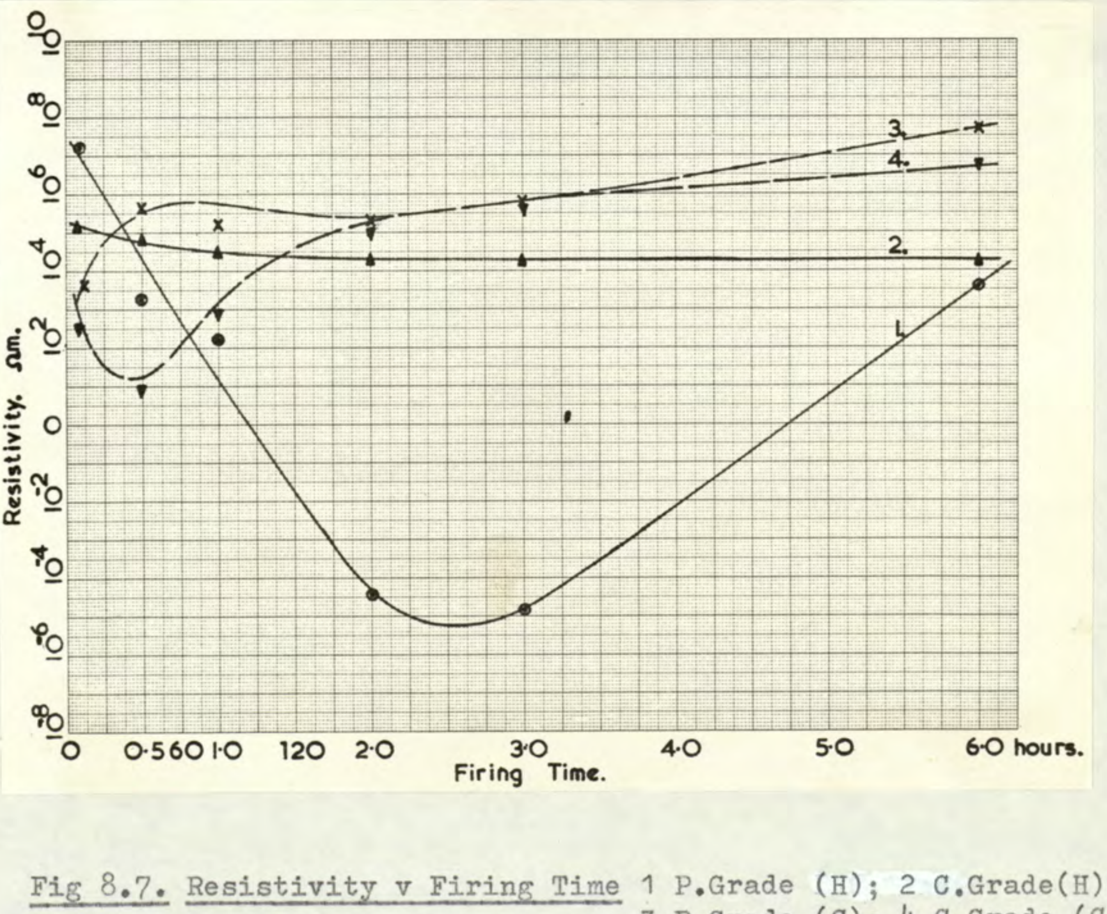

Fig 8.7. Resistivity v Firing Time 1 P.Grade (H); 2 C.Grade(H); 3 P.Grade (C); 4 C.Grade (C).

8.3.2. Hydrostatically Pressed Commercial Grade Material

8.3.2.1. Relative Permittivity

As with the pure grade material, the relative permittivity of the fired test pieces rose quickly over the first hour of firing, but in this case the rate of increase was higher (at 2,550/hour).

A maximum of 3,200 was reached shortly after one hour firing time, but beyond this point the value fell away almost as rapidly as it had increased earlier.

Later (for firing times above two hours) this high rate of decrease slackened off quickly and the permittivity of the materials fired for periods longer than three hours assumed an almost constant value (1,860).

(See Figure 8.6).

8.2.2.2. Resistivity

The resistivity of the material was found to decrease slowly with increasing firing time. A logarithmic relationship of the form:-

$$\rho_0 = \rho_1 t^{-m}$$

was proved, where t is in hours, $\rho_1 = 5.72 \times 10^4.$

$m = 0.75.$

(See Figure 8.7.)

8.3.3. Conventionally Pressed Pure Grade Powder

8.3.3.1. Relative Permittivity

The permittivity of the fired test pieces was seen to rise very quickly over the first 1½ hours of firing time, the value of permittivity rising at the rate of 1,475 per hour during this period. A maximum of 3,200 was reached for a firing time of 1¾ hours, but beyond this point the value of permittivity fell away very rapidly, reaching a minimum of approximately 750 after 3¼ hours firing time.

Later, the value increased slowly to 1,080 for test pieces fired for 6 hours.

(See Figure 8.6).

8.3.3.2. Resistivity

The resistivity of the material rose quickly at first but, in the materials fired for periods longer than half an hour, the measured values increased very slowly, a value of 1.67 x 10^7 Ωm being recorded for the test pieces fired for 6 hours.

(See Figure 8.7).

8.3.4. Conventionally Pressed Commercial Grade Powder

8.3.4.1. Relative Permittivity

The relative permittivity of the commercial material was seen to follow much the same characteristic with increasing firing time as the pure-grade powder. The maximum point occurred slightly earlier (after 1½ hours) and was somewhat smaller in magnitude (2300). The minimum point occurred at the same time as that of the pure material but, again, it was of lower magnitude (approximately 550). The sample permittivity then increased slightly with further increase in firing time, reaching 792 after a total of 6 hours.

(See Figure 8.6).

8.3.4.2. Resistivity

The resistivity of the material was seen to drop quickly from 4.04 x 10^2 Ωm for a five minute firing to a minimum of 90Ωm for a thirty minute firing. Beyond this point the resistivity increased rapidly until, after 3 hours firing, the rate slackened and the values obtained corresponded to those of the pure-grade material pressed by the same method.

(See Figure 8.7).

CHAPTER 9

9. THE FERROELECTRIC-PARAELECTRIC TRANSITION

When barium titanate is cooled through the transition temperature (120°C.) it is transformed from a cubic paraelectric state to a ferroelectric state, where the polar axis may develop along any one of the original cubic axees. The change requires gross motion of the crystal surfaces and, if this motion is impeded, the crystal twins repeatedly in order to reduce the overall change in dimensions and minimize the internal stress.

In polycrystalline barium titanate, the constraints applied to each individual crystal will be complex and the physical phenomena exhibited by the material will be altered considerably by the internal stress distribution within the crystal matrix.

The parameters of the ferroelectric-paraelectric transition in polycrystalline barium titanate are therefore determined by the crystal texture of individual test pieces, and a detailed study of variations in the transition point of the test pieces produced during the project yields information relevant to the state of the materials in their room temperature form.

The effects of mechanical and electrical forces on the ferroelectric phase transitions of $BaTiO_3$ have been discussed earlier (Chapter 3).

The measurements made during the transition period were, therefore, made under conditions of low electrical stress, in order that the variation in properties of the polycrystalline samples from those of the single crystal could be attributed solely to mechanical forces.

9.1. VARIATION OF PRESSING FORCE

9.1.1. Hydrostatically Pressed Pure Grade Material

9.1.1.1. Transition Temperature

The transition temperature of the individual test pieces was found to rise very slightly from 134.2°C (for a pressing force of 5 tons) to a maximum of 136°C (at 8 tons force) before falling to 134°C at maximum force.

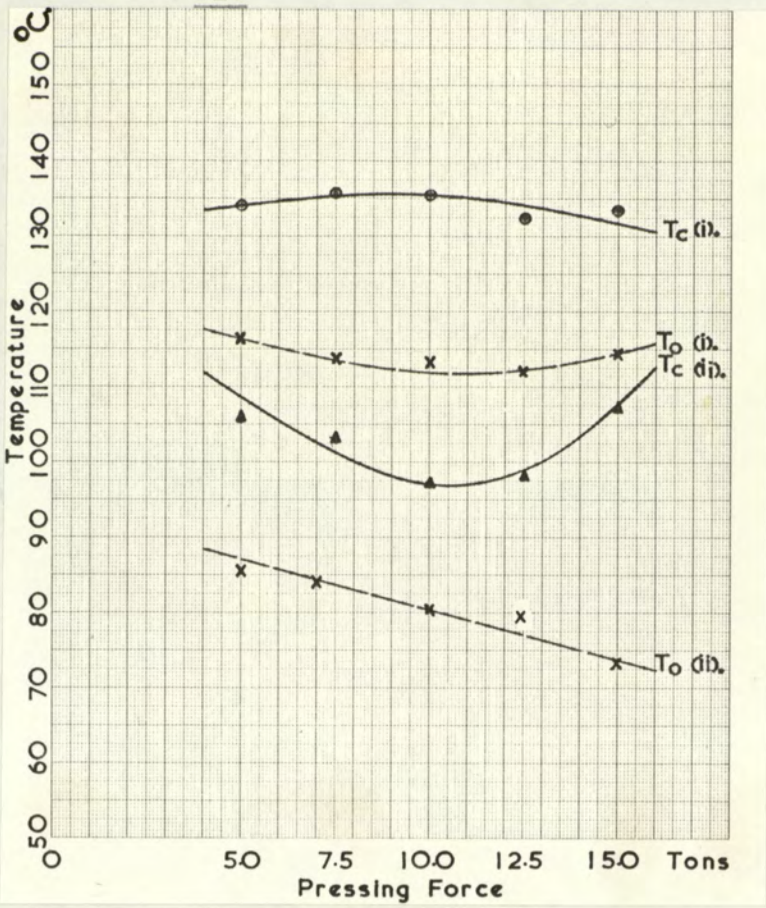

Fig 9.1. T_c & T_o v Pressing Force.
1 Pure Grade.
2 Commercial Grade.

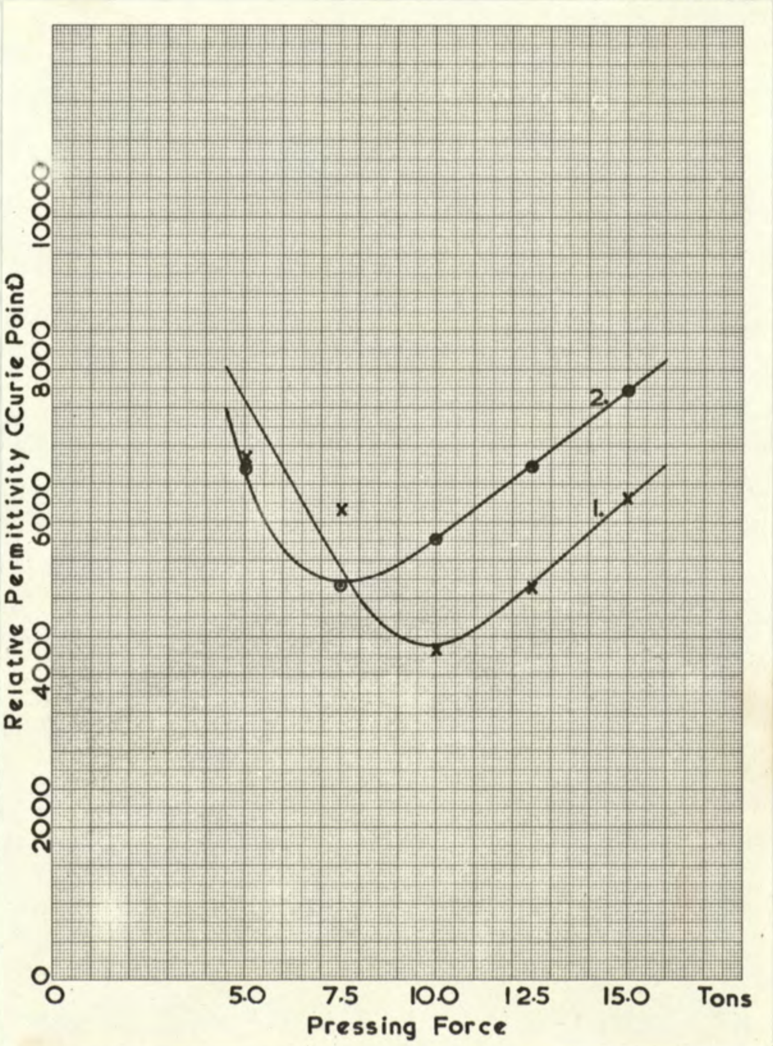

Fig 9.2. Relative Permittivity (C.P.). v Pressing Force.
Pure Grade Commercial Grade.

9.1.1.2. T_o.

The value of T_o fell with increasing pressing force from 106.2°C, for a force of 5 tons, to a minimum of 95°C, at 10½ tons force, before rising to 107.5°C, at 15 tons force.

(See Figure 9.1).

9.1.1.3. Relative Permittivity

The relative permittivity of the test pieces fell from an initial value of 6,740 to a minimum of 5,160 at 7.5 tons force. The value of permittivity then rose quickly (at the rate of 391 per ton force increase), reaching 7,735 for samples pressed at 15 tons force.

(See Figure 9.2).

9.1.1.4. Curie Constant

The Curie Constant of the test pieces fell slightly at first, from an initial value of 1.88, to 1.68 for materials pressed at 7.5 tons. The respective value of the Curie Constant then rose very quickly with increasing force, reaching 5.75 for samples pressed at 15 tons force.

(See Figure 9.3).

9.1.1.5. Nature of Transition

The permittivity characteristics of these test pieces rose very sharply immediately before the Curie Temperature, the change becoming almost instantaneous in the final stages. The peak permittivities were high, although this value decreased sharply immediately.

9.1.2. Hydrostatically Pressed Commercial Grade Material

9.1.2.1. Transition Temperature

The transition temperature of the test pieces fell from 116.5°C (for samples pressed at 5 tons force) to a minimum of 112.6°C (at 10.0 tons force) before rising to 114.6 at maximum pressing force (15 tons force).

(See Figure 9.1).

9.1.2.2. T_o.

The value of T_o fell linearlly (at the rate of 1.3°C per ton force) as the pressing force was increased. At the highest pressing force T_o assumed a value of 73.1°C.

(See Figure 9.1).

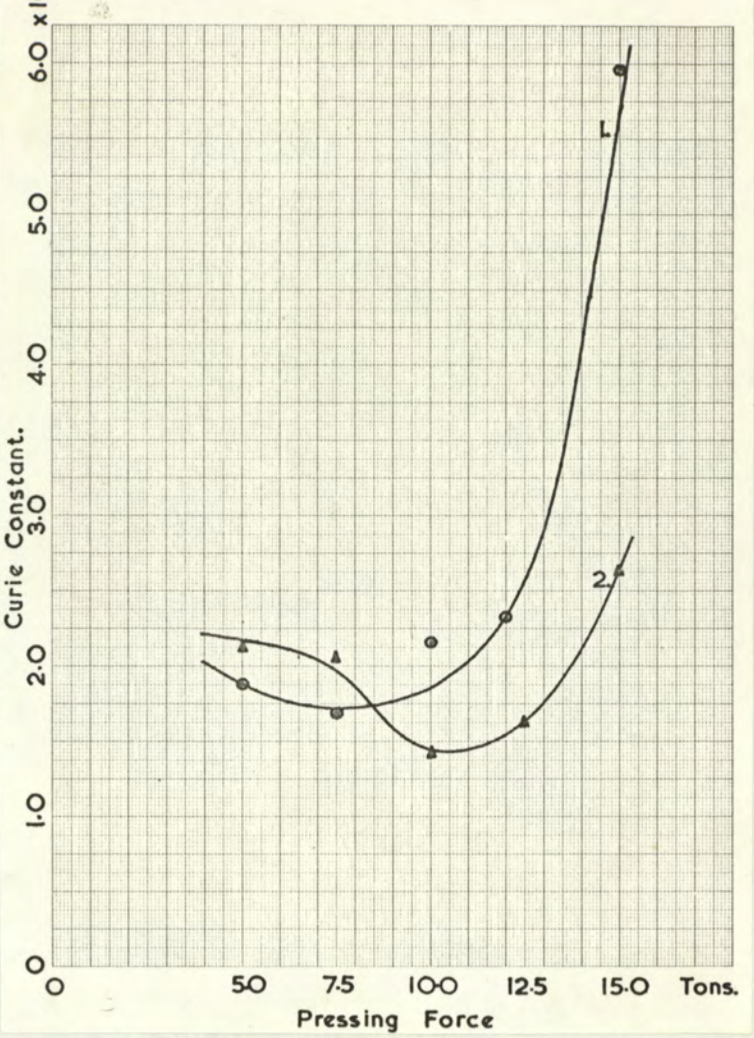

Fig 9.3. Curie Constant v Pressing Force. 1 Pure Grade;
2 Commercial Grade.

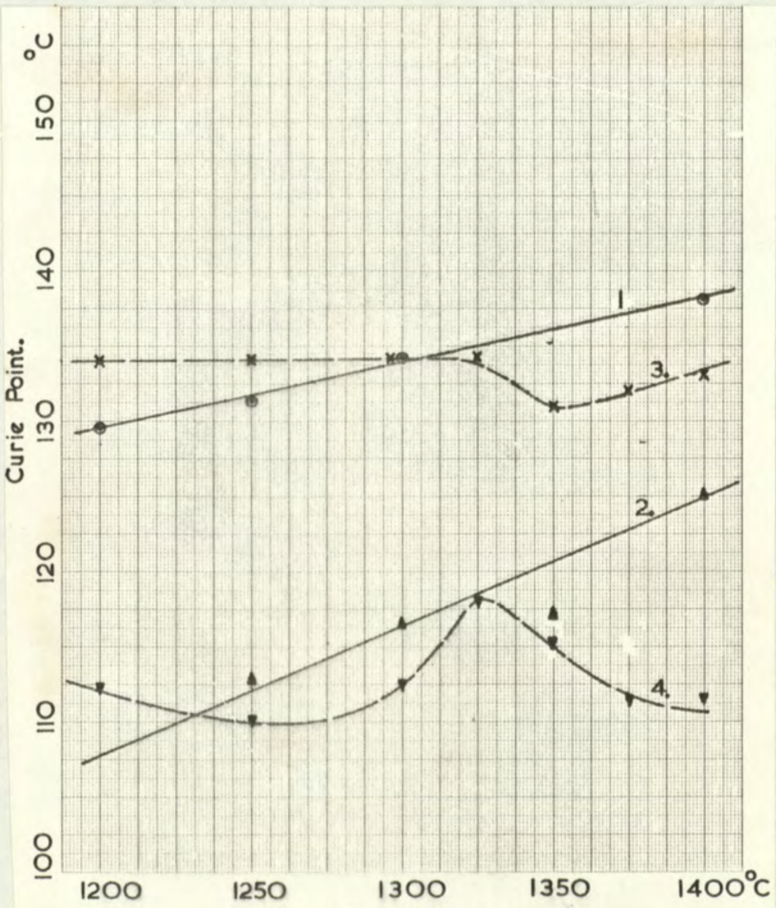

Fig 9.4. T_c v Firing Temperature. 1 P.Grade(H); 2 C.Grade(H);
3 P.Grade(C); 4 C.Grade(C).

9.1.2.3. Relative Permittivity

The relative permittivity of the test pieces at their Curie points showed a linear increase with increasing pressing force beyond 7.5 tons applied force. The value of permittivity increased at the rate of 400 per ton force and reached 6,320 at maximum force.

(See Figure 9.2).

9.1.2.4. Curie Constant

The Curie Constant, C, of the specimens fell to a minimum of 1.412 x 10^5 (in materials pressed at 10.0 tons force), but later recovered and assumed a value of 2.62 x 10^5 in samples pressed at maximum force (15 tons).

(See Figure 9.3).

9.1.2.5. Nature of Transition

The characteristic of these test pieces showed similar changes to those of the pure grade material. The permittivity rose sharply before the transition temperatures, although the rate of increase and subsequent decrease from the maximum values was reduced. Maximum permittivity values became depressed slightly in the later stages of the pressing range.

9.2. VARIATION IN FIRING TEMPERATURE

9.2.1. Hydrostatically Pressed Pure Grade Material

9.2.1.1. Transition Temperature

The transition temperature of the fired test pieces rose linearly with increasing firing temperature, the rate of rise being 4.2° per 100°C increase in firing temperature.

(See Figure 9.4).

9.2.1.2. T_o.

At first the calculated temperature, T_o, rose quickly with increasing firing temperature, but above 1,250°C the rate of increase slackened considerably and the temperature, T_o, then increased at the reduced rate of 3° per 100°C increase in firing temperature. At maximum firing temperature (1,400°C) the value of T_o was 118.9°C.

(See Figure 9.5).

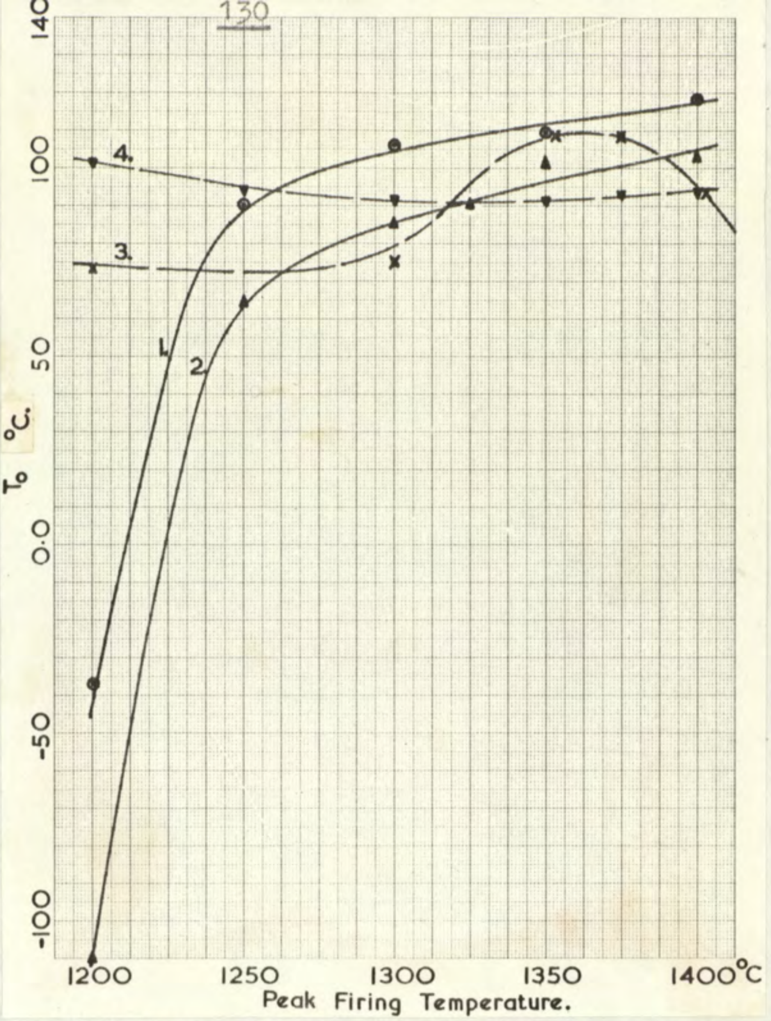

Fig 9.5. T_o v Firing Temperature. 1 P.Grade(H); 2 C.Grade(H); 3 P.Grade(C); 4 C.Grade (C).

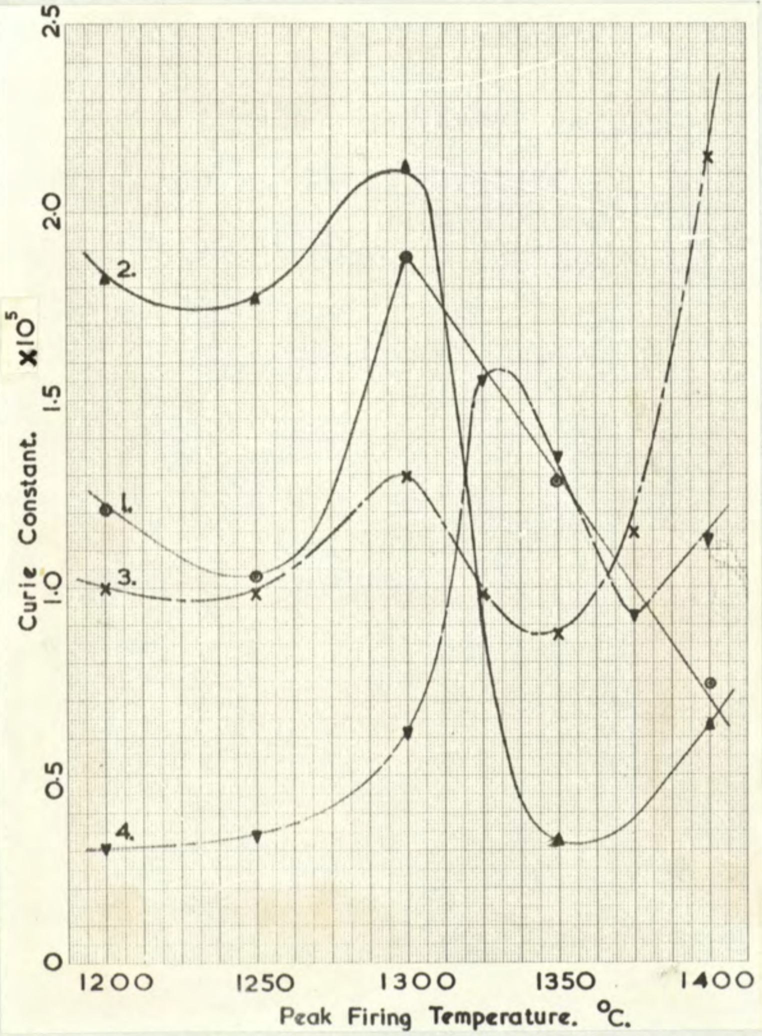

Fig 9.6. Curie Constant v Firing Temp. 1 P.Grade(H) 2 C.Grade(H) 3 P.Grade(C) 4 C.Grade(C)

9.2.1.3. Curie Constant

Initially, the value of the Curie Constant, C, fell with increasing firing temperature but, above 1,250°C, rose suddenly to a maximum of 1,88 at 1,300°C. Subsequent increase in firing temperature reduced the value of C at the rate 0.54 per 100°C.

(See Figure 9.6).

9.2.1.4. Relative Permittivity

The relative permittivity for the test pieces at their respective Curie points increased from a very low value for 1,200°C firings (357) to 6,750 for materials fired in the range 1,300-1,350°C. Further increase in firing temperature produced a slight decrease in permittivity (to 6,420 for 1,400°C firings).

(See Figure 9.7).

9.2.1.5. Nature of Transition

The permittivity characteristics of these test pieces showed only slight increase in permittivity at the transition temperatures, the change occurring over 5-10°C. With increasing firing temperature the values of maximum permittivities increased, the characteristics assuming the more usual sharp-fronted form.

9.2.2. Hydrostatically Pressed Commercial Grade Material

9.2.2.1. Transition Temperature

Above 1,250°C, the transition temperature of the test pieces rose linearly with increasing firing temperature. The rate of increase in transition temperature was 4.25°C per 100°C increase in firing temperature.

(See Figure 9.4).

9.2.2.2. T_o.

The calculated value of the temperature, T_o, rose very quickly at first but above 1,250°C proceeded at the reduced rate of 13.7°C per 100°C increase in firing temperature, reaching 113°C in materials fired at 1,400°C.

(See Figure 9.5).

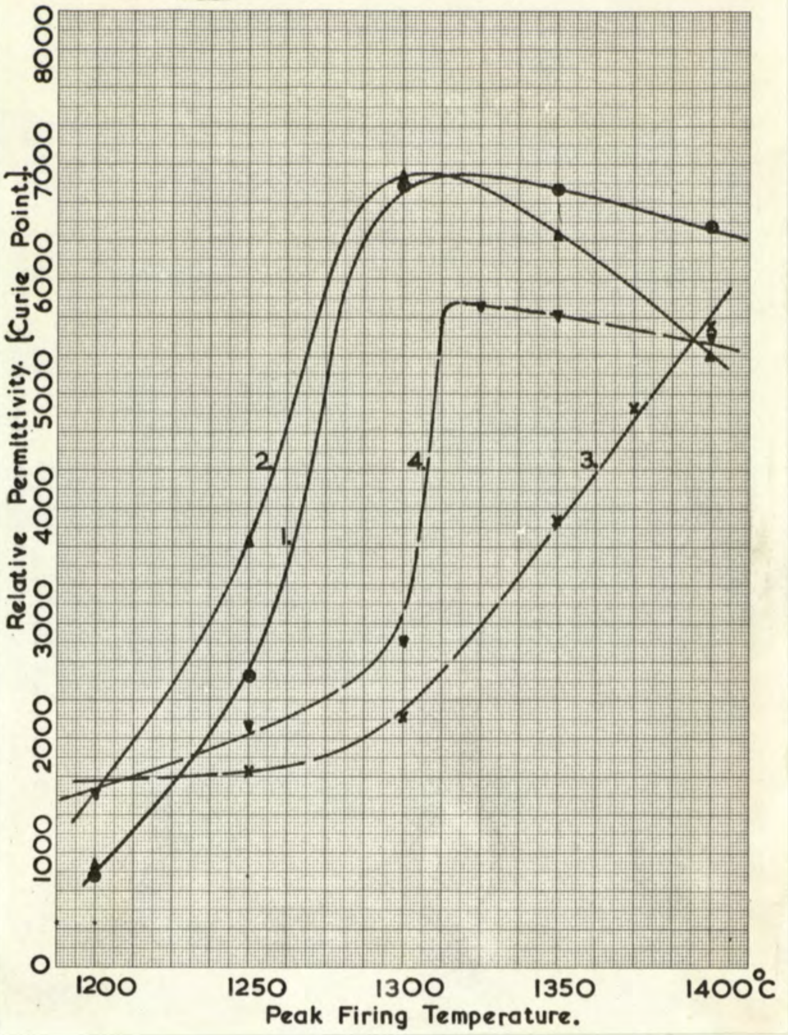

Fig 9.7. Relative Permittivity (C.P.). v Firing Temperature.

1 P.Grade (H); 2 C.Grade (H).
3 P.Grade (C); 4 C.Grade (C).

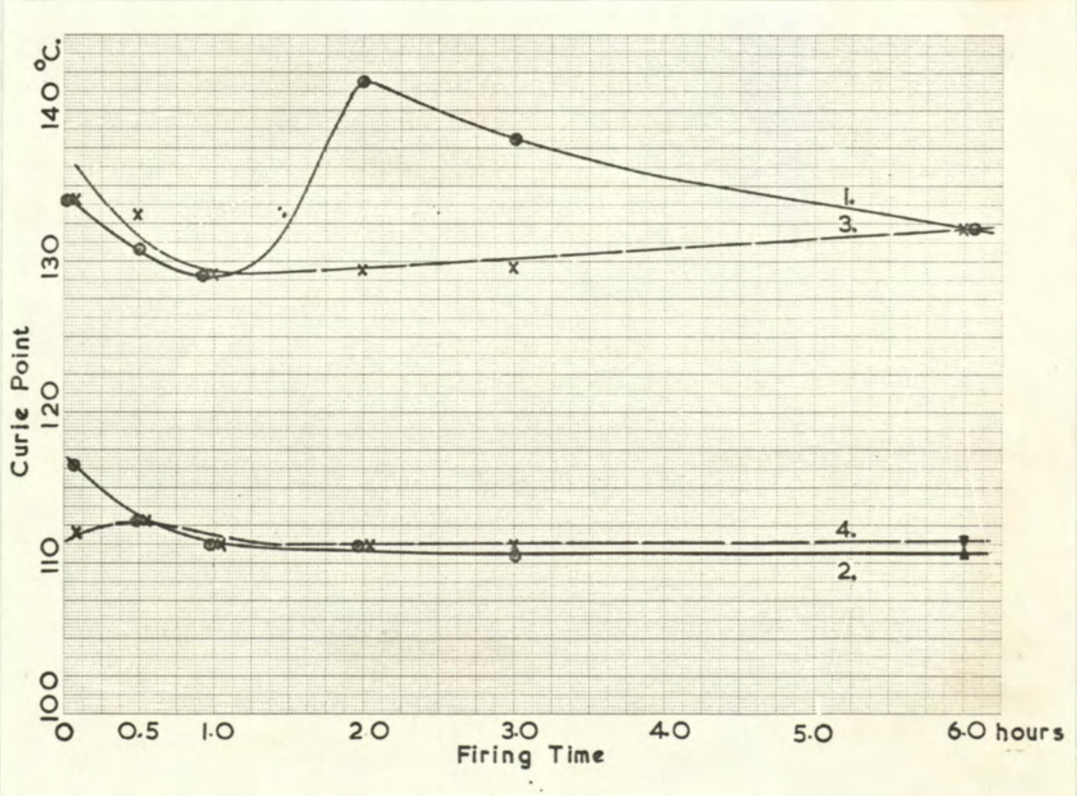

Fig 9.8. Curie Point v Firing Time. 1 P.Grade(H); 2 C.Grade(H).
3 P.Grade(C); 4 C.Grade(C).

9.2.2.3. Curie Constant

The Curie Constant, C, of the test specimens fell slightly at first but above 1,2750°C rose slowly to a maximum of 2.125 x 10^5 at 1,300°C. The value of C then fell very quickly to 0.325 x 10^5 at 1,350°C, but recovered slightly above this point.

(See Figure 9.6).

9.2.2.4. Relative Permittivity

The relative permittivity of the fired samples at their Curie point increased quickly as the firing temperature was increased. A maximum point was reached at a firing temperature just above 1,300°C, but above this point the value of maximum permittivity decreased at a fairly high rate and reached 5,290 in materials fired at 1,400°C.

(See Figure 9.7).

9.2.2.5. Nature of Transition

The permittivity characteristics of these test pieces showed only slight increase in permittivity at the transition temperatures, the change occurring over 5-10°C. With increasing firing temperature the values of maximum permittivities increased, the characteristics assuming the more usual sharp-fronted form.

9.2.3. Conventionally Pressed Pure Grade Material

9.2.3.1. Transition Temperature

The transition temperature of the fired test pieces remained constant at 134°C over the firing range 1,200°-1,325°C. The value of T_c then dropped suddenly at 131°C (above 1,325°C), but then recovered slowly, reaching 133°C in test specimens fired at 1,400°C.

(See Figure 9.4).

9.2.3.2. T_o.

The value of the calculated temperature T_o remained constant at 74°C over the first half of the firing range but at firing temperatures above 1,300°C, the value of T_o increased and reached a maximum of 109°C at 1,360°C. Beyond this point, the value T_o fell away quickly

(See Figure 9.5).

9.2.3.3. Curie Constant

Initially, the value of the Curie Constant of the fired materials rose (to a maximum of 1,292 x 10^5 for materials fired at 1,300°C). There was then a reduction in C, and a minimum value 0.875 x 10^5 was reached at a firing temperature 1,345°C. Above this point the value of C increased very quickly, reaching 2.15 x 10^5 at a firing temperature of 1,400°C.

(See Figure 9.6).

9.2.3.4. Relative Permittivity

The relative permittivity of the samples at their Curie point remained constant at 1,650 for the first part of the firing range. The value of relative permittivity then increased linearly with increasing firing temperature (1,310 per 100°C increase), later reaching 5,530 for samples fired at 1,400°C.

(See Figure 9.7).

9.2.3.5. Nature of Transition

The permittivity characteristics of the conventionally-pressed samples at their transition temperatures had the same form as those of the hydrostatically-pressed samples although the values of maximum permittivity were considerably reduced over the major part of the firing range.

9.2.4. Conventionally Pressed Commercial Grade Material

9.2.4.1. Transition Temperature

The transition temperature of the test pieces fell slightly at first but above 1,250°C. the value of Tc recovered and a maximum of 118°C. was reached with materials fired at 1,325°C. The transition temperature then fell away with increasing firing temperature and a value of 112.6 was obtained for samples fired at 1,400°C.

(See Figure 9.4).

9.2.4.2. T_o.

The value of the calculated temperature, T_o, fell slowly with increasing firing temperature, a minimum of 91°C occurring at 1,325°C. Above this point the value of T_o recovered slowly and reached 97.3 for materials fired to 1,400°C.

(See Figure 9.5).

9.2.4.3. Curie Constant

The value of the Curie Constant, C, rose quickly with increasing firing temperature, from an initial value of 0.306×10^5 to a maximum of 1.548×10^5 at 1,325°C. Above this point, the value of C fell quickly to a minimum of 0.921×10^5 at 1,375°C, but recovered slightly later.

(See Figure 9.6).

9.2.4.4. Relative Permittivity

The value of relative permittivity of the test pieces at their Curie point rose slowly at first, but above 1,350°C increased very rapidly reaching a maximum of 5,690 slightly before 1,300°C. Above this temperature, the value of permittivity fell away slowly (130 per 100°C increase).

(See Figure 9.7).

9.2.4.5. Nature of Transition

The permittivity characteristics of the conventionally-pressed samples at their transition temperatures had the same form as those of the hydrostatically-pressed samples, although the values of maximum permittivity were considerably reduced over the major part of the firing range.

9.3. VARIATION OF FIRING TIME

9.3.1. Hydrostatically Pressed Pure Grade Material

9.3.1.1. Transition Temperature

At first, the transition temperature of the fired test pieces fell quickly with increasing firing time, but later (after one hour) a sudden change occurred, the temperature Tc rising to 142°C before falling away at the rate of 5°C per one hour increase in firing time.

(See Figure 9.8).

9.3.1.2. T_o.

The value of the calculated temperature, T_o, assumed an almost constant value of 110°C throughout the firing range.

(See Figure 9.9).

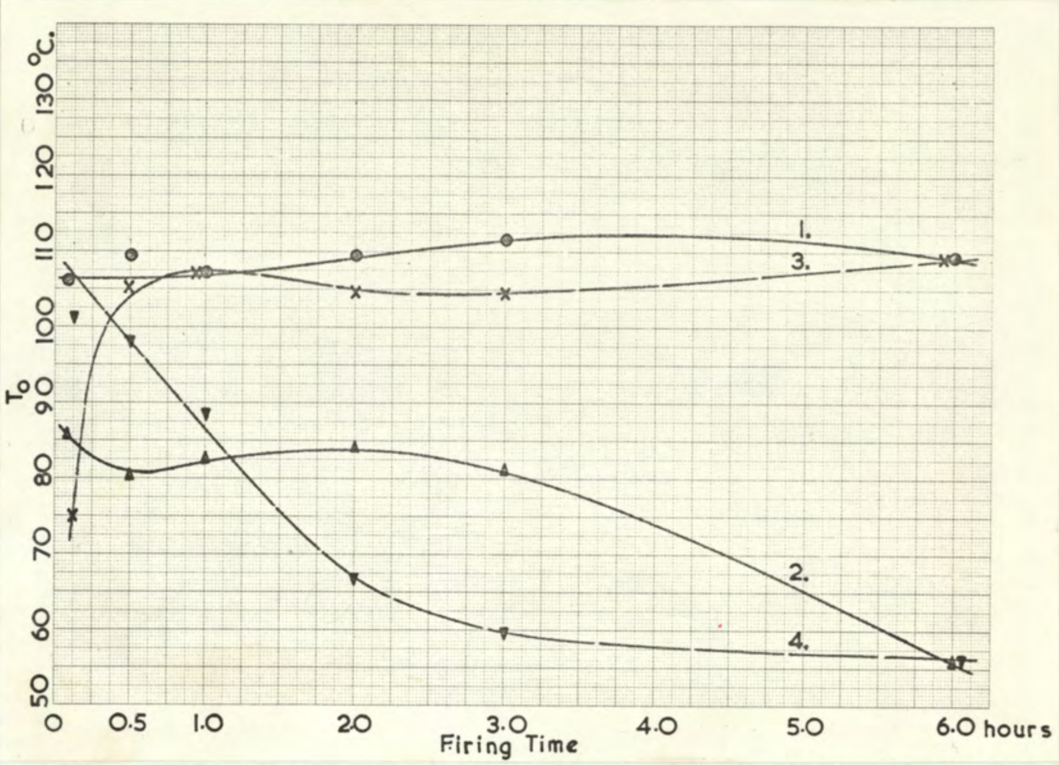

Fig 9.9. T_o v Firing Time. 1 P.Grade(H); 2 C.Grade(H);
3 P.Grade(C); 4 C.Grade(C).

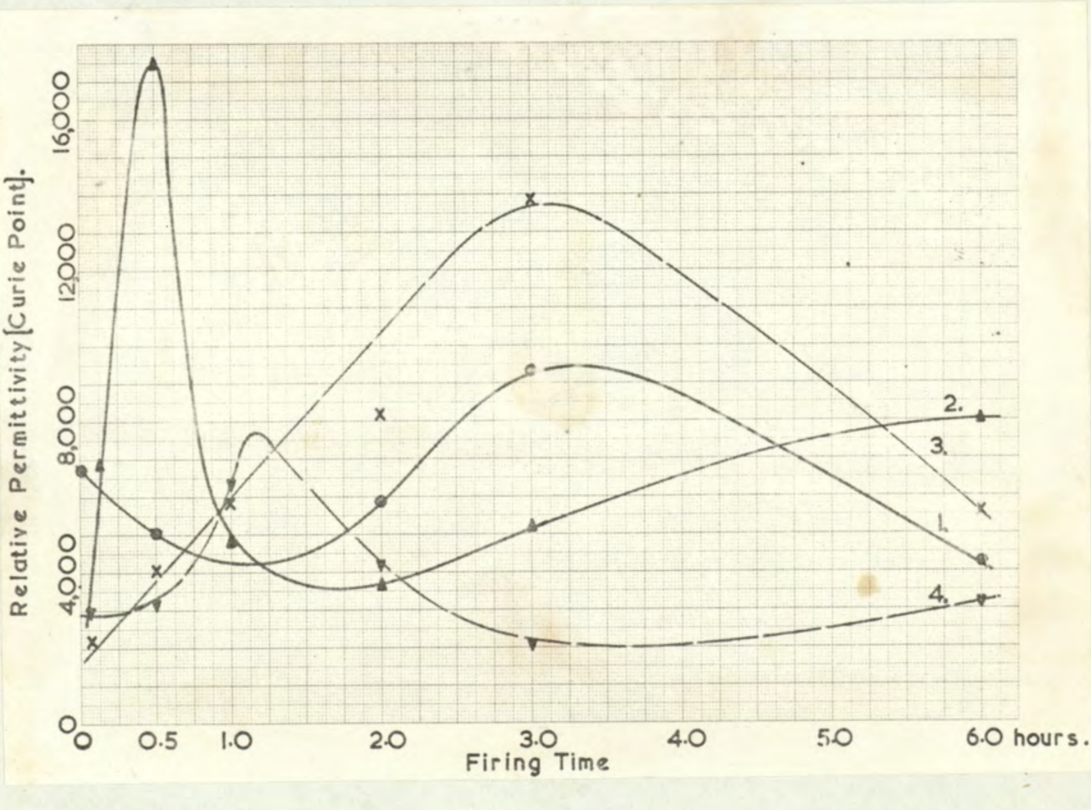

Fig 9.10. Relative Permittivity (C.P.). 1 P.Grade(H); 2 C.Grade(H)
3 P.Grade(C); 4 C.Grade(C)

9.3.1.3. Relative Permittivity

Initially, the relative permittivity of the test pieces at their Curie point fell fairly quickly with increasing firing time. However, for firing periods greater than one hour, the value of permittivity began to increase and a maximum of 9,400 was obtained in samples fired for 1 hour 20 minutes. The permittivity of the test pieces then fell away fairly quickly, reaching 4,326 in test pieces fired for 6 hours.

(See Figure 9.10).

9.3.1.4. Curie Constant

The Curie Constant, C, of the test pieces was seen to fall at first (to a minimum of 1.09×10^5 in samples fired for 45 minutes). The value of C then increased to 2.305×10^5, before falling away to 1.0×10^5 in samples fired for 6 hours.

(See Figure 9.11).

9.3.1.5. Nature of Transition

The permittivity/temperature characteristics of these samples at their Curie Points had sharp fronted high maxima. With increasing firing time the relative height of the maximum values decreased markedly, but later this value recovered quickly.

9.3.2. Hydrostatically Pressed Commercial Grade Material

9.3.2.1. Transition Temperature

At first, the transition temperature, Tc, of the fired test pieces dropped slowly with increase in firing, but for firing periods greater than one hour Tc assumed a constant value of 111°C.

(See Figure 9.8).

9.3.2.2. T_o.

At first the value of the calculated temperature, T_o, fell with increasing firing time but later (after one hour) increased slightly, before falling quite quickly to 56°C with samples fired for 6 hours.

(See Figure 9.9).

9.3.2.3. Relative Permittivity

The relative permittivity of the test pieces at their Curie point rose

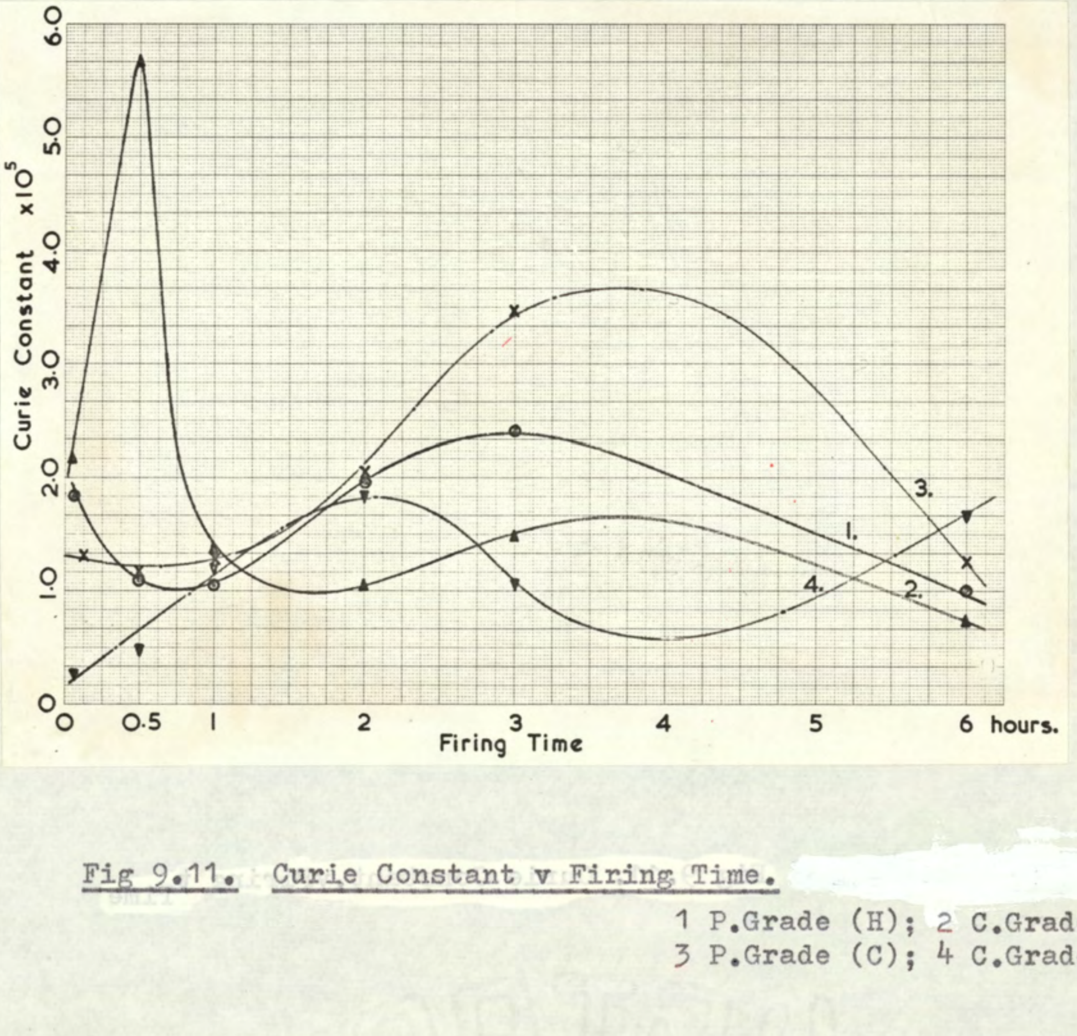

Fig 9.11. Curie Constant v Firing Time.

1 P.Grade (H); 2 C.Grade (H);
3 P.Grade (C); 4 C.Grade (C).

sharply from an initial value of 6,880 to 17,560 for samples fired for 30 minutes. The value of permittivity then fell sharply, but for firing periods greater than 2 hours began to increase again and a value of 6,000 was obtained from samples fired for 6 hours.

(See Figure 9.10).

9.3.2.4. Curie Constant

The Curie Constant of the fired materials rose sharply from 2.12 x 10^5 to a peak of 5.67 x 10^5 for 30 minute firings. The value of C then dropped quickly, but later (after 2 hours firing time) recovered somewhat before falling again to 0.73 x 10^5 for a firing period of 6 hours.

(See Figure 9.11).

9.3.2.5. Nature of Transition

The permittivity characteristics of the samples at their Curie Points had sharp fronted maxima. At first, the relative height of the maximum values increased rapidly with increasing firing time, but then quickly fell away, only to recover again later.

9.3.3. Conventionally Pressed Pure Grade Material

9.3.3.1. Transition Temperature

At first, the transition temperature, Tc, of the test specimens fell quickly with increasing firing time but for firing times greater than one hour the value of Tc recovered slightly, rising from 129°C at one hour to 132°C at 6 hours.

(See Figure 9.8).

9.3.3.2. T_o.

The value of the calculated temperature, T_o, rose very quickly at first reaching a maximum of 106.8°C for samples fired for one hour. The value of T_o then decreased slowly but later recovered and reached 109.6°C in specimens fired for 6 hours.

(See Figure 9.9).

9.3.3.3. Relative Permittivity

The relative permittivity of the test samples at their Curie point rose from 2,190 for samples fired for 5 minutes to 13,820 (for samples fired for 3 hours). The permittivity then fell away sharply, reaching a value of 5,570 in test pieces fired for 6 hours.

(See Figure 9.10).

9.3.3.4. Curie Constant

The Curie Constant, C, of the samples rose from an initial value of 1.3 x 10^5 to a maximum of 3.5 x 10^5 (for materials fired for 3 hours 45 minutes). The value of C then fell away rapidly, being reduced to 1.249 x 10^5 in materials fired for 6 hours.

(See Figure 9.11).

9.3.3.5. Nature of Transition

The permittivity characteristics of these materials **had** sharp fronted maxima. Initially the values of maximum permittivity were depressed in comparison with those of similar hydrostatically-pressed materials, but later the relative height of the maxima increased rapidly, the value becoming very large in latter part of the firing range.

9.3.4. Conventionally Pressed Commercial Grade Material

9.3.4.1. Transition Temperature

The transition temperature of the fired test pieces rose slightly, from the initial value of 112°C to 113°C for samples fired for 30 minutes. Samples fired for longer periods assumed a constant transition temperature of 111°C.

(See Figure 9.8).

9.3.4.2. T_o

The value of the calculated temperature, T_o, fell from the initial value of 101.2°C, to 66.6°C for materials fired for 2 hours. The rate of decrease then slackened considerably and, for samples fired for 6 hours the value of To was 56°C.

(See Figure 9.9).

9.3.4.3. Relative Permittivity

The value of the relative permittivity of the test pieces at their transition temperature rose quickly from an initial 2,820 to a maximum of 7,700 (for samples fired slightly above one hour). Beyond this point, the value of permittivity decreased quickly, but above firing times of 4 hours recovered slightly, reaching 3,120 for specimens fired at 6 hours.

(See Figure 9.10).

9.3.4.4. Curie Constant

The value of the Curie Constant, C, rose slowly at first and a maximum of 1.84×10^5 was reached for materials fired for 2 hours. The value of C then fell away, but above 4 hours recovered and reached 1.653×10^5 (for materials fired for 6 hours).

(See Figure 9.11).

9.3.4.5. Nature of Transition

The permittivity characteristics at their Curie Points had sharp-fronted maxima. The relative heights of these maxima were, however, somewhat smaller than those of the similar hydrostatically-pressed materials, this being particularly noticeable in the first part of the firing range.

CHAPTER 10

10. DISCUSSION

10.1. PRODUCTION OF PRESSING POWDERS

From very early on in the project, it was realized that the pressing powders used by other workers could be classified into two broad groups:-

(i) relatively coarse grained powders, produced by the calcination of intimate mixtures of $BaCO_3$ and TiO_2 at high temperatures, and

(ii) fine grain powders formed by other chemical means.

Both groups would appear to exhibit somewhat differing physical phenomena (especially electrical permittivities and transition points) and several attempts were made to produce powders of suitable quality for direct comparison.

The efforts to produce these powders met with considerable difficulty due to the unsatisfactory nature of some of the processes involved.

Samples of pressing powders generally available were therefore obtained and representive powders of both groups were examined. The difference in the structure of the grains of both types of powder immediately revealed considerable difference between each group (electronmicrographs 1 and 2) and this was thought to be responsible for the difference in densification rates when the two types of powders were pressed over a range of pressures (Figure 6.1, Page 74).

The pure-grade powder, which is seen to be composed of very fine regular grains, compacts linearly with increasing pressure, whilst the commercial grade powder, which is made up from a range of irregular grains, compacts in a similar fashion at first, but later reaches a state where further increase in compaction is no longer possible.

The difference in fired density can be explained by reasoning that, as the commercial grade powder consists of a range of grain sizes, it will have a greater 'packing factor' than the pure powder and will therefore form denser compacts.

10.2.FABRICATION PROCESSES

In every case of previous investigations,all experimental measurements had been made on specimens formed from powders pressed in a punch and die.

This particular method was found to be most unsatisfactory for the production of high-quality test pieces, the test pieces formed containing density gradients produced by the deformation of the agglomerates during pressing. This effect was most noticeable on the major surfaces of the fired specimens,and was further complicated by deposition of metallic particles from the walls of the die onto the sides of the pressed powders during pressing, the powder being quite abrasive.

In addition to this problem, shear lines were set up within the pressings (Plate 3, page 44), and this problem could not be overcome without the use of organic binders.

No such patterns were observed in the isostatically-pressed ceramics fired for short periods at low temperatures although there were a number of high-density areas present within the bulk of the material. These particular areas were not thought to be caused by variation in pressure during the forming process,but rather by chance preferential arrangement of the grains. The areas had no specific shape, were usually confined to 5 to 10 crystals,and were of random distribution; many were,in fact,observed on the thicker conventionally-pressed specimens.

As firing times or temperatures increased,the structure all the test pieces changed radically and,although there was considerable difference between batches of specimens pressed under different conditions, the mechanisms of the changes appeared to be the same in each case.

In every case,increasing time or temperature produced rearrangement in the grains within the crystal matrix. Groups of crystals initially bonded together by thin sinter bridges formed compact groups, some microporosity remaining within the group. The trapped micro-pores then moved along the crystal boundaries within the groups,eventually linking and forming large pores at the edge of the crystals mass.

These large pores then began to migrate throughout the material during the firing period, many evaporating from the free surfaces and the materials densified quickly.

These processes continued until all microporosity had been expelled from the crystal agglomerates. Secondary or duplex crystals then formed, the restraints on the grain boundaries having been removed with the loss of the micropores. Further increase in firing parameters then only served to raise the size of these 'duplex' crystals and increase their numbers.

Similar crystals have in the meantime formed in quantity at the surfaces(by the same mechanism as those in the bulk of the material). The crystals do,in fact,form much earlier than those in the centre,because they lie on a free surface, which may in itself be abnormally dense. It is also conceivable that the impurities (if any) deposited on this surface during pressing may form initiation sites for such grain growth.

In many cases,distinct layers of these crystals are formed and these effectively block pores migrating from the bulk of the material to the free surface,and a very porous layer is formed immediately below the surface layer (see photomicrograph 17c).

The addition of organic binders to the conventionally-pressed specimens obviously affected the basic structure changes occurring during firing, the crystal structure of the materials forming more quickly with increase in firing temperature, although the opposite effect was noticed with increasing firing time.

10.2.3. Summary

10.2.3.1. Fabrication

The microstructure of ceramic barium titanate undergoes considerable alteration when the fabrication process is altered. The unsatisfactory nature of the conventionally-pressed test piece was demonstrated and a defect-free ceramic material is proposed for the processes of electrical investigation.

10.2.3.2. Grain Growth

It is suggested that primary grain growth in ceramic barium titanates is controlled by the motion of micropores along the grain boundaries of the constituent crystals and that the speed of migration is controlled by the free-surface energy of the grain boundaries. General pore movement within the bulk of the material, on the other hand, is controlled by vapour transport mechanisms and at the free surface or at the surface of very large pores by evapouration.

The process of secondary crystal growth is seen to be substantially different from that of primary growth; direct observation indicates that secondary grains are formed from thin plates, although they retain their characteristic shape.

A pronounced decrease in the values of fired density is always observed in the materials containing duplex crystals when surface evaporation is still occurring in places. It must therefore be assumed that the larger crystals are responsible for the change, the crystals swelling during the growth process.

The addition of organic binders alters the mechanisms of crystal growth, this presumably being caused by the reduction of the crystal surfaces (by particles of carbon from the binder remaining in the matrix after the initial firing period). In general, the growth processes are deccelerated by this effect.

10.3. X-RAY STRUCTURE STUDY

Every sample subjected to x-ray examination gave sharp distinct x-ray diffraction profiles. Examination of Figure 7.1 shows that, with variation in pressing force, the x-ray particle size of the pure-grade material stayed constant but that of the commercial-grade powder increased. It was, therefore, concluded that some grain growth did occur in the commercial-grade powder as a direct result of increasing the pressing force, and that this occured as a result of forming denser compacts from powders of irregular grain size, there being more chance of dense agglomerates forming under pressure with this type of powder.

Both types of sample showed similar characteristics with results obtained from materials fired over a range of temperatures. The value of the calculated particle size fell quickly with increasing temperature over the lower part of the temperature range,but above 1,300°C both materials assumed an almost constant value. This,presumably,would indicate that the crystallites within the pressing powders(although large and irregular at first) assumed constant size only in regular well-ordered crystals(such as would be found in powders fired above the vitrification temperature).

The characteristics obtained with increasing firing time at constant temperature showed that this process was fundamentally different to that occurring when the firing temperature was varied.

In the case of the pure-grade material,the size of the crystallites within the crystal matrix of the test pieces was seen to rise quickly(to a maximum at a position corresponding to a firing time of 2 hours 15 minutes) and then fall slightly to a value which remained constant over the remaining part of the firing range. Crystallite growth was thus thought to have occurred in the initial stages,but when 'duplex' crystals began to form crystallite growth stopped and assumed a constant value.

With the commercial-grade powder,a different process occurred, the crystallite size remained constant over the first half of the firing range, and it was only in the latter section that any growth occurred. Study of the relevant photomicrographs (16) indicates that this may indeed have been the case with respect to the full crystal structure,as crystal growth in the bulk of the samples appears to occur only in the latter stages of the firing cycle. The initial process seems to be one of rearrangement of the crystal and pore structure within the samples.

10.4. APPLICATION OF ELECTRODES

The most convenient form of electrode for use with ceramic materials is vacuum deposited metal.

In this process the metal electrode is uniformly deposited over the entire surface of the material(which may be very crystalline in form, Electronmicrograph 3), and penetrates any pores or crevices in the surface. Unfortunately, this may interfere with measurements in some cases, the electrode material clamping the surface crystals and altering their electrical and structural properties; in others, the points of metal formed within the pores may act as areas of high stress during electrical tests at high voltages and so precipitate nucleation of domains or breakdown of the material.

Other types of electrode may be useful in some cases but, for the purposes of electrical investigation, must be considered suspect, due to difficulties in application to the surfaces of the test pieces or in their bonding properties with the surfaces concerned.

In general, cut or polished surfaces are considered superior to fired specimens due to their uniformity and reduced surface area. Comparison of electronmicrographs 3 and 4 illustrates this point.

10.5. DIELECTRIC STUDIES

It was not found difficult to make low-stress measurements on the test pieces, even at either extreme of temperature. The results obtained were thought to be as near electrical-stress free as was possible; so any variations found between samples could be attributed to mechanical forces inherent in the structure of the material.

Tests made at high levels of electrical stress were not so successfull, as repeated d.c. switching caused premature aging and deterioration of the specimen, and high a.c. stress causing heating in some cases(where insulation oil was used to prevent surface breakdown). The elctrode material was found to deteriorate at high temperature, the metal film being lifted off, so reducing the effective electrode area.

Tests with insulating gases, in particular sulphur hexafluoride, effectively prevented surface breakdown of the sample, but there is evidence that the electrical properties of barium titanate may be influenced by the atmosphere in which the samples are placed during measurement. The results obtained could not, therefore, be considered to be useful without a conclusive investigation of this point.

In general, the high stress a.c. measurements obtained were inconsistent and no firm conclusions could be drawn from this work. Switching measurements were equally inconclusive, although the difficulties experienced could have been due to the structure of the materials, charges building up on the pore surfaces during the switching and back switching the domains within the crystals later. A more complete investigation of these phenomena is therefore required.

10.6. CORRELATION BETWEEN ELECTRICAL AND STRUCTURAL PROPERTIES IN CERAMIC BARIUM TITANATE

10.6.1. General

The properties of ceramic $BaTiO_3$ differ from those of the single-crystal material, because of the random orientation of the constituent grains and because of porosity. A simple correction, such as given in Appendix 3, is sufficient to compensate for deficiences in density, but it is difficult to asses the effect of internal strain within the material (as the detailed stress distribution in an individual grain will depend upon the particular orientation of neighbouring grains and the degree of mutual bonding which exists between the grains in the polycrystalline matrix).

It can be expected, however, that some of these strains will be of a type tending to suppress the spontaneous tetragonal deformation of the $BaTiO_3$ crystal and, by analogy with the conditions which exist at the tetragonal-cubic transition point, that is a condition of high intrinsic permittivity. It can be argued that any material possessing a room-temperature permittivity greater than that which is obtained by averaging a and c for a $BaTiO_3$ single crystal and compensating for porosity, does so by reason of the internal forces within the crystal which tend to force each grain back towards its cubic state.

10.6.2. Effect of Grain Size

Applying the principle outlined above, the strains similar to those which exist at the Curie point are present within ceramic materials at room temperature. It is reasonable to presume that the constituent crystallites will themselves reorientate where possible, in order to relieve these stresses.

Such effects are evident in the test pieces investigated. Individual crystals are seen to have twinned to form butterfly-shaped crystals (electronmicrograph 7) and extremely complex domain patters are observed in the larger duplex crystals.

It is therefore probable that the smallest crystals are under much greater stress than the larger crystals, and will therefore exhibit a much higher relative permittivity as a result. There is evidence to indicate that this is, in fact, the case.

During early work test pieces were produced from coarse-grained powders and these were found to be composed solely of very large grains, (photomicrograph 22). Electron measurements showed that these test pieces always possessed relatively-low dielectric constants (approximately 1,000 at room temperature, Figure 8.1) having values which could not be directly attributed to the effects of impurities or to porosity.

The effect of this phenomenon is of direct importance in considering the relationship between electrical and physical properties in ceramics of the type investigated.

The test pieces are found to be composed of three types of material:-

(i) samples consisting of primary grains only

(ii) samples consisting of primary grains surrounded by a thin layer of secondary duplex crystals

(iii) samples consisting of a mixture of primary and duplex grains surrounded by thick layers of duplex crystals.

It is to be expected, therefore, that test pieces in group 1 will exhibit high permittivity regardless of the method of pressing. Test pieces in group 2 will, however, show depressed values of permittivity in conventionally pressed samples, as the low permittivity surface layers will take over the electrical properties exhibited by the bulk of the material. Hydrostatically-pressed specimens, however, only show depressed electrical properties when the firing parameters are raised sufficiently to form duplex crystals within the bulk of the material, the test pieces having no surface material with the influence of electroded surfaces. This point is best illustrated by reference to Figure 8.5, page 122, in which the sudden depression in the value of relative permittivity is observed in both conventionally-pressed specimens at the onset of duplex grain growth at the surface of the specimens. This is in direct contrast with the results obtained from the hydrostatically-pressed test pieces where the value of permittivity only falls slightly over the last stages of the firing range, this being due to the progressive formation of duplex crystals within the bulk of the material.

In the latter stages of the firing cycle, the value of permittivity rises slightly, which is presumably due to the growth of the surface layer and the formation of duplex crystals within the bulk of the material.

These particular effects are also observed in the materials fired over the range of peak temperatures (Figure 8.4, page 119). It must be assumed however, that the pure hydrostatically-pressed material consists solely of primary grains, even in samples fired at 1,400°C, although complex domain structure was clearly visible. A careful re-examination of the polished specimens in question confirmed that this was probably still the case, as the individual grain boundaries were evident although very faint.

The individual crystals were thus ordering generally but remained under considerable local stress from adjacent grains. It is probable that the material was fired to a point approaching the onset of true secondary crystallization and that a slight increase in firing time or temperature would have, indeed, produced this effect, although it was not possible to check this point.

10.6.3. Grain Surface States

The changes in resistivity observed in barium titanate ceramics are generally depicted with the aid of the model of barrier layers at the grain boundaries but, in fact, although their existance is accepted, their precise nature is relatively unknown.

Generally, however, it is considered that the chemical conditions prevailing in these layers dictate the resistivity characteristics obtained for any particular sample. Analysis of the experimental measurements made during this project indicates that this is, indeed, the case far the conventionally-pressed samples, but certain structural relationships are evident from the measurements made with hydrostatically-pressed materials.

10.6.3.1. Hydrostatically Pressed Materials

From results obtained with materials pressed over a range of pressing forces, it is evident that distinct changes in resistivity occur at the same points as similar abrupt changes occurred in Transition Temperatures, (see Figure 8.3, page 117 and Figure 9.1, page 126).

The changes in resistivity would therefore seem to indicate a dependence of resistivity on structural properties, in both the pure and commercial grade materials.

Similar related changes occur in hydrostatically-pressed materials fired over a range of soak times. With the pure-grade material, the abrupt change in resistivity (seen in Figure 8.7, page 122) is parallelled by an equally abrupt change in Transition point at the same time.

The characteristics of the commercial-grade material does not show any specific change in either quantity, but the form of both curves is exactly the same over the entire firing range.

The relationships shown above do not apply to the hydrostatically pressed materials fired over a range of peak temperatures. However, it is known that the mechanisms of structure change in these materials is one of primary-grain growth, as distinct from rearrangement of individual grains. The total length of the grain boundaries therefore reduces with increase in firing temperature, whereas in the previous examples the average length of grain boundary per grain probably remained approximately constant over the total firing or pressing range.

10.6.3.2. Conventionally Pressed Materials

These materials differ from the hydrostatically-pressed test pieces in that they almost certainly contained carbon particles during most, if not all, of the firing ranges. The presence of this material within the crystal matrix is seen to have had considerable effect upon the structure of the material, the rate of growth of grains or changes in orientation of the grains being changed by its presence.

The carbon particles present can be assumed to cover the individual crystals because of the method of adding the binder and so on firing to high temperatures, substantial reduction of the surface layers of the grains probably occurs.

The materials should, therefore, have fairly low values of resistivities in the ceramic form before the carbon particles burn off; the values of resistivity should then progressively increase and assume a relatively-high value when all the carbon has gone completely. If the effect is independent of impurity effects, similar values of resistivity should be obtained for both the pure and commercial-grade powders.

Examination of Figure 8.5, page 119, and Figure 8.7, page 122 shows that this is indeed the case.

10.6.4. The Ferroelectric-Paraelectric Transition

10.6.4.1. General

In terms of the dielectric properties, there would appear to be little to distinguish between the general form of the permittivity-temperature characteristics for any of the samples tested, if those samples fired over a range of temperatures are temporarily disregarded. The general form observed indicates that the change itself took place over a small temperature range and in fact, with samples made from the pure-grade powder the changes were almost discontinuous in nature.

These changes, therefore, allow conclusions to be made regarding the state of these materials at their Curie Points, as the degree of discontinuity must be taken as a measure of the homogenity of the crystalline matrix. The pure-grade materials were, therefore, considered to be much more regular in terms of crystal structure than the commercial-grade powder.

The changes noticed in test pieces fired at varying changes gave results which were somewhat different, due to the inclusion of firing temperatures below the temperature at which vitrification occurs.

With these materials, the transition period was found to initially extend over 5-10°C, with a very low peak value of permittivity. With increase in firing temperature to 1,300°C and above, the characteristics resumed the characteristic shape, i.e. sharp fronted maxima.

The cause of this effect is easily seen by studying the structure of these test pieces; the powders within the compacts are just beginning to bond together and numbers of groups of these crystals are present. Each group will therefore have its own separate stress system set up within itself on cooling, and this will dictate the transition point of that particular group. The material thus consists of many of these small groups, all of which have separate distinct Curie points and permittivities, and the overall characteristics obtained from these materials are the sum of the characteristics of the individual crystal groups.

10.6.4.2. Structural Changes and Internal Stress

When a free single crystal of $BaTiO_3$ is cooled through its Curie point it is transformed from the cubic paraelectric state to the tetragonal ferroelectric state.

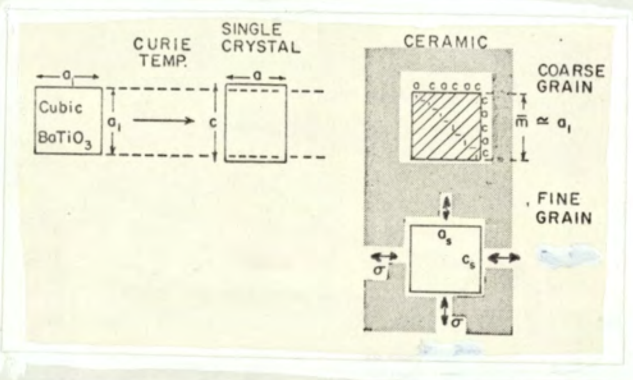

Figure 10.1. Two dimensional model showing origin of internal stress in $BaTiO_3$.

If external constraints are applied to the crystal, such as two-dimensional pressures (causing compression along it's C axis) or complex stresses (having the same overall effect) such would be found if the crystal was situated in a ceramic body, there is a tendency for the spontaneous deformation at T_c to be suppressed and the material to be forced back to the cubic state. Change in the direction of the applied forces only serve to reverse the effect but, in either case, the Curie point of the material must be altered from its single free domain value of 120°C.

It is of interest to compare the values for the Curie point determined for both pure and commercial grade powders. In every batch of test pieces used during the course of the project, the values of T_c determined for the samples made from the pure grade powder were generally 10-20°C above the single-crystal Curie point and those from samples made from commercial grade powder 10°-20°C, below. These completely opposite effects observed in the test materials must therefore indicate that two entirely separate systems are operating within the powders.

In either case, it must be supposed that an overall change in lattice parameters within the materials is responsible for these effects. It is suggested that the changes in the pure-grade material are caused by inherent stresses set up within the individual crystals of the matrix, and those in the commercial-grade material by doping of the material by the impurities(the impurity ions entering the crystal lattice of the material).

Individual variations in Curie point occurring between test pieces of either group are therefore produced as a result of changes in the overall stress distribution in the crystal matrix(caused by structural changes as a result of change in firing parameters).

These changes can be observed in the test pieces formed over a range of pressing forces (see Figures 9.1 and 9.2, page 126). In pure-grade specimens, there is slight decrease in transition temperature with increase in pressing forces above 7.5 tons, and these changes are accompanied by increase in permittivity in every case, as would be expected. The opposite effect is observed in the commercial-grade powders, decreases in transition temperature being accompanied by decrease in transition permittivity, and increases accompanied by rises in permittivity.

The changes observed in the hydrostatically-pressed test pieces fired over a range of temperature also reveal some substantial variation in the transition temperature of many of the test pieces. The true effects are, however, masked by the formation of duplex crystals within the materials in the later section of the firing ranges (where peak value of permittivity becomes progressively depressed with increase in firing temperature) although the Curie Point of both sets of samples still shows a linear increase in the same region.

As before, increase in the transition temperature of the pure materials is accompanied by a fall in the relative permittivity of sample when at that temperature, although this effect may be masked slightly by the effects of secondary crystallization.

Similarly, commercial-grade material shows a decrease in permittivity with increase in transition temperature, in direct contrast to the previous result and, in this case, the transition temperature in fact exceeds the single-crystal transition temperature of 120°C in the later stages of the firing range.

In both cases, it is assumed that the crystals become subjected to progressively increasing stress on raising the firing temperature, the stress being such as to restrain the change of the grains from the tetragonal to the cubic state(that is a compression along the 'a' axis of the crystal or stretching along the 'a' axis). The linear increase in To above 1,300°C tends to support this view, it becoming more difficult to force the material into the psuedo-cubic state by application of electric fields. The situation prevailing in the materials fired over varying time schedules is more complex than in other test pieces, as the alterations in crystal structure are due to the re-arrangement of the constituent crystals instead of growth of individual grains.

Both pure and commercial grade hydrostatically-pressed samples show a high maximum point in the values obtained for permittivity at individual transition points. The peak observed in the commercial grade materials is very high (approximately 18,000), but no specific change in the transition temperature of this sample was observed. There is a definite change in both quantities in the pure-grade material, a very distinct change in transition temperature being accompanied by a peak in the value of permittivity at that point (see Figure 9.8, page 132 and Figure 9.10, page 136).

10.7. APPLICATIONS OF BARIUM TITANATE CERAMICS

Ceramic barium titanate is widely used in industry both in its pure and doped form for the manufacture of capacitors, transducers and many other items of electrical equipment. Further comment on this subject is not necessary, therefore, except that new types of ceramic having greatly improved operating characteristics are possible as improved fabrication techniques are evolved.

CHAPTER 11

11. CONCLUSIONS

11.1. General

It is concluded that the results obtained during the project were indicative of the precise changes in electrical and physical properties of the materials tested, and that the results obtained from the tests made upon the hydrostatically-pressed materials represented an accurate account of the true properties of barium titanate ceramics.

11.2. Fabrication

The fabrication techniques tested gave some indication of the relative merits of each method in general use. It was seen that improved methods of fabrication are necessary to produce test pieces for scientific research.

In particular, it was noticed that improved powder production methods are necessary to produce high-density test pieces and binders have a generally detrimental effect on the subsequent structure of the material.

11.3. Structural Dynamics

Overall densification of both types of samples in all the systems investigated took the same general form. The fired density of the test pieces rose from fairly low initial values to a peak at some specific temperature or time, then fell away due to the onset of secondary crystallization.

Optical examination of polished etched test pieces showed that the densification rate was, in fact, controlled during the firing process by the migration of micropores along the grain boundaries (the grain boundaries being restrained by their presence), by volume diffusion of the larger pores within the bulk of the material, and by evaporation of the larger pores in the imediate area of the free surface.

Secondary crystallization was seen to occur slightly after the point at which all microporosity had been expelled from crystal agglomerates.

Electron microscopy revealed a difference in the structure of duplex crystals when compared with primary crystals, the secondary crystals growing in the form of plates 0.3 microns thick. This observation lends weight to the idea that duplex crystals have a lower density than primary crystals, and that their presence in ceramics produces a decrease in overall density of the material.

11.4. Dielectric Properties

The low-stress dielectric properties observed were considered to be the properties of the material as determined by the mechanical state of the crystal.

High-stress measurements were not successful ,but further work is indicated to determine the mechanism of domain switching in this type of $BaTiO_3$ ceramic.

11.5. Correlation of Properties

Several distinct changes in the structure of the test pieces were observed at various specific points in the tests,and these were correlated with changes observed in the corresponding dielectric properties. The changes that were observed in the permittivity of the materials,and the specific variation in transition temperatures,were attributed to changes in the stress system set up within the material as a result of cooling the material through its Curie point during fabrication.

In general,it was observed that the smaller crystals possessed high room temperature permittivities, whilst the large crystals(especially the secondary 'duplex' crystals) had low values of room-temperature permittivity.

The formation of duplex crystals in surface layers was found to distort electrical measurements in general and were probably responsible for any discrepancies in previous works.

The more general displacement of the transition temperatures of both pure and commercial grade material from that of a single crystal of $BaTiO_3$ was thought to be due to inherent strain within the grains of the pure material (causing elevation of the transition temperature) and to doping of the impure material by reason of the inclusion of impurity ions within the crystal lattice (causing depression of the transition temperature).

Resistivity is seen to be dependent upon structural changes in the hydrostatically-pressed material (although the mechanism was not clear) and on the inclusion of carbon particles in the conventionally-pressed specimens (causing low values of resistivity initially, but high values later, due to reduction of the surface layers of the grains within the crystal matrix).

CHAPTER 12

12. FUTURE WORK

The physical properties of ceramic $BaTiO_3$ are becoming increasingly well documented. There are, however, several areas in which discrepancies occur, or where there is a distinct lack of positive information. Several of these areas of study are described below for inclusion in future work.

12.1. Aging

Due to unfortunate circumstances, the mechanisms of dielectric aging in $BaTiO_3$ ceramics could not be investigated during the course of this project. The effect in single-crystal $BaTiO_3$ is generally attributed to rearrangement of the domain walls within the crystal, but in ceramics there is the possibility that subsidary effects, such as microcracking, might be responsible for part of the observed effect.

12.2. Switching

The results obtained for switching ferroelectric domains in polycrystalline $BaTiO_3$ were inconclusive. The problem is seen to be extremely complex although the general mechanisms of switching as observed in single crystal $BaTiO_3$ probably occur in practice.

It was not considered possible to adequately investigate this problem during the project but it is suggested that the problem could be approached by observing switched and partially switched material as outlined by DeVries and Burke (21), paying due account to the resistivity and crystal structure of the materials concerned.

12.3. Measurement of Particle Size and Structural Strain

The amount of strain present in any particular $BaTiO_3$ ceramic may be measured by comparing the x-ray diffraction peak of the material with that of a pure strain-free reference material (Wilson 1962 and 1963 (61)(62)).

In this method, the variances of the wavelength spread and of the diffraction profile, which are very large, are used as a measure of the particle size and strain of particular material.

12.3.1. Particle Size

The size of the constituent crystallites within a particular specimen may be measured more accurately by the variance method than the half-height width method used in the project. The method is more laborious however.

12.3.2. Structural Strain

An estimate of structural strain may be made by the comparison of the x-ray characteristic of a particular sample with that of a strain-free pure standard of the same material. This was not possible from the method of measurement of half-height width for a single diffraction line used during the project.

In the variance method, the mean square breadth in 2θ can be expressed in the form

$$W_{2\theta} = \frac{K.\lambda.\delta.(2\theta).}{2\pi^2.p.\cos\theta} - \frac{L.\lambda^2.}{4\pi^2 p^2.\cos^2\theta.}$$

where: p is the cube root of particle volume 2θ is the range of 2θ used in evaluating $W_{2\theta}$. K analogous to the Scherrer constant.

L is a quantity depending upon the decrease in area of cross-section of the crystallites in the hkl direction. For non spherical crystals K and L are functions of hkl and are evaluated for certain simple crystal shapes.

A computor programme is given below, which enables the strain in particular specimens to be calculated. Detailed x-ray profiles are required for both the standard and the test specimens. These are usually taken over 2-3° in 0.02° steps.

The computor input then takes the form of:

(i) number of points; (ii) range step (0.02°); (iii) background step; (iv) first 2θ angle; (v) step between points and (vi) second 2θ angle.

The strain is then computed in terms of

$$W = \frac{\langle e\rangle^2 - \langle e\rangle^2}{d^2}$$

where e = local strain and d is the interplanar spacing.

The strain within a particular ceramic specimen can therefore be measured and, by suitable adaption of the specimen holder in the goniometer the variation of strain with temperature could be measured (and would be of particular interest in the region of the Curie Point of the material).

```
BEGIN INTEGER I,J,K,M,N, REAL CLASS,B,BN,D,DN,R,SUM,SY,SXY,SN1,XF,DELTAX,
                          XL,SN2,XBA,XPHY,Z,T,W,VAR,RANGE,ONE,TWO'
                         REAL ARRAY Y(*:300)'
                         SWITCH S:=REPEAT,EXIT,CONTINUE,NEXTB'
REPEAT: READ N'
        IF N LESSEQ 0 THEN GOTO EXIT'
        READ CLASS,Z,XF,DELTAX,XL'
        SY:=SXY:=SUM:=0'
        FOR 1:=1 STEP 1 UNTIL N DO READ Y(I)'
        D:=Y(N)-Y(1)'    B:=0.5*(Y(N)+Y(1))'
        FOR 1:=* STEP 1 UNTIL N DO
            BEGIN SY:=SY+Y(I)'
                  SUM:=SUM+I*Y(N-I+1)'
            END'
        SUM:=SUM/SY-1'
        T:=SY*CLASS'     R:=B*N/SY'
        SY:=(SUM+R*(SUM-0.5*(N-1)+(N+1)*D/(12*B))/(1-R)'
        XBA:=XL-SY*CLASS'
        K:=SY'
        PRINT XBA,PREFIX(££S3??).T'
        FOR BN:=B STEP (-Z) UNTIL (B-5*Z) DO
        BEGIN     PRINT ££L3??,BN,££L??'
                   J:=N'  M:=N-2*K'
         CONTINUE:IF (J-M) LESSEQ 0 THEN GOTO NEXTB'
                  SY:=SUM:=SXY:=XPHY:=0'
                  W:=J-M'  DN:=W*D/(N-1)'
                  FOR I:=M STEP 1 UNTIL J DC
                      BEGIN T:=I-M+1'
                            XPHY:=XPHY+Y(I)*(W-T+1)*(W-T+1)'
                            SUM:=SUM+T*Y(J+M-I)'
                            SY:=SY+Y(I)'
                      END'
                  XPHY:=XPHY/SY'
                  SUM:=SUM/SY-1
                  RANGE:=(J-M)*DELTAX'
                  SN2:=XPHY-W*(2*W+1)/6+W*(W+2)*DN/(12*BN)'
                  SN1:=SUM-0.5*W+(W+2)*DN/(12*BN)'
                  R:=w*BN/SY'
                  SY:=R/(1-R)'
                  ONE:=(XPHY+SY*SN1)*CLASS*CLASS'
                  TWO:=(SUM+SY*SN1)*CLASS'
                  VAR:=ONE-TWO*TWO'
                  XBA:=XF+(J-1)*DELTAX-TWO'
                  PRINT FREEPOINT(4),RANGE,PREFIX(££S3??),FREEPOINT(6),
                                                              XBA,VAR'
                  M:=M+1'  J:=J-1'   GOTO CONTINUE'
       NEXTB:END'
         GOTO REPEAT'
 EXIT:END'
```

Fig 12.1 Computor Programme for the determination of strain in ceramic bodies.

Appendix Ia

Material Pure Grade

Pressing Hydrostatic , Variable Pressing force.

Firing Peak temperature ,Constant Soak Time 5mins.

Batch No.	Pressing Tons. f.	Crystal Size Å.	Fired Density gm/ml.	ϵ_r 20°C.	ϵ_r C.P.	T_c °C.	T_o °C.	C $\times 10^5$	ϱ_o Ω m.
HE1	5.0	2060	4.716	1077	6740	134.2	106.2	1.888	2.58×10^7
HE2	7.5	2060	4.91	2150	5160	135.8	103.2	1.68	1.75×10^6
HE3	10.0	2060	5.02	2500	5780	135.71	97.4	2.155	2.85×10^6
HE4	12.5	2060	5.19	2900	6730	132.6	98.2	2.315	2.43×10^6
HE5	15.00	2130	5.31	3050	7735	133.9	107.5	5.97	6.79×10^6

Appendix I b

Material Pure Grade

Pressing Hydrostatic

Firing Variable Peak Temperature, Soak Time 5mins.

Batch No.	Firing Temp. °C	Crystal Size °A.	Fired Density gm/ml.	ϵ_r 20°C.	ϵ_r C.P.	T_c °C.	T_o °C.	C $\times 10^5$	ρ_o Ω m.
HE6	1200	5500	4.57	357	725	129.5	-37	1.208	0.334
HE7	1250	2630	4.47	924	2490	131.4	90	1.03	1.93
HE8	1300	2060	4.716	1077	6740	134.2	106.2	1.88	2.58
HE9	1350	1950	5.67	1428	6760	136.2	109	1.283	2.51
HE10	1400	1925	5.47	1747	6420	138	118.9	0.72	2.28

Appendix I c

Material Pure Grade

Pressing Hydrostatic

Firing Variable Time, Peak Temperature Constant (1300°C)

Batch No.	Firing Time mins	Crystal Size Å.	Fired Density gm/ml.	ϵ_r 20°C.	ϵ_r C.P.	T_c °C.	T_o °C.	C x10^5	ρ_o Ωm.
HE11	5	2060	4.716	1077	6740	134.2	106.2	1.88	2.584×10^{7}
HE12	30	2130	5.16	2090	5062	130.8	109	1.092	2.304×10^{3}
HE13	60	2400	5.47	3030	4270	129.7	104.8	1.061	2.05×10^{2}
HE14	120	3250	5.41	3150	5960	141.8	109	1.954	5.014×10^{-5}
HE15	180	3070	5.35	2735	9375	138.0	113.4	2.305	1.523×10^{-5}
HE16	360	3070	5.34	2134	4236	132.0	112	1.0	5.521×10^{3}

Appendix I d

Material Commercial Grade

Pressing Hydrostatic Variable pressing force

Firing Peak temperature constant 1300°c Soak time 5 mins.

Batch No.	Pressing Tons.f.	Crystal Size Å.	Fired Density gm/ml.	ϵ_r 20°C.	ϵ_r C.P.	T_c °C.	T_o °C.	C $\times 10^5$	ϱ_o Ωm.
HC 1	5.0	3480	5.32	1238	6880	116.5	85.6	2.125	1.27×10^5
HC 2	7.5	3250	5.37	1870	6160	113.8	76.9	2.065	1.51×10^5
HC 3	10.0	3300	5.43	1824	4320	113.3	80.6	1.412	5.6×10^5
HC 4	12.5	3480	5.44	1714	5110	112.1	80.3	1.624	2.66×10^5
HC 5	15.0	3720	5.439	1714	6310	114.6	73.1	2.62	1.042×10^5

Appendix I e

Material Commercial Grade

Pressing Hydrostatic

Firing Variable Peak Temperature 5 min soak time

Batch No.	Firing Temperature	Crystal Size Å.	Fired Density gm/ml.	ϵ_r 20°C.	ϵ_r C.P.	T_c °C.	T_o °C.	C $\times 10^5$	ρ_o Ωm.
HC 6	1200	5300	4.825	606	799	118.5	-110	1.827	0.376×10^5
HC 7	1250	4350	4.895	1042	3730	112.2	64.9	1.772	0.491×10^5
HC 8	1300	3470	5.32	1238	6880	116.5	85.6	2.125	1.271×10^5
HC 9	1350	3470	5.00	1596	6370	117.9	111.9	0·3.25	5.852×10^5
HC 10	1400	3250	5.04	2540	5290	125	113	0·6.35	91.94×10^5

Appendix I$_f$

Material Commercial Grade

Pressing Hydrostatic

Firing Variable time Peak temperature Constant (1300°c)

Batch No.	Firing Time	Crystal Size Å.	Fired Density gm/ml.	ϵ_r 20°C.	ϵ_r C.P.	T_c °C.	T_o °C.	C x10^5	ρ_o Ω m.
HC 11	5	3480	5.32	1238	6880	116.5	85.6	2.125	1.271x 10^5
HC 12	30	3480	5.35	2100	17,560	112.8	80.5	5.67	0.829 x 10^5
HC13	60	3480	5.4	3060	4820	111.2	82.8	1.371	0.575 x 10^5
HC 14	120	3250	5.51	2186	3680	112.3	84.0	1.041	0.3113 x 10^5
HC 15	180	3480	5.52	2000	5220	110.6	82.0	1.493	0.249 x 10^5
HC 16	360	4020	5.46	1860	6000	109	56 82.0	1.620 0.73	0.157 x 10^5

Appendix I g

Material Pure Grade

Pressing Conventional

Firing Variable peak temperature 5 min soak time.

Batch No.	Firing Temp °C	Crystal Size Å.	Fired Density gm/ml.	ϵ_r 20°C.	ϵ_r C.P.	T_c °C.	T_o °C.	C $\times 10^5$	ϱ_o Ω m.
CE 1.	1200	—	3.17	55.6	1650	134	73.4	1.00	2.32×10^7
CE 2	1250	—	3.96	970	1640	134	74.0	0.983	7.69×10^6
CE 3	1300	—	5.16	2063	2910	134	75.0	1.292	5.4×10^3
CE 4	1325	—	5.63	2283	2960	134	90.9	0.98	3.99×10^3
CE 5	1350	—	5.2	1920	3905	131	108.6	0.875	4.34×10^3
CE 6	1375	—	5.1	1463	4870	132	108.5	1.146	2.894×10^4
CE 7	1400	—	5.06	1338	5530	133	94.2	2.142	5.183 x 105

Appendix I ^{h}

Material Pure Grade

Pressing Conventional

Firing Variable time Peak Temperature constant (1300°C)

Batch No.	Firing time Mins	Crystal Size °A.	Fired Density gm/ml.	ϵ_r 20°C.	ϵ_r C.P.	T_c °C.	T_o °C.	C $\times 10^5$	ϱ_o Ωm.
CE 8	5	—	5.16	1338	2190	134	75	1.292	5.4×10^3
CE 9	30	—	5.48	1642	4095	133	105.2	1.138	6.14×10^6
CE 10	60	—	5.51	2780	5830	129	106.8	1.293	2.032×10^6
CE 11	120	—	5.54	3180	8140	129.3	104.5	2.02	2.75×10^6
CE 12	180	—	5.66	856	13820	129.5	104.5	3.46	8.53×10^6
CE 13	360	—	5.74	1080	5570	132	109.6	1.249	1.67×10^7
		—							

Appendix I ;

Material Commercial Grade

Pressing Conventional

Firing Variable Peak Temperature 5 mins soak time

Batch No.	Firing Temperature	Crystal Size °A.	Fired Density gm/ml.	ϵ_r 20°C.	ϵ_r C.P.	T_c °C.	T_o °C.	C $\times 10^5$	ϱ_o Ω m.
CC1	1200	—	3.85	728	1486	112	101.2	0.306	1.205×10^5
CC2	1250	—	5.19	956	2090	110	94	0.334	1.32×10^4
CC3	1300	—	5.23	1750	2820	112	91.3	0.612	4.0×10^2
CC4	1325	—	5.46	1534	5690	118	90.8	1.548	1.375×10^2
CC5	1350	—	5.45	1278	5610	115	90.9	1.352	17.1
CC6	1375	—	5.49	1886	4750	112.6	93.2	0.921	7.98×10
CC7	1400	—	5.51	1622	5460	112.6	97.3	1.123	5.183×10^5

Appendix I.j.

Material Commercial Grade

Pressing Conventional

Firing Variable time Peak Temperature Constant (1300°c)

Batch No.	Firing Time Mins.	Crystal Size °A.	Fired Density gm/ml.	ϵ_r 20°C.	ϵ_r C.P.	T_c °C.	T_o °C.	C $\times 10^5$	ρ_o Ω m.
CC8	5	—	5.23	1750	2820	112	101.2	0.2482	404×10^2
CC9	30	—	5.3	2105	3112	113	98	0.466	86.1
CC10	60	—	5.38	2035	6300	109.8	88.6	1.34	74.3×10^2
CC11	120	—	5.52	2240	4115	112.3	66.6	1.84	8.21×10^4
CC12	180	—	5.69	624	2058	111.2	59.7	1.058	5.67×10^5
CC13	360	—	5.49	792	3120	108.9	56	1.653	6.12×10^6

Appendix 2

Definitions of Porosity and their inter-relation (B.S.1598.1964)

(i) British Standard Porosity

$$\text{B.S.P.} = \frac{[100 \text{ mass of water sat. specimen} - \text{mass of dry specimen } \%]}{[\text{mass of dry specimen}]}.$$

Obtained by double weighing under specified procedure.

(ii) Void Fraction Porosity

$$\text{V.F.P.} = \frac{100 \times (\text{mass of } H_2O \text{ sat. specimen} - \text{mass of dry specimen})}{\text{Volume}} \%$$

Obtained by double weighing and volume measurements.

$\text{V.F.P.} = \rho_1 \times \text{BSP}$ $\rho_1 =$ apparent density of material.

(iii) Density Defect Porosity (D.D.P.) or Absolute Porosity

$$\text{D.D.P.} = 100 \times \frac{(\rho_0 - \rho_1)}{\rho_1} \%$$

Obtained from a single weighing and volume measurement.

Single crystal density of $BaTiO_3 = 6.10$ gm/cm^3 by x-ray technique. If all the pores in the ceramic are interconnected, the D.D.P. of the substance is equal to the V.F.P.

$$\text{as D.D.P.} = \frac{(\text{dry mass})\,(V - v) - \dfrac{(\text{dry mass})}{V}}{(\text{dry mass})\,(V - v)} = \frac{v}{V} = \text{V.F.P.}$$

$V =$ volume of specimen $v =$ volume of pores in specimen

Any difference found in practice will give an indication of the volume fraction of isolated pores.

Test for porosity by water absorption

Heat test pieces to 110°C in a dry atmosphere for up to two hours and cool in a desiccator. Weigh test pieces and then immerse in distilled water which is then boiled for up to 30 minutes. Allow to cool for up to six hours in the water, then wipe surface with damp but well rung cloth and support in still air for five minutes and then before ten minutes from time of removal from the water reweigh the test pieces

$$\%\ \text{Water absorption} = \frac{\text{weight of moisture absorbed} \times 100\%}{\text{initial weight of test pieces}}$$

Temperature Coefficient of Capacitance

$$\text{T.C.C.} = \frac{(C_2 - C_1) \times 10^6}{C_1 (T_2 - T_1)} \quad \text{parts per million per } {}^\circ\text{C.}$$

C_1 = cap. of sample at T_1°C.

C_2 = cap. of sample at T_2°C.

The temperature coefficient of capacitance of a material is idential with that of a capacitor having that material as dielectric and constrained in such a manner that the change in capacitance with temperature is determined solely by the properties of the dielectric and not by the electrodes. This implies that the electrodes should consist of thin continuous films, firmly attached to the surface of the material, so that the thermal expansion of the electrodes is controlled by the dielectric.

Appendix 3

Porosity Corrections

The permittivity of the continuous phase in $BaTiO_3$ is very much greater than that of the discontinuous phase.

Using Wieners' Law

$$\left[\frac{\epsilon_A - \epsilon_2}{\epsilon_A + \epsilon_2}\right] = X_1\left[\frac{\epsilon_1 - \epsilon_2}{\epsilon_1 + 2\epsilon_2}\right]_2$$

ϵ_A = apparent permittivity

ϵ_1 = permittivity of displaced phase (assumed spheres)

ϵ_2 = permittivity of continuous phase

X_1 = volume fraction of dispersed phase

In $BaTiO_3$ $\epsilon_1 = 1$ and $\epsilon_2 \gg \epsilon_1$

therefore $$\frac{\epsilon_A - \epsilon_2}{\epsilon_A - 2\epsilon_2}_{\,2} = -\frac{X_1}{2}$$

therefore $$\epsilon_2 = \left[\frac{\epsilon_2 + X_1}{2(1 - \epsilon_1)}\right] \cdot \epsilon_A$$

or for very low values of ϵ_1

$$\epsilon_2 = \left(1 + \frac{3}{2} \cdot X_1\right) \cdot \epsilon_A$$

N.B. X_1 = absolute porosity

$$X_1 = \frac{\rho_o - \rho_1}{\rho_o}$$

ρ_1 = apparent density

ρ_o = x-ray density = 6.1 gm/ml.

APPENDIX 4

Spectrographic Analysis of $BaTiO_3$ Samples

(i) Powder Samples

Element	Pure Material % Content	Commercial Material % Content
Fe	0.002	0.004
B	N.D.	N.D.
Si	0.002	0.02
Sr	N.D.	D.
Mn	N.D.	D.
Ph	0.002	0.002
Ba	*	*
Ge	Trace	Trace
Mg	0.002	0.002
Sn	0.03	0.06
Al	0.002	0.008
Ca	0.02	0.04
Cu	0.002	0.002
Na	0.002	0.01
Ti	*	*
Lr	N.D.	N.D.

* Main constituent
N.D. Not detected
D. Detected but quantity unknown

(ii) Hydrostatically Pressed Powder

Ceramic samples show no difference in impurity content.

Spectrographic Analysis Plate 1

Samples 1. Pure grade powder. 2. Commercial grade powder.

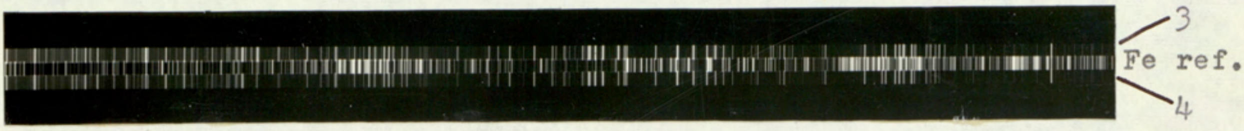

Spectrographic Analysis Plate 2.

Samples 3. Ceramic sample commercial grade. 4. Ceramic sample pure grade.

APPENDIX 5

Capacitor Voltage Dividers

Capacitor voltage dividers are used on power systems for the measurement of E.H.T. voltages in excess 66 kV, as economic considerations precludes their use below this level.

The usual arrangement is shown schematically below:-

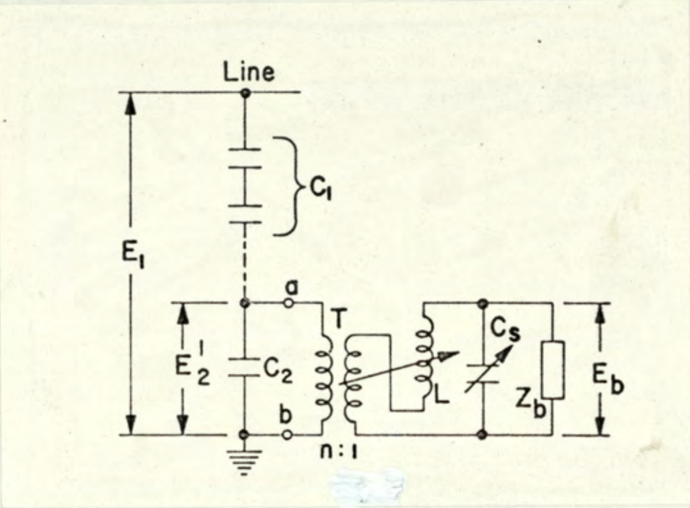

Capacitor Voltage Divider (Schematic)

The phase relationship between the input and burden voltages is controlled by varying the value of the secondary reactance L, the reactance usually required being that required to produce resonance with the capacitor C_1, as $C_1 \gg C_2$.

In this case, the maxoutput is given by $i_2 \times V_{c2}$.

Usually, the capacitors have the value $C_1 = 200$pF and $C_2 = 3{,}000$pF, C_1 being a standard air gap and C_2 a paper oil capacitor.

Disadvantages

(i) This type of divider suffers from the disadvantage that, under transient conditions, the system inevitably suffers from ferroresonent oscillations and a secondary circuit must be introduced to minimize this effect.

(ii) The accuracy of the instrument is subject to errors due to many factors, the most important being: (a) temperature variations within the divider stack; (b) changes of frequency in the system voltage; (c) nonlinearity of the inductive components and (d) external contamination of the stacks by atmospheric pollutants.

Ceramic Voltage Dividers

The values of capacitance required for normal voltage-divider components may be obtained easily using ceramic components. The types of material studied during the preceding project are eminently suitable for such a task, the ceramic bodies produced having a combination of high permittivity and dielectric strength in every case.

In work carried out in the University, several voltage transformers were constructed using ceramic discs 1 cm in diameter and approximately 1 mm thick with circular copper electrodes $\frac{1}{2}$ cm in diameter deposited on the major surfaces of each disc(by high-vacuum technique)$\frac{1}{2}$ cm in diameter.

The discs were stacked within an insulating column with conducting carbon pads placed between eachlayer. Sulphur hexafluoride gas was used as an insulatant.

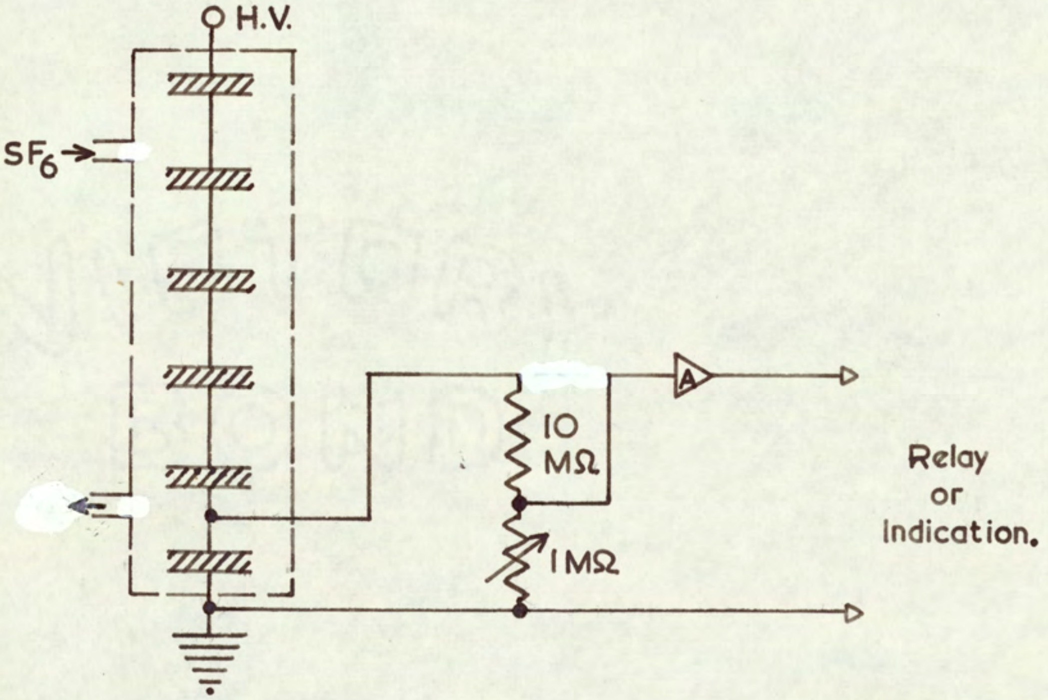

Ceramic Voltage Divider

The output of the device, a tapping between the ultimate and penultimate discs, was fed into an a.c. amplifier having a very-high input impedance.

The output of the amplifier was then used to feed indicating meters of relay coils.

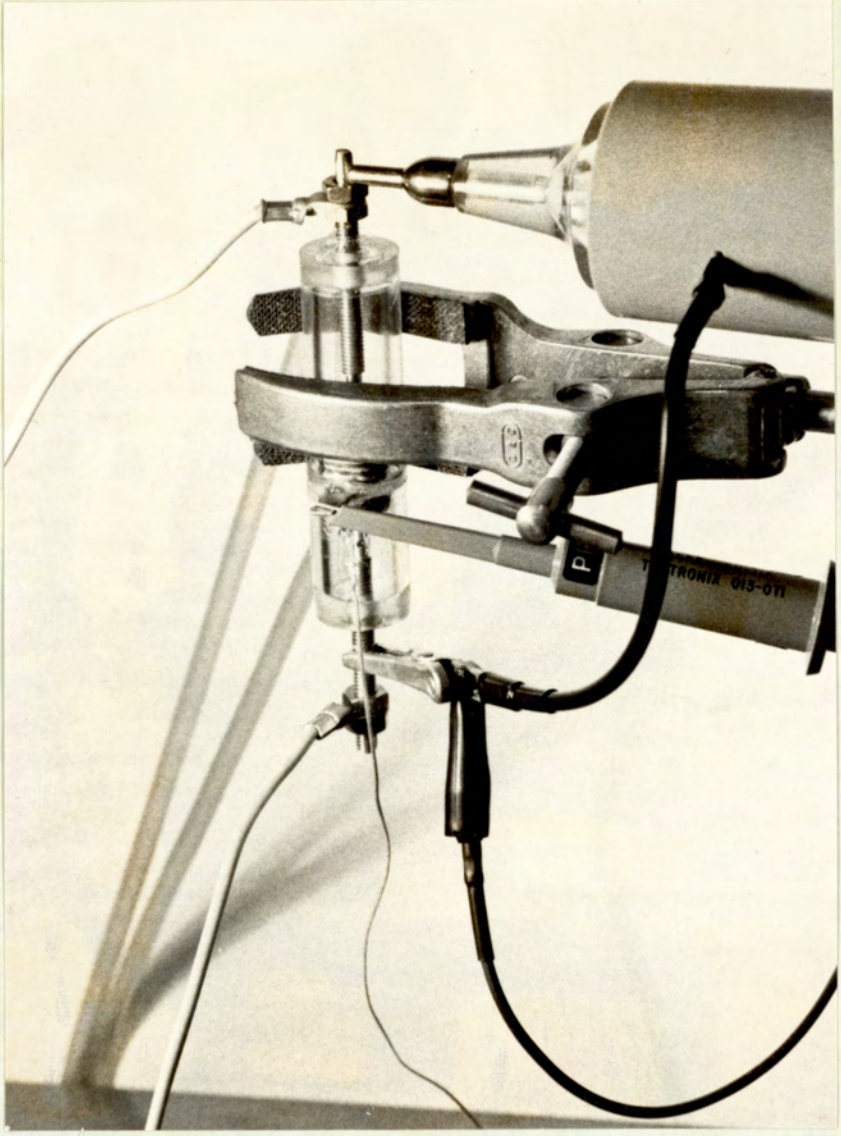

Plate 6. Ceramic Voltage Divider.

Testing

(i) Voltage Ratio Test

The unit was tested up to maximum voltage of 7kv R.M.S., the voltage ratio being measured at several points over this range.

(ii) Frequency Test

The divider was tested using a varying-frequency a.c. supply, the voltage ratio being measured for varying frequency at constant applied voltage.

(iii) Transient Test

The supply voltage to divider was changed suddenly by switching the tappings of the supply transformer, the response of input and output voltages being recorded on ultra-violet recorder.

Results

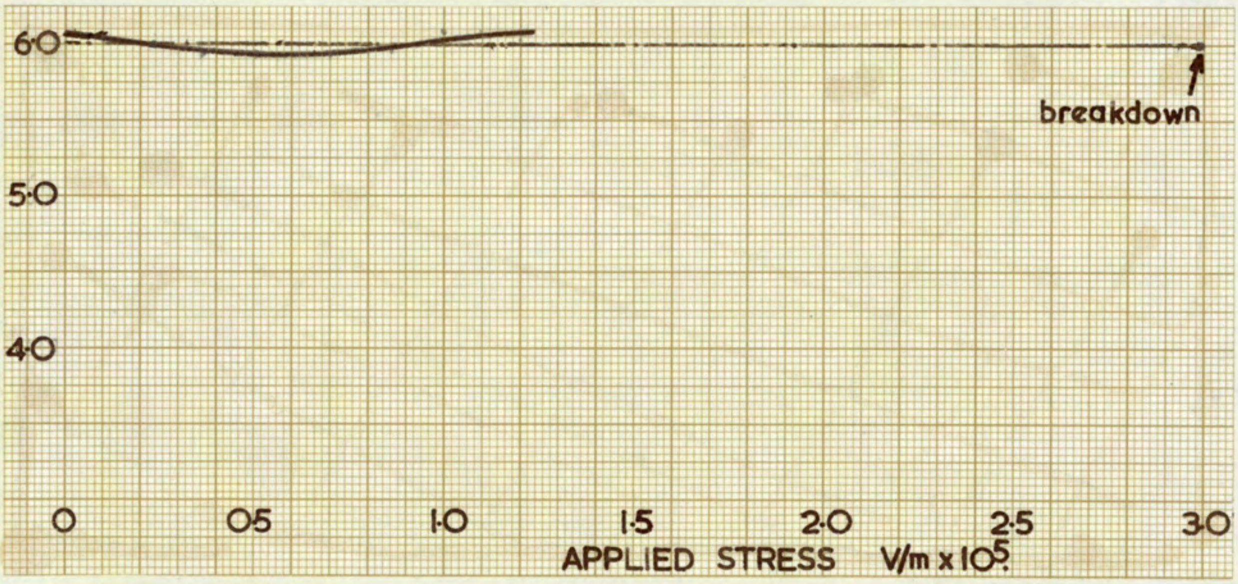

1. Input/output ratio for varying applied voltage

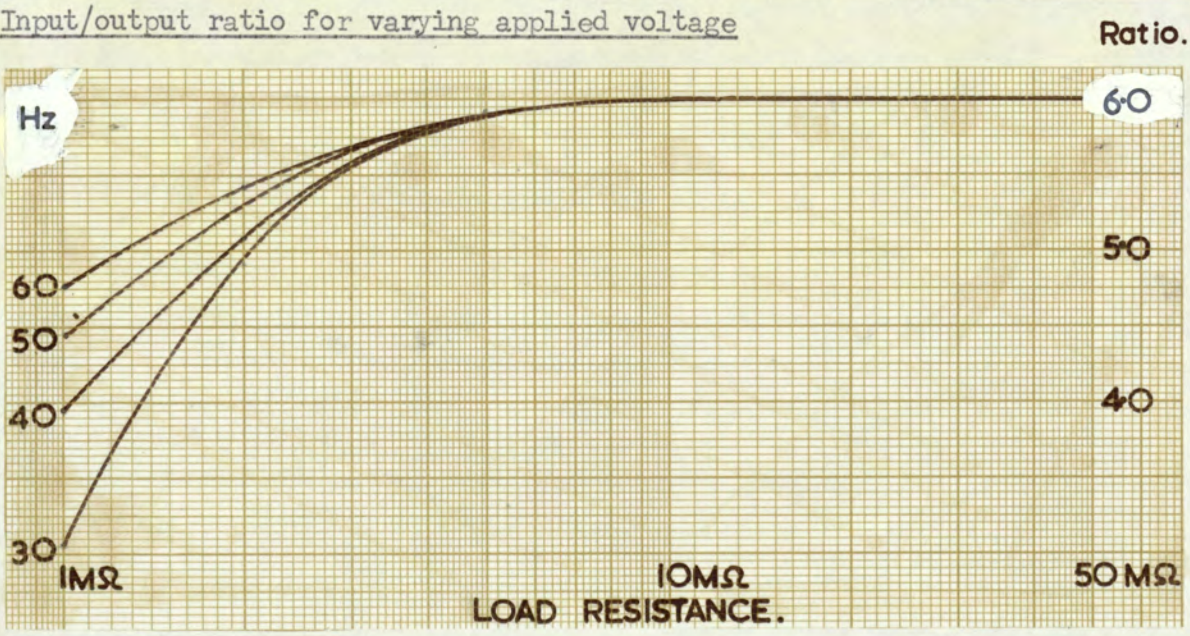

2. Frequency response

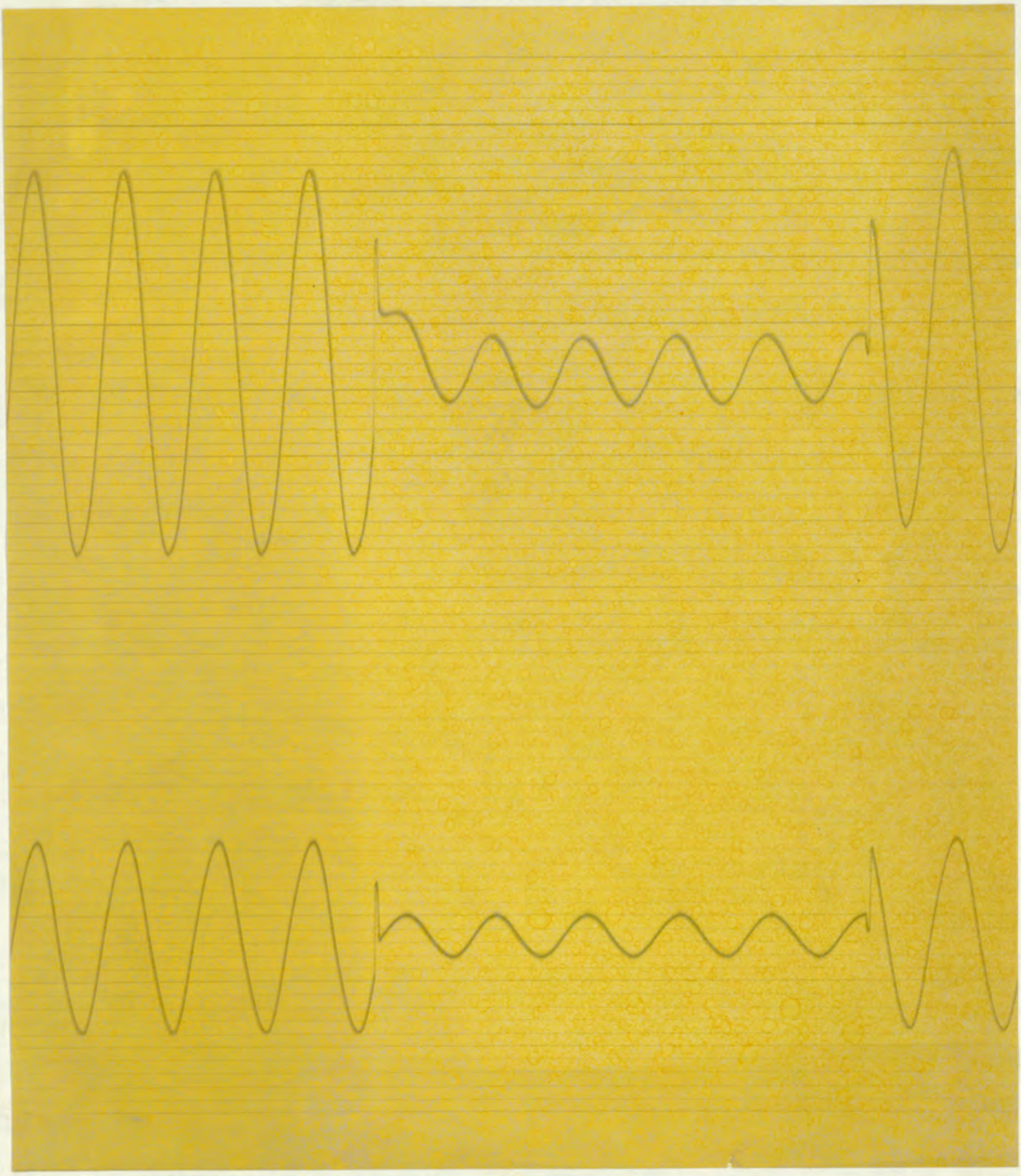

3. Typical Transient Response.

See opposite.

3. Transient response (typical)

Discussion

The type of divider described above would appear to have superior operating characteristics to the dividers presently in use on power systems, especially where transient response is concerned.

Dividers constructed using these materials are cheap and robust and could easily be applied to low-voltage systems, the unit being placed possibly in the inside of post-type insulators and insulated with epoxy resin. For higher voltages, sealed stacks of ceramic material insulated with SF_6 might be employed, the resultant unit having a very much smaller bulk than the present units.

In all of these proposed units, the output VA is controlled only by the type of amplifier employed in the secondary circuit and, as the trend at present is towards solid-state protective devices which only require small input powers, the cost of a suitable amplifier is therefore low and not of great importance from the economic standpoint.

REFERENCES

1. B.Vul and I.M.Goldman. C.R. Acad.Sci. U.R.S.S., 46, 139, (1945).
2. H.F.Kay and P.Vouden. Phil.Mag., 40, 1091, (1949).
3. W.J.Merz. Phys.Rev., 76, 1221, (1949).
4. W.J.Merz. Ibid., 78, 52, (1950).
5. W.Kanzig and N.Maikoff. Helv.Phys. Acta., 24, 175, (1957).
6. P.W.Forsbergh. Phys.Rev., 93, 686, (1954).
7. W.Kanzig and N.Maikoff. Helv.Phys. Acta., 24, 343, (1951).
8. W.J.Merz. Phys.Rev., 91, 513, (1953).
9. W.J.Merz. Ibid., 95, 690, (1954).
10. R.C.Mular and A.Savage. Ibid., 112, 755, (1958).
11. H.L.Stadler. J.Appl.Phys., 29, 1485, (1958).
12. H.F.Kay. Acta.Cryst., 1, 229, (1948).
13. R.C.Millar. Phys.Rev., 111, 736, (1967).
14. H.D.Megaw. Proc.Phys.Soc., 58, 133, (1946).
15. D.F.Rushman and M.A.Strivens. Trans Faraday Soc., 42A, 231, (1946).
16. B.M.Vul. J.Phys.(U.S.S.R.), 10,2, 95, (1946).
17. L.Egerton and S.E.Koonce. J.Am.Cer.Soc., 38,11, 412, (1955).
18. W.R.Eubank; F.J.Rogers; L.E.Schilberg; S.Solnik. Ibid., 35,11, 16, (1952).
19. F.Kulcsar. Ibid., 39,1, 13, (1956).
20. W.R.Cook. Ibid., 39,1, 17, (1956).
21. R.C.DeVries and J.Burke. Ibid., 40, 6, 200, (1957).
22. J.A.Tennery and A.F.Anderson. J.App.Phys., 29, 755, (1958).
23. L.A.Templeton and J.A.Pask. J.Am.Cer.Soc., 42,5, 212, (1959).
24. D.E.Rase and R.Roy. Ibid., 38,3, 102, (1955).
25. H.Kruepkamp and W.Heywang. Z.Angew Phys., 6,9, 385, (1954).
26. P.K.Gallagher; F.Schrey and F.V.DiMarcello. J.Am.Cer.Soc., 46,8, 359, (1963).
27. P.K.Gallagher and F.Schrey. Ibid., 46,12, 567, (1963).
28. K.Kiss; J.Magder; M.S.Vukasovich and R.J.Lockhart. Ibid., 49,6, 91, (1966)

29. T.M.Harkulich; J.Magder; M.S.Vukasovich and R.J.Lockhart. Ibid., 49,6, 295, (1966).

30. W.H.Payne and H.U.Anderson. Ibid., 50,9, 491, (1967).

31. P.Baxter; N.J.Hellical and B.Lewes. Ibid., 42,10, 465, (1959).

32. E.C.Henry and A.V.Illyn. J.Can.Cer.Soc., 34, 137, (1955).

33. H.D.Megaw. Trans Faraday Soc., 42A, 231, (1946).

34. T.N.Verbitskaya; G.S.Zhdanor; In.N.Venevtsev and S.P.Soloviev. Soviet Phys.Cryst., 3,2, 182, (1958).

35. G.A.Smolenskii and V.A.Isupor. Dokl.Akad.Nauk., 96,1, 53, (1954).

36. W.H.Payne and V.J.Tennery. J.Am.Cer.Soc., 48,8, 413, (1965).

37. E.C.Subbarao and G.Shirane. Ibid., 42,6, 279, (1959).

38. P.R.VanLoan and M.R.Chakrabarty. Ibid., 49,5, 276, (1966).

39. W.J.Merz and J.R.Anderson. Bell Lab.Record., 33, 335, (1955).

40. B.H.Marks. Electronics, 21,8, 116, (1948).

41. K.W.Plessner. Proc.Phys.Soc., 69,12, 1261, (1956).

42. J.Valasek. Phys.Rev., 17, 475, (1921).

43. C.B.Sawyer and C.H.Tower. Ibid., 35, 269, (1930).

44. J.A.Hooton and W.J.Merz. Ibid., 98, 409, (1955).

45. R.L.Coble. J.App.Phys., 32,5, 795, (1962).

46. W.D.Kingery and B.Francois. J.Am.Cer.Soc., 48,10, 546, (1965).

47. W.D.Kingery and J.Berg. J.App.Phys., 26, 1205, (1955).

48. F.A.Nichols. J.App.Phys., 37,13, 4599, (1966).

49. A.Arias. J.Am.Cer.Soc., 49,11, 621, (1966).

50. A.F.Devonshire. Phil.Mag., 40,309, 1040, (1949).

51. W.A.Weyl and T.Forland. Indust.Engng.Chem., 42, 257, (1950).

52. S.S.Flaschen and L.G.Van Uitert. J.App.Phys., 27, 190, (1956).

53. H.A.Sauer and S.S.Flaschen. Am.Cer.Soc.Bull., 39,6, 304, (1960).

54. R.Sussman and V.Ern. J.Am.Cer.Soc., 48,10, 543, (1965).

55. G.W.Marks; D.W.Waidelich and L.A.Monson. Trans.A.I.E.E., Pt.1, 75, 469, (1956).

56. G.Busch. Helv.Phys.Acta., 21, 212, (1948).

57. W.Heywang. Solid State Electron, 3, 51, (1961).

58. W.Heywang. J.Am.Cer.Soc., 47,10, 484, (1964).

59. S.N.Ruddlesden and A.C.Airey. Trans.British Cer.Soc., 66, 587, (1967).

60. A.G.King and K.Fuchs. J.Am.Cer.Soc., 50,6, 328, (1967).

61. A.J.C.Wilson. Proc.Phys.Soc., 80, 268, (1962).

62. A.J.C.Wilson. Proc.Phys.Soc., 81, 41, (1963).